

UNIVERSITA' DEGLI STUDI DI NAPOLI "FEDERICO II"  
DOTTORATO DI RICERCA IN INGEGNERIA AEROSPAZIALE,  
NAVALE E DELLA QUALITA'  
XXIV CICLO



**New Approach and Results on the Stability  
and Control of Airship**

TUTORS:

Prof. Ing. Leonardo Lecce

Prof. Ing. Claudio Pensa

Prof. Ing. Agostino De Marco

CANDIDATE:

Ing. Maria Acanfora

November 2011

## Acknowledgments

The authors acknowledge the support received by **Airship Italia s.r.l.** and by **CIRA-Italian Aerospace Research Center**, who provided some important data and information that have been very useful in carrying out this work.

# Contents

<b>1</b>	<b>Introduction</b>	<b>7</b>
1.1	Airship history and the Italian heritage . . . . .	7
1.2	Airship classification . . . . .	8
1.3	Airship characteristics and applications . . . . .	9
1.4	Airship actual projects . . . . .	10
1.5	State of art . . . . .	11
1.5.1	Airship static stability . . . . .	12
1.5.2	Airship control . . . . .	13
<b>2</b>	<b>Unmanned Airship AIUX15</b>	<b>14</b>
2.1	The AIUX15 prototype . . . . .	14
2.2	Airship configurations . . . . .	14
2.3	Airship aerodynamic data . . . . .	16
<b>3</b>	<b>Linear Airship Model</b>	<b>26</b>
3.1	General equation of motion . . . . .	26
3.2	Linearized airship model . . . . .	29
3.2.1	Longitudinal equations . . . . .	30
3.2.2	Lateral-directional equations . . . . .	31
3.3	The airship static stability . . . . .	32
3.4	Longitudinal trim . . . . .	34
3.5	Application of the method . . . . .	34
3.5.1	“Cross” configuration results . . . . .	35
3.5.2	“Inverted Y” configuration results . . . . .	36
<b>4</b>	<b>Longitudinal Simulation Model</b>	<b>40</b>
4.1	Longitudinal equation of motion . . . . .	40
4.2	The Simulink 3DoF model . . . . .	42
4.3	Method comparison . . . . .	46
<b>5</b>	<b>Six-degree-of-freedom Simulation Model</b>	<b>54</b>
5.1	Implemented equation of motion . . . . .	54
5.2	The implemented Simulink model . . . . .	57
<b>6</b>	<b>Airship Control in Steady Air</b>	<b>66</b>
6.1	Implemented equation of motion . . . . .	66
6.2	The pole placement method . . . . .	67
6.3	Applications and results . . . . .	68

<i>CONTENTS</i>	3
<b>7 Airship Control in Turbulent Air</b>	<b>72</b>
7.1 The turbulence model . . . . .	72
7.2 The pole placement with noise . . . . .	73
7.3 Linear quadratic optimal control . . . . .	75
<b>8 General Layout of the Experimental Tests</b>	<b>81</b>
8.1 Introduction . . . . .	81
8.2 The mathematical model . . . . .	81
8.3 Preliminary analysis . . . . .	83
8.4 Model test arrangement . . . . .	84
<b>9 Conclusion</b>	<b>86</b>
9.1 Linear analysis . . . . .	86
9.2 Simulation model . . . . .	87
<b>A The Added Mass</b>	<b>88</b>

# List of Figures

1.1	The Norge Airship . . . . .	8
1.2	The Hindenburg Airship . . . . .	9
1.3	The Goodyear non-rigid Airship . . . . .	10
2.1	The AIUX15 prototype . . . . .	15
2.2	The AIUX15 propeller outline . . . . .	15
2.3	AIUX15 empennage configurations . . . . .	17
2.4	Cross configuration – Drag coefficient . . . . .	17
2.5	Cross configuration – Lateral force coefficient . . . . .	18
2.6	Cross configuration – Lift coefficient . . . . .	18
2.7	Cross configuration – Rolling moment coefficient . . . . .	19
2.8	Cross configuration – Pitching moment coefficient . . . . .	19
2.9	Cross configuration – Yawing moment coefficient . . . . .	20
2.10	Inverted Y configuration – Drag coefficient . . . . .	20
2.11	Inverted Y configuration – Lateral force coefficient . . . . .	21
2.12	Inverted Y configuration – Lift coefficient . . . . .	21
2.13	Inverted Y configuration – Rolling moment coefficient . . . . .	22
2.14	Inverted Y configuration – Pitching moment coefficient . . . . .	22
2.15	Inverted Y configuration – Yawing moment coefficient . . . . .	23
2.16	Airship control surfaces aerodynamic data. Four-empennage configuration. . . . .	24
2.17	Airship control surfaces aerodynamic data. Three-empennage configuration. . . . .	25
3.1	Reference frame . . . . .	27
3.2	AIUX15 cross configuration-longitudinal response to a 5° elevators step . . . . .	37
3.3	AIUX15 inverted Y configuration-longitudinal response to a 5° elevators step . . . . .	37
3.4	AIUX15 cross configuration-lateral response to a 5° rudders step . . . . .	38
3.5	AIUX15 inverted Y configuration-lateral response to a 5° rudder step . . . . .	39
4.1	Reference frame with origin in the $CG$ . . . . .	41
4.2	Airship 3DoF implemented Matlab/Simulink model . . . . .	42
4.3	Airship longitudinal response to 10° elevator step . . . . .	43
4.4	Airship longitudinal response to +5° –5° elevator input . . . . .	44
4.5	Airship longitudinal response to 10% thrust increase . . . . .	44

4.6	Airship longitudinal response to 10 % thrust increase with $\mu = 45^\circ$	45
4.7	Case 1: Axial Forces	46
4.8	Case 1: Normal Forces	47
4.9	Case 1: Pitching Moments	48
4.10	Case 2: Axial Forces	48
4.11	Case 2: Normal Force	49
4.12	Case 2: Pitching Moments	49
4.13	Case 3: Axial Forces	50
4.14	Case 3: Normal Force	50
4.15	Case 3: Pitching Moments	51
4.16	Case 4: Axial Forces	51
4.17	Case 4: Normal Force	52
4.18	Case 4: Pitching Moments	52
4.19	Neutral buoyancy condition: model responses comparison	53
4.20	Non-neutral buoyancy condition: model responses comparison	53
5.1	6DoF implemented Simulink model	58
5.2	6DoF aerodynamic subsystem	59
5.3	6DoF gravitational subsystem	59
5.4	6DoF propulsive subsystem	60
5.5	6DoF added mass subsystem	60
5.6	6DoF implemented model responses – velocity in the body-fixed frame	61
5.7	6DoF implemented model responses – angular rates in body-fixed axes	62
5.8	6DoF implemented model responses – Euler rotation angles	63
5.9	6DoF implemented model responses – position in inertial axes	64
5.10	6DoF implemented model responses – incidence, airspeed and $f_{tail}$	65
6.1	Block diagram of the linear system with state feedback.	67
6.2	simulink roll response with feedback control to an initial rudder step of $25^\circ$	68
6.3	rudder input with feedback control, from the initial step of $25^\circ$	69
6.4	simulink roll response with feedback control to an initial rudder step of $15^\circ$ , aileron case	69
6.5	aileron deflection after and before the saturation block	70
6.6	Cross configuration lateral responses without and with control	70
6.7	Inverted Y configuration lateral responses without and with control	71
7.1	Block diagram of the linear system with turbulence and state feedback.	73
7.2	Matlab/Simulink 6Dof airship model with turbulence control, pole placement method.	74
7.3	Cross configuration lateral responses in turbulence.	75
7.4	Inverted Y configuration lateral responses in turbulence.	76
7.5	root locus analysis, cross configuration	77
7.6	root locus analysis, inverted Y configuration	78
7.7	Matlab/Simulink 6Dof airship model with turbulence optimal control method.	78
7.8	Optimal control responses in turbulence, cross configuration	79

7.9	Optimal control responses in turbulence, inverted Y configuration	79
7.10	Surface deflections efforts in turbulence atmosphere. . . . .	80
8.1	The towing tank of the DIN . . . . .	82
8.2	Cross flexure pivot . . . . .	84
8.3	Voice coil actuator . . . . .	85

# List of Tables

2.1	AIUX15 main characteristics . . . . .	16
2.2	AIUX15 main aerodynamic data . . . . .	16
3.1	AIUX15 trim conditions . . . . .	35
3.2	AIUX15 cross configuration-stability results . . . . .	36
3.3	AIUX15 inverted Y configuration-stability results . . . . .	38
6.1	Control characteristics and controller gains . . . . .	67
7.1	Controller gains with turbulence . . . . .	73
7.2	LQR controller gains with $\alpha = 1.1$ . . . . .	77
8.1	Towing tank characteristics . . . . .	81
8.2	Airship model characteristics . . . . .	83
8.3	Frequency comparison . . . . .	84
8.4	Cross flexure pivot main dimensions . . . . .	85

# Nomenclature

$a_x, a_y, a_z$	= airship center of gravity coordinates with respect to center of volume in body frame
$b_x, b_y, b_z$	= airship center of buoyancy coordinates with respect to center of volume in body frame
$c$	= $\nabla^{1/3}$ airship reference length
$d_x, d_y, d_z$	= thrust application point coordinates with respect to center of volume in body frame
$f_{\text{tail}}$	= tail enhanced authority factor due to propeller wash
$\mathbf{k}$	= gain vector in steady atmosphere
$\mathbf{k}_p$	= gain matrix in steady atmosphere
$\mathcal{L}, \mathcal{M}, \mathcal{N}$	= rolling, pitching, and yawing moments
$m$	= airship mass
$p, q, r$	= airship angular velocities
$\dot{p}, \dot{q}, \dot{r}$	= airship angular accelerations
$x_n$	= noise vector
$\mathbf{A}$	= plant matrix
$\mathbf{B}$	= control matrix
$\mathbf{F}$	= noise coefficient matrix
$D, Y, L$	= aerodynamic forces, in wind axes
$\mathbf{K}$	= gain vector in turbulent atmosphere
$\mathbf{K}_p$	= gain matrix in turbulent atmosphere
$\mathbf{K}_{p\alpha}$	= optimal control gain matrix
$L_u, L_v, L_w$	= turbulence scale lengths
$S$	= $\nabla^{2/3}$ airship reference surface
$S_{\text{prop}}$	= propeller section
$T$	= total propeller thrust
$U, V, W$	= airship linear velocities
$V_a$	= airspeed
$\dot{X}_{\dot{U}}, \dot{X}_{\dot{q}}, \dot{Y}_{\dot{V}}, \dot{Y}_{\dot{p}}, \dot{Z}_{\dot{W}}, \dot{Z}_{\dot{q}}, \dot{\mathcal{L}}_{\dot{p}}, \dot{\mathcal{L}}_{\dot{V}}, \dot{\mathcal{L}}_{\dot{r}}, \dot{\mathcal{M}}_{\dot{U}}, \dot{\mathcal{M}}_{\dot{q}}, \dot{\mathcal{M}}_{\dot{W}}, \dot{\mathcal{N}}_{\dot{r}}, \dot{\mathcal{N}}_{\dot{V}}, \dot{\mathcal{N}}_{\dot{p}}$	= added mass coefficients
$\ddot{U}, \ddot{V}, \ddot{W}$	= airship linear accelerations
$X, Y, Z$	= force components in body axes
$\alpha$	= exponential decay rate
$\delta_a, \delta_e, \delta_r$	= aileron, elevator, and rudder deflection angles
$\mu$	= thrust angle
$\nabla$	= airship volume
$\phi, \theta, \psi$	= roll, pitch, and yaw angles
$\rho$	= air density at sea level

$\omega$	= turbulence circular frequency
$\Delta D, \Delta Y, \Delta L$	= aerodynamic force variations, in wind axes, due to the control surface deflections
$\Delta \mathcal{L}, \Delta \mathcal{M}, \Delta \mathcal{N}$	= aerodynamic moment variations, in wind axes, due to the control surface deflections
$\Phi_u, \Phi_v, \Phi_w$	= turbulence velocity spectra
$\Phi_p, \Phi_q, \Phi_r$	= turbulence angular rate spectra

# Chapter 1

## Introduction

### 1.1 Airship history and the Italian heritage

THE airships are aerospace vehicles that get most of their lifting capability from aerostatic or buoyant lift, using gases which are lighter than air. They were widely used in the first half of the 20th century, for a variety of purposes. During this period the airships were employed for military applications by the US Army performing search and patrol operations.

In 1921 the US Army acquired the Italian semi-rigid airship “Roma”, the largest semi-rigid airship in the world. After its crash in 1922, the US started to use helium instead of hydrogen as the lifting gas.

Another important Italian airship in the history was the semi-rigid airship “Norge” (see Figure 1.1) that carried out what many consider the first verified overflight of the North Pole on May 12, 1926. Norge was the first N class semi-rigid airship, designed by Umberto Nobile, and it was the first Italian airship to be provided with a four empennages cruciform tail (“cross” configuration).

Airships were also used for commercial passenger-carrying. For example the “Akron” airship in 1931 could carry 270 persons and 5 fighters for a distance of 16 000 km.

The German rigid airship “Hindenburg” (see Figure 1.2), by the Zeppelin Company, was the longest class of flying machine and the largest airship by envelope volume, for passenger transatlantic transportation, filled with hydrogen. It was characterized by a length of about 245 m, an envelope volume of 200 000 m<sup>3</sup> and a maximum speed of 140 km/h. The Hindenburg disaster took place in 1937 and was the subject of spectacular newsreel coverage and photographs, destroying the idea of airship safety. This event represented the end of the huge rigid airship time. However during and after the second world war the US Navy continued to use the airships for military purposes: at first as a weapon against the submarines and later for the “early warning” radar system (the radars were collocated inside the airship envelope in order to be protected by the weather, to be hidden and to reduce the drag).

Although airships were no longer used for passenger transportation, they continued to be used for other tasks such as advertising and sightseeing.

In the last years, the widespread concerns about climate change, the ef-



Figure 1.1: The Norge Airship

fects of economic and political turmoil on the price of petroleum and the need for security organizations to maintain persistent surveillance in a cost-effective manner, were causing a fundamental reassessment of the utility of airships. A number of organizations are now beginning to explore the use of LTA vehicles for different roles in today's society.

## 1.2 Airship classification

The airships have been conventionally classified into three different types based upon their physical structure: “rigid airships”, “non-rigid airships” and “semi-rigid airships”. More recently, there have been further proposals to construct vehicles which derive most of their lift from aerostatic principles, but rely very much upon aerodynamic lift for useful cargo capacity. These innovative vehicle concepts have become known generically as “hybrid airships”.

The rigid airship, such as the Hindenburg (Figure 1.2), contained an internal framework constructed of a lightweight but strong material providing a rigid structure within which were the lifting gas cells, machinery, fuel and living/working space. A separate cover went over the outside of the framework to provide streamlining and weatherproofing. The last rigid airship was dismantled in 1940.

The semi-rigid airship (for an example see the airship in Figure 1.1), consists of a rigid keel, sometimes running the whole length of the ship, suspended below an envelope containing the lifting gas. The keel provides the prime attachment of the gondola. The gondola is the airship's cabin containing the cockpit, engine compartment and facilities for crew, passengers and cargo. The semi-rigid airship maintains its shape mainly by the pressure of the lifting gas



Figure 1.2: The Hindenburg Airship

in the envelope.

The non-rigid airship or blimp, such as the famous advertising Goodyear blimps (see Figure 1.3), in its simplest form is a streamlined envelope, containing the lifting gas, with a gondola suspended below it, with the crew accommodation, propeller and fuel. The envelope is the primary structure containing the helium gas and the ballonets. The ballonets are air bags which regulate the internal pressure, shape and trim: air is squeezed out of the ballonets as the gas expands with increasing altitude and forced back in again as the helium contracts when the airship descends. Most of the airships today used for surveillance tasks are non-rigid ones and unmanned aerial vehicles (UAVs) [1], [3], [10].

### 1.3 Airship characteristics and applications

Nowadays the interest in using airships for several applications is increasing worldwide, due to their advantageous characteristics.

The lift of airships is mainly aerostatic and compared to other aerial vehicles, airships spend most energy moving and compensating wind disturbances, rather than trying to keep themselves on air. For this reason, they need less powerful engines, leading to a lower energy consumption, as well as less noise or vibrations. They possess a long endurance and they can fly at low speeds or even hover. However the airship could reach maximum speeds over 140 km/h.

The deadweight of an airship is strictly linked to its dimensions; greater airship volume means greater cargo capacity. Although the huge dimensions represent a problem in term of construction, maintenance and infrastructure costs they allow the airship to offer a unique service in the transport of bulky cargo. For the passengers instead great spaces would mean comfort.



Figure 1.3: The Goodyear non-rigid Airship

The airship can also operate in areas without airports, thanks to its possibility of a vertical take-off and landing, also aided by thrust vectored propellers. However a relevant problem remains the need of huge infrastructures and hangars for storage and maintenance.

Although they are known especially for their disasters, the airships present high safety standards thanks to the slow degradation in case of failure. Moreover a lot of accidents were caused by the hydrogenous, by which were filled the airships, nowadays substituted by the helium.

Considering these characteristics, airships have a wide spectrum of applications as observation and data acquisition platforms. They can be used in several fields related to biodiversity, ecological and climate research and monitoring.

Inspection oriented applications cover different areas such as mineral and archaeological prospecting, agricultural and livestock studies, crop yield prediction, land use surveys in rural and urban regions, fire detection and also inspection of man-made structures such as pipelines, power transmission lines, dams and roads [33].

With such a wide spectrum of applications, and considering the quest for autonomy, airships present characteristics and competitive costs when compared to other aircrafts, certainly constituting an important option for research, development and also experimental validation in autonomous aerial robotics.

## 1.4 Airship actual projects

The dawn of the 21st century saw a variety of advanced technologies resurrecting the concept of the airships besides their use in advertising and leisure flights. Worldwide companies are starting several projects concerning innovative airship

applications.

The US/LTA conducts remote sensing experiments with airships since 1992. In 2000, SkyKitten maiden flight takes place in Cardiff. The Russian company RosAeroSystem commercializes the Au-30 Patrol Airship series. The Total Pole Airship Project, for instance, aims to measure the thickness of the pack ice layer covering the Arctic Ocean, using one of the series. Two others are used for surveillance of power lines in Russia and one other is scheduled to monitor traffic conditions in Moscow. With a more humanitarian purpose, Mineseeker is an airship-based mine detection system with optical, electro-optical and ground penetrating radar sensors, tested in Kosovo by the United Nations.

In 2009, Lockheed Martin received a DARPA/Air Force contract to build and fly a demonstrator airship and scaled-down ISiS sensor system by 2013. The ISiS airship would use dual-band UHF ground-tracking radar and X-band radar to spot UAVs and cruise missiles. The Army's LEMV (long endurance multintelligence vehicle), being built by Northrop Grumman and the U.K.'s Hybrid Air Vehicles, was fully funded in 2010 to complement the PTDS (persistent threat detection system), a Lockheed Martin-built tethered aerostat, to support coalition forces with long-endurance communications.

Actually the research projects involving unmanned airships are: AURORA, LOTTE and DIVA. Project AURORA [5] [8] [31] – Autonomous Unmanned Remote Monitoring Robotic Airship – focuses on the establishment of the technologies required to substantiate autonomous operation of unmanned robotic airships for environmental monitoring and aerial inspection missions. This includes sensing and processing infrastructures, control and guidance capabilities, and the ability to perform mission, navigation, and sensor deployment planning and execution. Other important researches related to outdoor autonomous airships in the world at this moment are the Lotte Project in Germany [24] [38] [37], regarding also new techniques in evaluating the aerodynamic coefficients. Recently, Project DIVA – *Dirigível Instrumentado para Vigilância Aérea* – has started in Portugal, sharing a partnership with the AURORA Project.

Recently an Italian society “The Airship Italia s.r.l.” is recollecting the old Italian heritage in the airship technology: a project involving an unmanned airship prototype (AIUX15) has been planned; the partnership of the University “Federico II” has led to this research work concerning new stability and control methods and approaches for airship.

## 1.5 State of art

The main objectives of the research work have been focused in this section. The whole study was concentrated to solve several problems on an unmanned airship prototype (that will be introduced in the following chapter) and to provide new tools for airship design. The need to evaluate and improve the airship stability, manoeuvrability and control have represented the basis of the work. Starting from what was already done in literature, at first the research have regarded the standard approaches to the static stability evaluation and the typical control strategies. Then the existing methods have been improved and new approaches have been developed.

### 1.5.1 Airship static stability

Stability and manoeuvrability have always been important aspects of airship design, and they mainly depend on the empennages configuration and on the weight and buoyant lift effects. The design criteria for the elevators and rudders of the conventional aircrafts, referring to the static stability, are not applicable to the airships as they are characterized by positive  $C_{m\alpha}$  and negative  $C_{n\beta}$ .

The most typical and easy airship equilibrium flight condition is characterized by neutral buoyancy ( $B = mg$ ), that allows the airship to flight at zero incidence meaning also the airship's weight could not exceed the buoyant lift. The airship could generate aerodynamic lift in a wide range of incidence, even if characterized by  $C_L$  lower than the conventional aircraft, but assuming that, it is possible to make the airship heavier than the buoyancy. According to this concept, a new method, developed on the based of previous work (detailed in the following), was introduced in this research work, in order to investigate on the effects of the weight on the longitudinal and lateral stability of the airship, taking also in account different empennages configurations.

Instead of previous works, such as [16], [12], and [17], the researched method wants to underline the impact of the weight and of the static lift on the stability of the airships: the analysis of the effects on the equilibrium flight conditions and on the longitudinal stability of an airship, with the weight exceeding the buoyant lift, has been evaluated.

The longitudinal static stability of an airship is ensured by the righting moment due to the buoyant lift that balances the effects of the positive value of the  $C_{m\alpha}$  of the whole body (envelope plus empennages). This is a typical airship characteristic at low angles of attack, because of a poor stability effects of the fins against the envelope instability. In order to estimate the stability of the airship, it was decided to investigate on the behavior of the dynamic system, when is constrained to In this way is possible to take in account all the stability contributions: not only from the  $C_{m\alpha}$ , but also from the aerodynamic damping coefficient  $C_{mq}$  and from the added mass effects.

Other works, such as [15] and [16], had derived and applied the equation of motion of an airship for the neutrally buoyant condition. The mathematical model for the level flight at zero incidence and the equilibrium equations or trim equations were given by *Cook* [15]; the stability of an airship was investigated by *Goineau* [16], applying non-linear methods.

The mathematical model and the trim equations [15], in the research work, have been fitted for the heaviness condition and the linearized longitudinal equations of motion, describing small perturbations about equilibrium condition, have been written in state space form: in this way the stability of the airship has been carried out by the analysis of the eigenvalues of the stability matrix.

A method [17], developed from the geometrical features and the aerodynamic coefficients of the airship, has been applied to define the state space problem, without the application of any non-linear methods [16]. This "method for airship modeling", has been proposed by *Kulczycki* and *Johnson* [17] for the longitudinal stability. Starting from this work, the method has been fitted in order to highlight the weight effects and, moreover, a method for the lateral-directional stability has been proposed. The application of this developed method has also allowed to compare the main characteristics of the "cross" configuration to the "inverted Y" configuration of the prototype airship (detailed in the following

chapter), demonstrating that it is possible to reduce airships empennages with benefits in terms of weight, without relevant effects on stability and control.

### 1.5.2 Airship control

The second part of the research work has regarded the development of airship lateral-directional control laws, both in steady air, both in turbulence. The flight dynamics models (FDM) of a three empennage configuration and a more conventional four empennage configuration for the same airship envelope have been discussed and implemented, based on a six-degrees-of-freedom (6DoF) mathematical model [9], [12], [13]. In all cases, the resulting system—for the airship prototype without ballast and ballonets system, and provided with electric engine—could be considered as an airframe characterized by a fixed center of gravity (CG). Given these assumptions, the developed FDM of the airship presented a body-fixed reference frame having its origin attached to the center of mass and not to the center of volume (CV), which represented the standard practice with ballasted airships [12], [13]. The added mass effects have not been included within the inertia of the airship, that was another standard assumption for the airship FDM, but have been modeled as external forces and moments occurring in accelerated flight. The effects of propulsion on aerodynamics have been introduced by taking into account the increase of tail efficiency due to the propeller arrangement [8].

The main goal has been the achievement of a satisfying roll control system that reduces the airship high-frequency oscillatory motions and the development of a lateral-directional control system in presence of turbulence and gusts. Two different control approaches have been introduced to reduce the rolling motions arising as undesired effect as a consequence of rudder deflections: these are an annoying source of trouble for the video and picture acquisition systems which represent the typical payload of the unmanned airship. The use of the ailerons for the lateral control has been discussed by other works, but only for typical four empennage configurations (AM phd, ALL STEP conDATI, e TESI TEDESCA); furthermore, no author focused the problem on the study of feedback control laws to limit the airship roll and lateral directional motions in turbulence, neither on the comparison of different strategies. For ailerons it means the elevators in the case of the cross configuration, when they are deflected anti-symmetrically. In the case of the inverted Y configuration the ailerons are the movable aerosurfaces placed on the two lower empennages (much like an inverted V-tail).

The control in turbulence has been carried out according to the pole placement with noise method [6] and according to the optimal control with exponential decay of rate technique [14]. The selection of an optimal control design technique has been motivated by the need to reduce the spending of energy required to move the control surfaces. The turbulent atmospheric conditions for the airship have been chosen following the work carried out on the *AURORA* airship [8], [5].

## Chapter 2

# Unmanned Airship AIUX15

### 2.1 The AIUX15 prototype

THE actual airship prototype, the *AIUX15*, represents a little jewel of state-of-the-art technology in this field. This airship is owned and developed by the Italian society “Airship Italia s.r.l.”, the only airship company operating in the Campania region. The actual research projects on this prototype are directed to improve its stability and control in order to meet all the mission requirements regarding research, monitoring operations and also safety and civil protection.

The *AIUX15* (see Figure 2.1) is totally powered by electric engines, with Lithium-ion battery of new generation, specially designed to provide long endurance of about 2 h. It has an autopilot that can enable automatic flight over pre-defined mission profiles. It is equipped with a GPS system that in addition to the automatic navigation will provide georeferenced scientific data.

The airship *AIUX15* has been totally developed and designed according to the modern aerospace techniques and built largely by composite materials. The drive mechanisms are in aerospace alloy materials processed by CNC machines. Electrical and electronic systems have been designed and constructed using high quality aerospace methods and materials. The two main electric engines are coupled with thrust vectored propellers able to rotate in the  $XZ$  plane (see Figure 2.2 of  $180^\circ$ ). In Table 2.1 are reported same quality features of the *AIUX15*.

In November 2009, this prototype was qualitatively tested in flight for about 15 min. The *AIUX15* represents the first airship to be designed and put in flight in the Neapolitan area, after the great experience of Prof. Nobile with his airship “ITALIA” designed and developed at the Aerodynamics Institute of the Engineering University in Naples.

### 2.2 Airship configurations

A picture of the actual *AIUX15* prototype is shown in Figure 2.1 during its first test flight. This airship is characterized by a tail with three empennages, while a former prototype of the same airship, developed in a previous research



Figure 2.1: The AIUX15 prototype

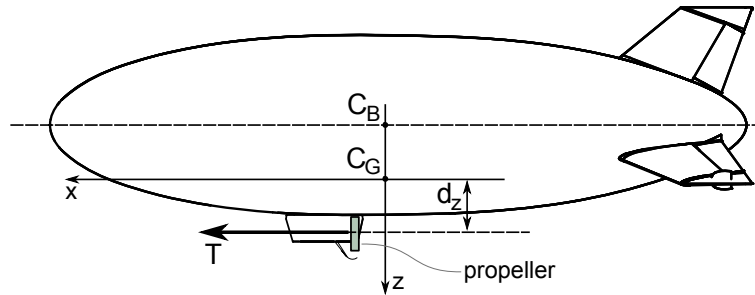


Figure 2.2: The AIUX15 propeller outline

project carried out by the CIRA [2], showed a four empennage configuration.

An engineering analysis and some preliminary tests performed on the prototype brought out the strong influence of the empennages in terms of weight and trim.

One of the purpose of my research was to compare the stability and the control of two different tail arrangement for the same envelope of the *AIUX15*.

In the four empennage configuration—see Figure 2.3(a)— the fins are arranged in a cross-like position; the three empennage configuration —see Figure 2.3(b)— has been obtained with the same fin dimensions of the first configuration, with three empennages placed at  $120^\circ$  and arranged in an inverted Y-like position. While the four empennages configuration represents a more conventional choice against the three empennage tail arrangement, the airship designers were more interested in the latter. The inverted Y configuration offers an improvement in terms of payload of approximately 10% with respect to the cross tail configuration applied to the same envelope.

Table 2.1: AIUX15 main characteristics

Airship		Empennages and Propulsion	
Envelope volume	123.06 m <sup>3</sup>	Fin surface area	3.20 m <sup>2</sup>
Overall length	15.12 m	Control surface area	0.76 m <sup>2</sup>
Max diameter	3.90 m	Vectorable propellers	2 units
Helium purity	0.97	Nominal thrust per unit	45 N
Max Speed	(50 km/h)	Thrust vectoring range	180°/pitch

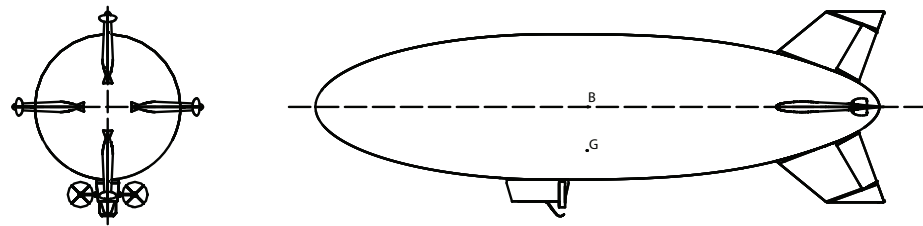
Table 2.2: AIUX15 main aerodynamic data

Item	Name	$C_{L\alpha}$	$C_{M\alpha}$	$C_{Y\beta}$	$C_{\mathcal{L}\beta}$	$C_{N\beta}$
a	Cross +	1.168	0.261	-1.168	0.000	-0.261
b	Inverted Y	0.950	0.659	-0.950	0.000	-0.659

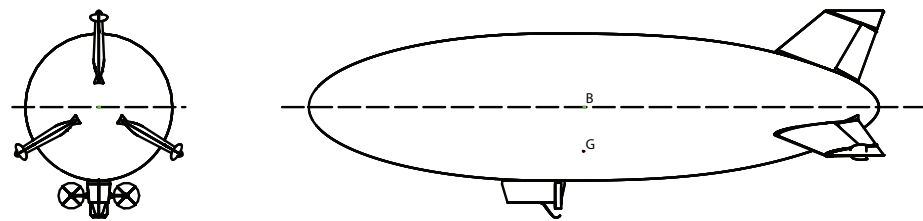
## 2.3 Airship aerodynamic data

The airship aerodynamic database comes from CFD (Computational Fluid Dynamics) analysis. In particular, it is built on the basis of a number of full three-dimensional RANS (Reynolds Averaged Navier-Stokes) computations [2]. This approach is considered more reliable and accurate compared to the available semi-empirical methods [11]. The CFD results have been validated by comparison with the experimental aerodynamic data of a known airship with four empennages.[2] The CFD analysis have been applied first on the cross configuration and then on the inverted Y airship with respect to the wind axis reference frame centered at the CV. The control coefficients have been calculated assuming as parameters the main aero-surface deflections. The obtained aerodynamic data are reported in the following. The terms  $p_n, q_n, r_n$  are the normalized angular velocity for the airship defined as follows in Eq. 2.1, where  $c$  is the airship reference length and  $V$  is the airspeed:

$$p_n = \frac{pc}{2V} \quad q_n = \frac{qc}{2V} \quad r_n = \frac{rc}{2V} \quad (2.1)$$



(a) "Cross" configuration



(b) "Inverted-Y" configuration

Figure 2.3: AIUX15 empennage configurations

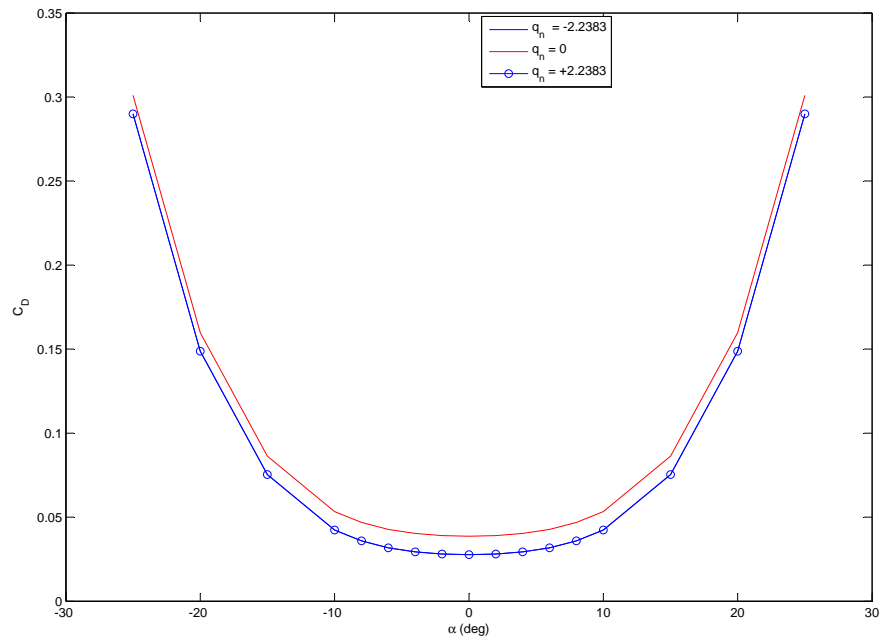


Figure 2.4: Cross configuration – Drag coefficient

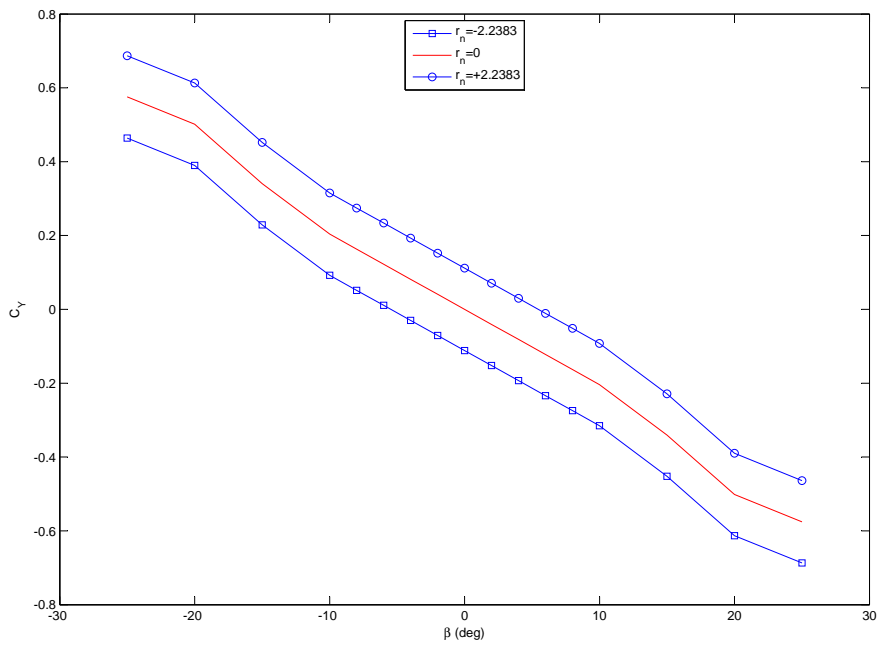


Figure 2.5: Cross configuration – Lateral force coefficient

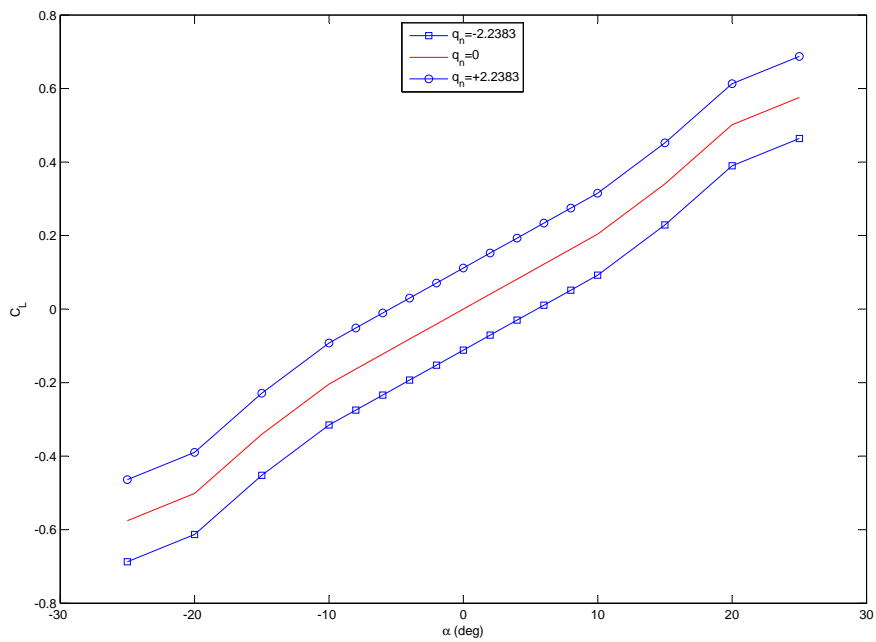


Figure 2.6: Cross configuration – Lift coefficient

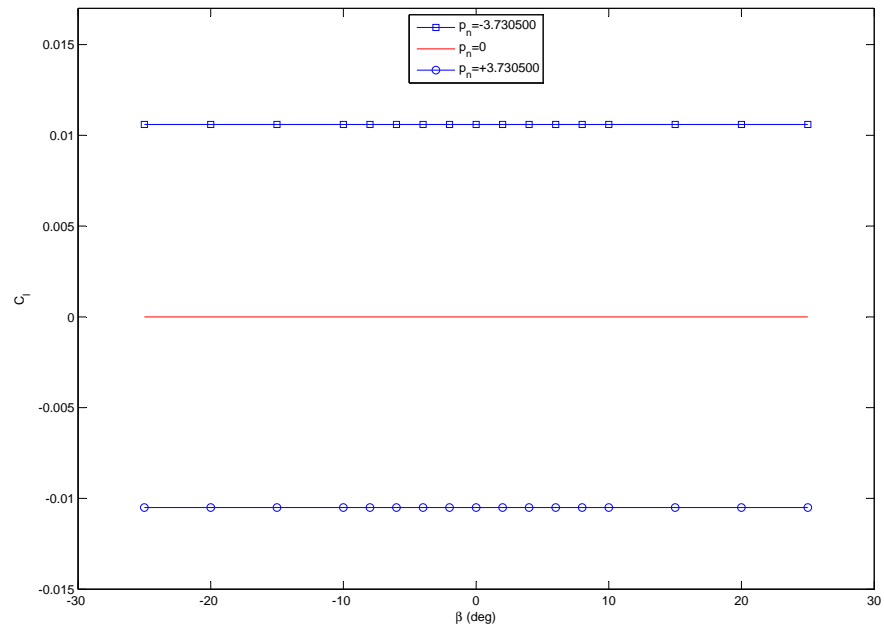


Figure 2.7: Cross configuration – Rolling moment coefficient

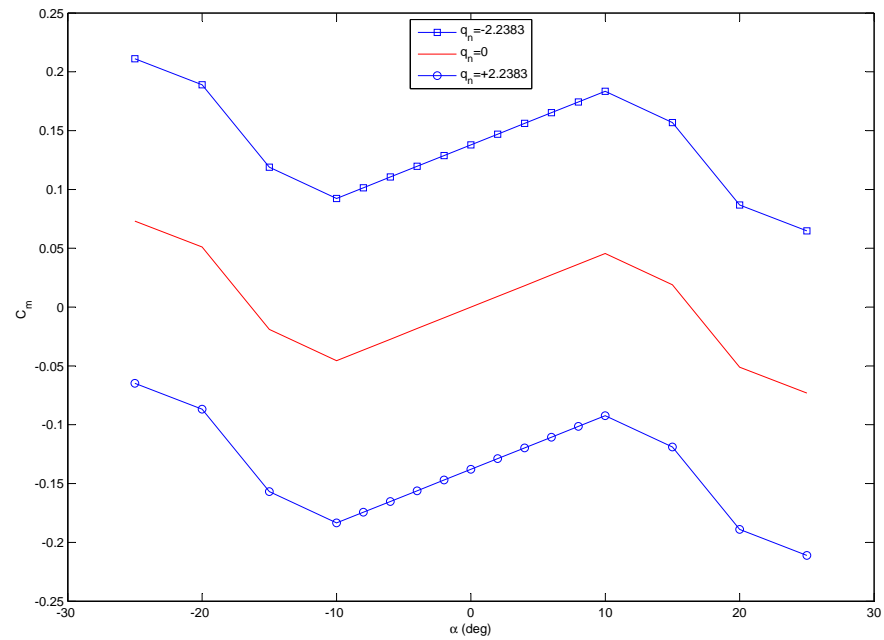


Figure 2.8: Cross configuration – Pitching moment coefficient

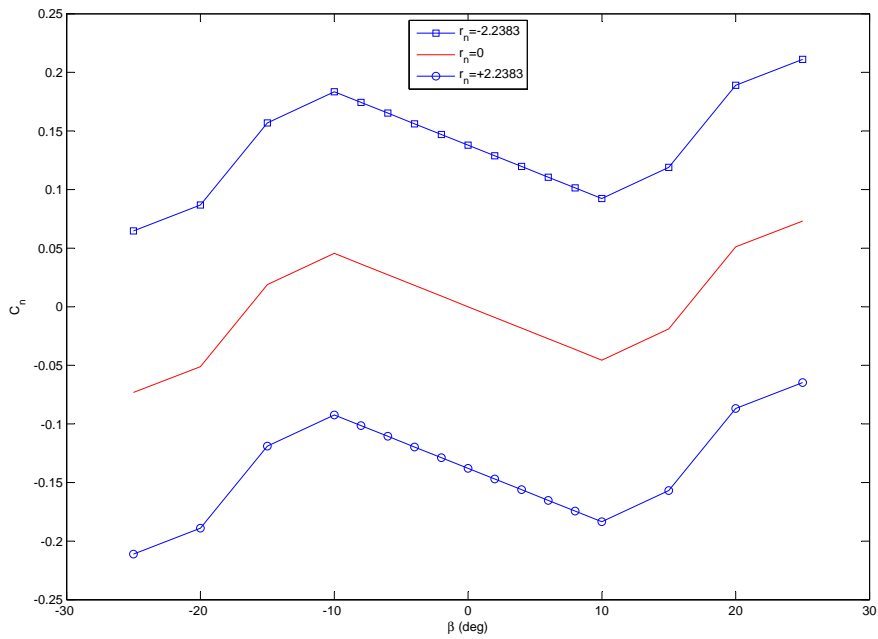


Figure 2.9: Cross configuration – Yawing moment coefficient

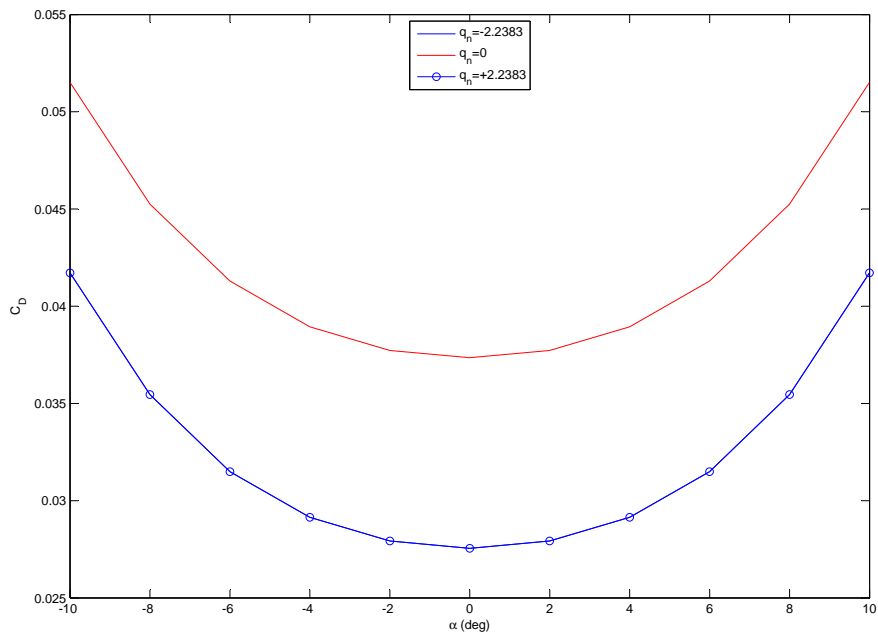


Figure 2.10: Inverted Y configuration – Drag coefficient

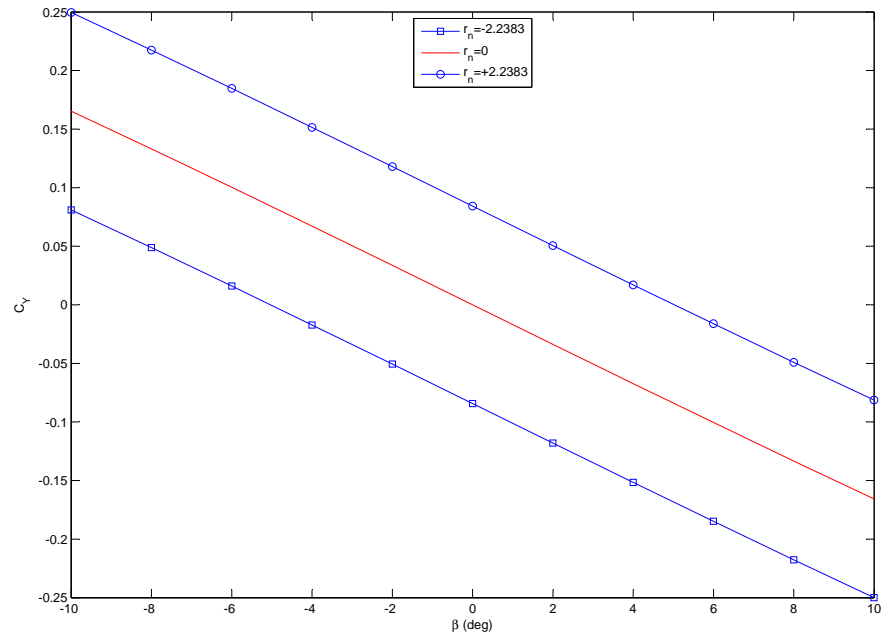


Figure 2.11: Inverted Y configuration – Lateral force coefficient

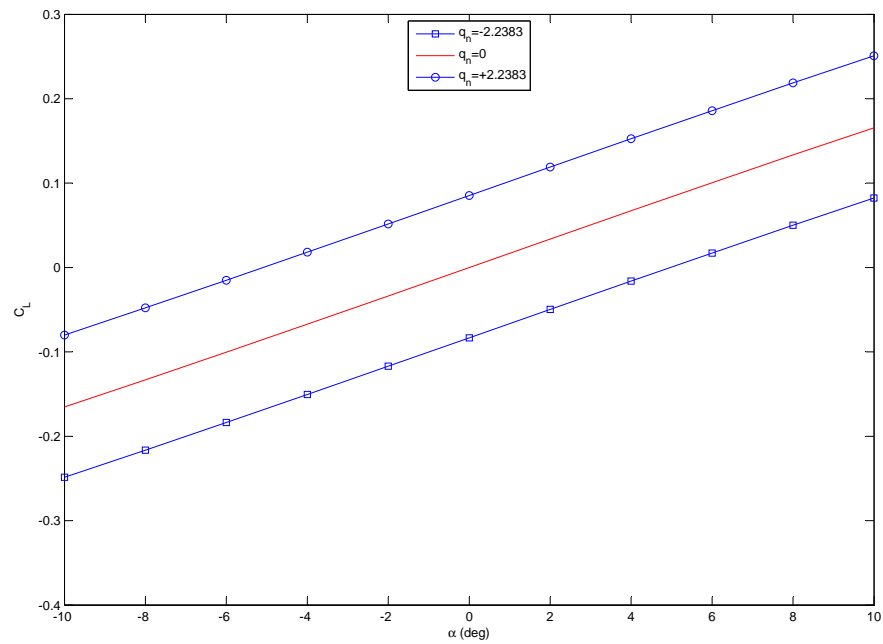


Figure 2.12: Inverted Y configuration – Lift coefficient

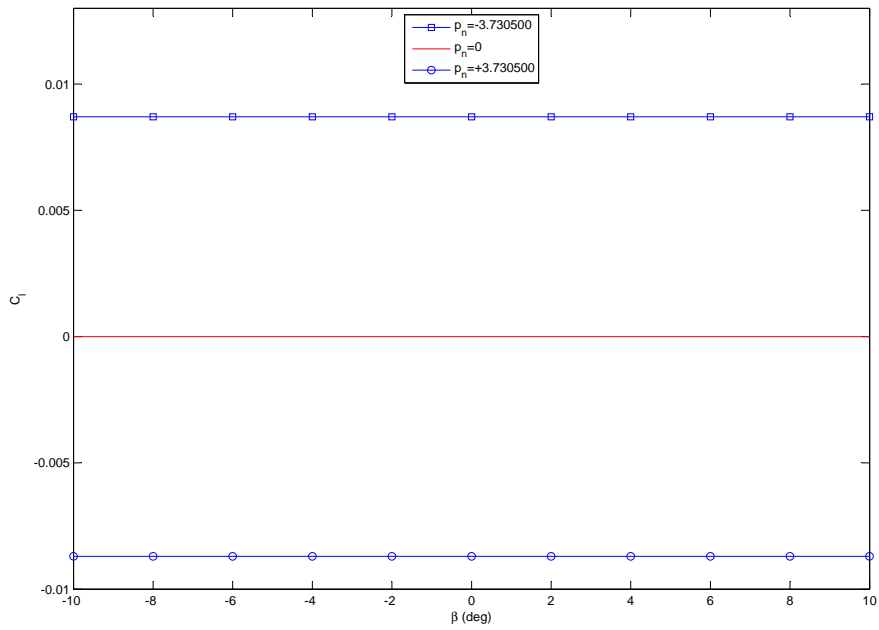


Figure 2.13: Inverted Y configuration – Rolling moment coefficient

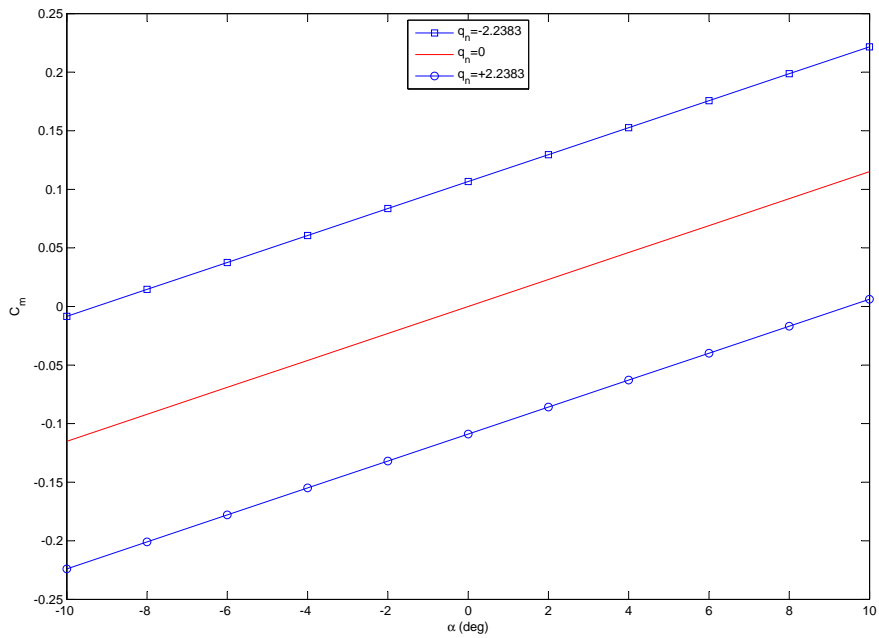


Figure 2.14: Inverted Y configuration – Pitching moment coefficient

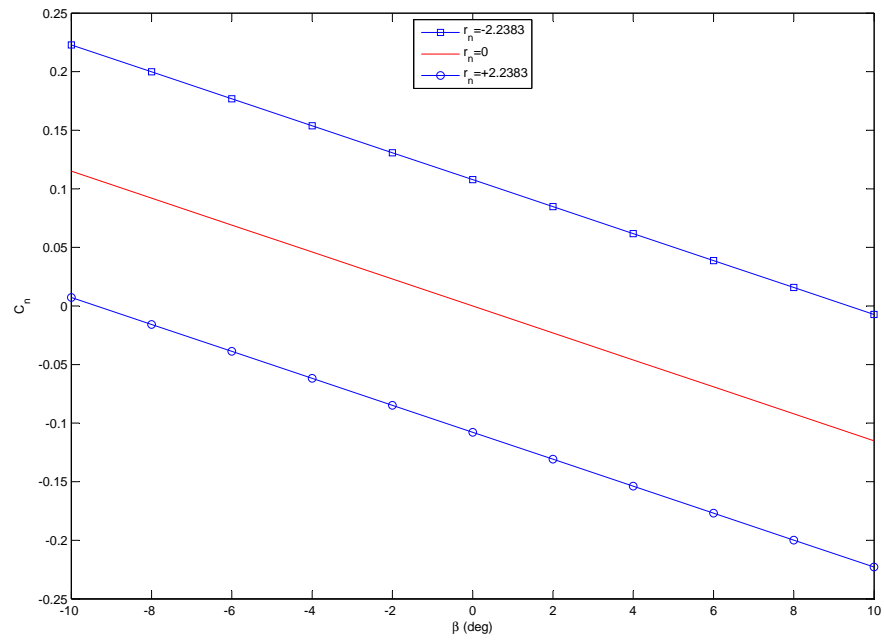
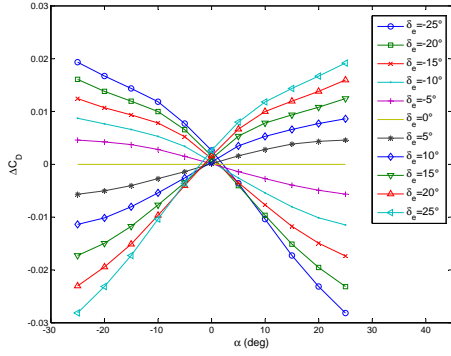
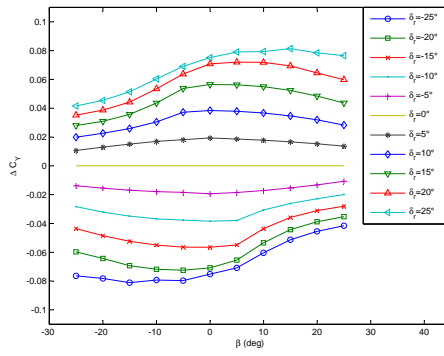


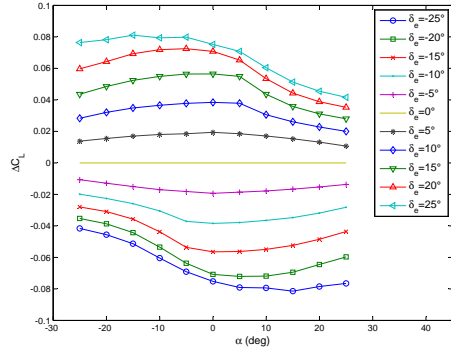
Figure 2.15: Inverted Y configuration – Yawing moment coefficient



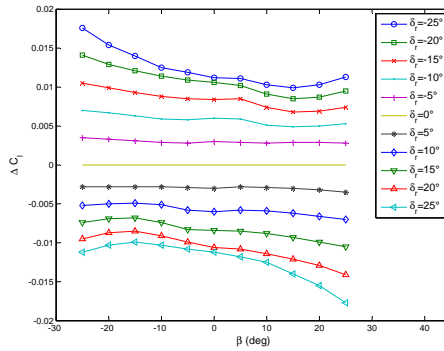
(a) Drag coefficient variation vs. alpha at different elevator deflections



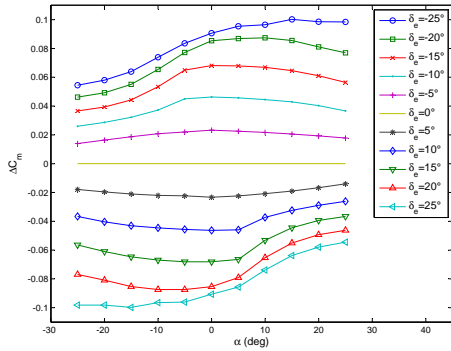
(b) Lateral force coefficient variation vs. beta at different rudder deflections



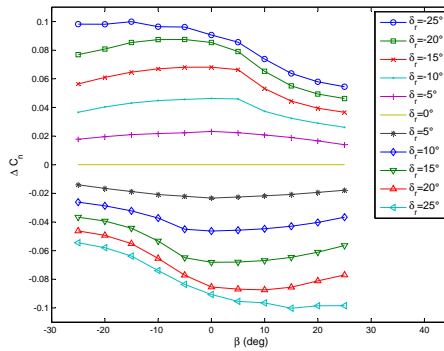
(c) Lift coefficient variation vs. alpha at different elevator deflections



(d) Rolling moment coefficient variation vs. beta at different lower rudder deflections

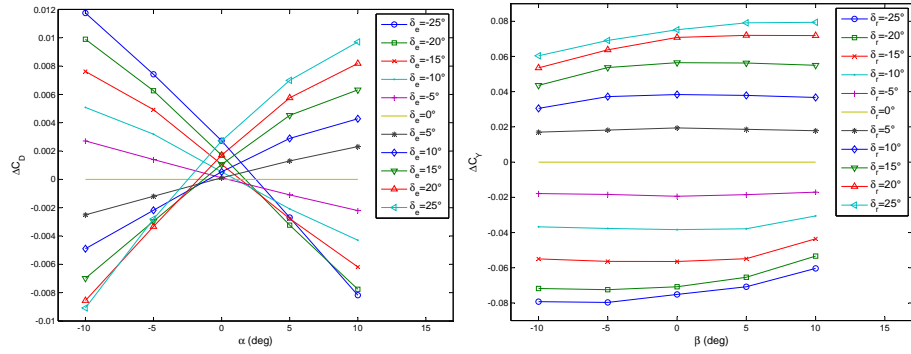


(e) Pitching moment coefficient variation vs. alpha at different elevator deflections

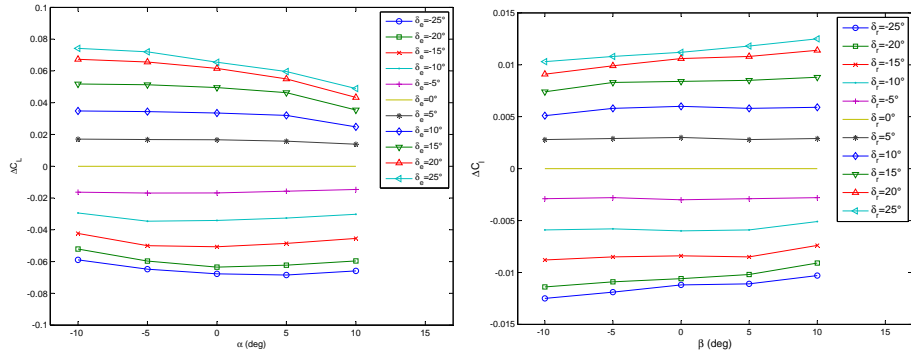


(f) Yawing moment coefficient variation vs. beta at different rudder deflections

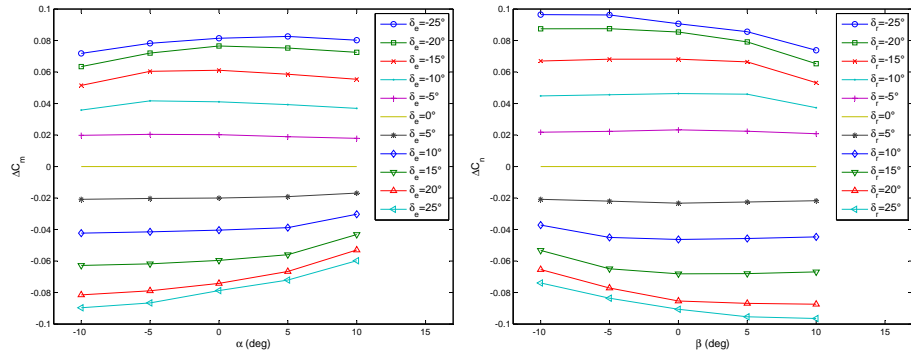
Figure 2.16: Airship control surfaces aerodynamic data. Four-empennage configuration.



(a) Drag coefficient variation vs. alpha at different elevator deflections (b) Lateral force coefficient variation vs. beta at different rudder deflections



(c) Lift coefficient variation vs. alpha at different elevator deflections (d) Rolling moment coefficient variation vs. beta at different lower rudder deflections



(e) Pitching moment coefficient variation vs. alpha at different elevator deflections (f) Yawing moment coefficient variation vs. beta at different rudder deflections

Figure 2.17: Airship control surfaces aerodynamic data. Three-empennage configuration.

## Chapter 3

# Linear Airship Model

### 3.1 General equation of motion

ANY scientific investigation on the stability and control requires a mathematical model built around the equations of motion. The airship mathematical model is based on a 6-DOF dynamic model. At first, the equations of motion of the airship have been developed on the basis of the standard following assumption:

- the airship mass remains constant;
- the airship is seen as a rigid body, meaning there are no aero-elastic effects;
- the airship is symmetric respect to the longitudinal plan, to which belong the airship centers of gravity and buoyancy;
- the airship is provided with control surfaces and two independent thrust vectored propellers;
- the airship equilibrium flight is rectilinear;
- there are no turbulence effects and the steady air model is assumed.

The body axes (see Figure 3.1) are conventionally centered at the airship  $C_V$  that represents a fixed point for the system. Assuming the symmetry of the problem, the center of gravity and the center of buoyancy will have  $a_y = b_y = 0$  and also the products of inertia will be  $I_{xy} = I_{yz} = 0$ .

In the following, under the above mentioned assumptions, the general dynamic equations of the airship 3.1 will be written; then the linearized equations of motion will be developed.

$$\begin{aligned}\frac{d\vec{Q}}{dt} &= \sum F_{est}^{\vec{}} \\ \frac{d\vec{K}_o}{dt} &= \sum M_{est}^{\vec{}}\end{aligned}\tag{3.1}$$

In addition to the usual aerodynamic terms the equations of motion of the airship will also include significant force and moment terms due to the static

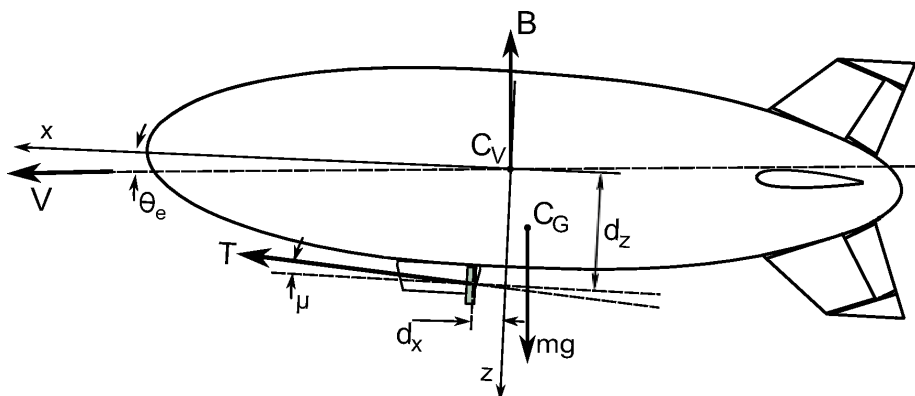


Figure 3.1: Reference frame

buoyancy and inertial terms due to the added mass of air displaced by the airship in acceleration. This mass of air gives rise to virtual mass and inertia effects, that are formally expressed as equivalent aerodynamic acceleration derivatives. The added mass and the added moments of inertia are introduced by the following expressions:

$$\begin{aligned}
 m_x &= m - \frac{\partial X}{\partial \dot{U}} = m - \dot{X}_{\dot{U}} & J_x &= I_x - \frac{\partial \mathcal{L}}{\partial \dot{p}} = m - \dot{\mathcal{L}}_{\dot{p}} \\
 m_y &= m - \frac{\partial Y}{\partial \dot{V}} = m - \dot{Y}_{\dot{V}} & J_y &= I_y - \frac{\partial \mathcal{M}}{\partial \dot{q}} = m - \dot{\mathcal{M}}_{\dot{q}} \\
 m_z &= m - \frac{\partial Z}{\partial \dot{W}} = m - \dot{Z}_{\dot{W}} & J_z &= I_z - \frac{\partial \mathcal{N}}{\partial \dot{r}} = m - \dot{\mathcal{N}}_{\dot{r}}
 \end{aligned} \tag{3.2}$$

In the following equations are defined the added products of inertia:

$$\begin{aligned}
 J_{xz} &= I_{xz} + \dot{\mathcal{L}}_{\dot{r}} = I_{xz} + \dot{\mathcal{N}}_{\dot{p}} \\
 J_{yz} &= I_{yz} + \dot{\mathcal{M}}_{\dot{r}} = I_{yz} + \dot{\mathcal{N}}_{\dot{q}} \\
 J_{xy} &= I_{xy} + \dot{\mathcal{L}}_{\dot{q}} = I_{xy} + \dot{\mathcal{M}}_{\dot{p}}
 \end{aligned} \tag{3.3}$$

According to the assumptions done before, the components of the momentum derivative  $\frac{d\tilde{Q}}{dt}$  have been written as follows:

1. axial component

$$m_x \dot{U} + (ma_z - \dot{X}_{\dot{q}})\dot{q} - m_y r V + m_z W q - (r^2 + q^2)a_x m + ma_z p r$$

2. lateral component

$$m_y \dot{V} + m_x U r - m_z p W - (ma_z + \dot{Y}_{\dot{p}})\dot{p} + (ma_x + \dot{Y}_{\dot{r}})\dot{r} + ma_x q p + ma_z q r$$

3. vertical component

$$m_z \dot{W} - (ma_x + \dot{Z}_{\dot{q}})\dot{q} + m_y p V + m_x U q - (p^2 + q^2)ma_z + ma_x p r$$

where:

$$\begin{aligned} \dot{X}_{\dot{q}} &= \frac{\partial X}{\partial \dot{q}}; & \dot{W}_{\dot{q}} &= \frac{\partial W}{\partial \dot{q}} \\ \dot{Y}_{\dot{p}} &= \frac{\partial Y}{\partial \dot{p}}; & \dot{Y}_{\dot{r}} &= \frac{\partial Y}{\partial \dot{r}} \end{aligned} \quad (3.4)$$

The angular momentum derivative components  $\frac{d\vec{K}_o}{dt}$  have been obtained assuming as pole the center of volume:

1. roll

$$J_x \dot{p} - J_{xz}(\dot{r} + pq) - (ma_z + \dot{\mathcal{L}}_{\dot{V}})\dot{V} - ma_z rU + ma_z Wp + rq(J_z - J_y)$$

2. pitch

$$J_y \dot{q} - (ma_x + \dot{\mathcal{M}}_{\dot{W}})\dot{W} - ma_x(Vp - Uq) + (ma_z + \dot{\mathcal{M}}_{\dot{U}})\dot{U} - ma_z(Vr - Wq) + pr(J_x - J_z) + J_{xz}(p^2 - r^2)$$

3. yaw

$$J_z \dot{r} + J_{xz}(rq - \dot{p}) + (ma_x - \dot{\mathcal{N}}_{\dot{V}})\dot{V} - ma_x(rU - pW) + pq(J_y - J_x)$$

In the above equation figure the following virtual mass terms:

$$\begin{aligned} \dot{\mathcal{L}}_{\dot{V}} &= \frac{\partial \mathcal{L}}{\partial \dot{V}}; & \dot{\mathcal{N}}_{\dot{V}} &= \frac{\partial \mathcal{N}}{\partial \dot{V}} \\ \dot{\mathcal{M}}_{\dot{W}} &= \frac{\partial \mathcal{M}}{\partial \dot{W}}; & \dot{\mathcal{M}}_{\dot{U}} &= \frac{\partial \mathcal{M}}{\partial \dot{U}} \end{aligned} \quad (3.5)$$

On the airship, in addition to the inertial generalized force, the aerodynamic, the control surfaces the gravitational and the propulsive forces and moments act. In the dynamic vector  $\mathbf{F}_d$  figure the terms obtained from the derivation of the momentum and of the angular momentum [3.1](#).

$$M \begin{bmatrix} \dot{U} \\ \dot{V} \\ \dot{W} \\ \dot{p} \\ \dot{q} \\ \dot{r} \end{bmatrix} = \mathbf{F}_d(U, V, W, p, q, r) + \mathbf{A}(U, V, W, p, q, r) + \mathbf{G}(\lambda_{13}, \lambda_{23}, \lambda_{33}) + \mathbf{C} + \mathbf{P} \quad (3.6)$$

The aerodynamic generalized force have been introduced as functions of the dimensional aerodynamic derivatives in the following  $6 \times 1$  vector, taking in account only the significative values (descending from the assumption of independence between longitudinal and lateral motion:

$$\mathbf{A} = \begin{bmatrix} X_a \\ Y_a \\ Z_a \\ \mathcal{L}_a \\ \mathcal{M}_a \\ \mathcal{N}_a \end{bmatrix} = \begin{bmatrix} \dot{X}_U U + \dot{X}_W W + \dot{X}_q q \\ \dot{Y}_V V + \dot{Y}_p p + \dot{Y}_r r \\ \dot{Z}_U U + \dot{Z}_W W + \dot{Z}_q q \\ \dot{\mathcal{L}}_V V + \dot{\mathcal{L}}_p p + \dot{\mathcal{L}}_r r \\ \dot{\mathcal{M}}_U U + \dot{\mathcal{M}}_W W + \dot{\mathcal{M}}_q q \\ \dot{\mathcal{N}}_V V + \dot{\mathcal{N}}_p p + \dot{\mathcal{N}}_r r \end{bmatrix} \quad (3.7)$$

In the same way have been also reported the control generalized force:

$$\mathbf{C} = \begin{bmatrix} X_c \\ Y_c \\ Z_c \\ \mathcal{L}_c \\ \mathcal{M}_c \\ \mathcal{N}_c \end{bmatrix} = \begin{bmatrix} \dot{X}_\delta \delta_e \\ \dot{Y}_\delta \delta_r \\ \dot{Z}_\delta \delta_e \\ \dot{\mathcal{L}}_\delta \delta_r \\ \dot{\mathcal{M}}_\delta \delta_e \\ \dot{\mathcal{N}}_\delta \delta_r \end{bmatrix} \quad (3.8)$$

The gravitational generalized force include the weight and the buoyant lift actions, as defined in the following  $6 \times 1$  vector:

$$\mathbf{G}(\lambda_{13}, \lambda_{23}, \lambda_{33}) = \begin{bmatrix} \lambda_{13}(mg - B) \\ \lambda_{23}(mg - B) \\ \lambda_{33}(mg - B) \\ -\lambda_{23}(mga_z + Bb_z) \\ -\lambda_{33}(mga_x + Bb_x) + \lambda_{13}(mga_z + Bb_z) \\ \lambda_{23}(mga_x + Bb_x) \end{bmatrix} \quad (3.9)$$

To describe the orientation of the airship as rigid body, the Euler angles  $\phi, \theta, \psi$  have been introduced. According to this assumption the directional cosine can be written as follows:

$$\begin{aligned} \lambda_{13} &= -\sin \theta \\ \lambda_{23} &= \sin \phi \cos \theta \\ \lambda_{33} &= \cos \phi \cos \theta \end{aligned} \quad (3.10)$$

The propulsive actions have been introduced in the following  $6 \times 1$  assuming two independent thrust vectored propellers:

$$\mathbf{P} = \begin{bmatrix} X_p \\ Y_p \\ Z_p \\ \mathcal{L}_p \\ \mathcal{M}_p \\ \mathcal{N}_p \end{bmatrix} = \begin{bmatrix} T_s \cos \mu_s + T_p \cos \mu_p \\ 0 \\ -T_s \sin \mu_s - T_p \sin \mu_p \\ (T_p \sin \mu_p - T_s \sin \mu_s)d_y \\ T_p(d_z \cos \mu_p - d_x \sin \mu_p) + T_s(d_z \cos \mu_s - d_x \sin \mu_s) \\ (T_p \cos \mu_p - T_s \cos \mu_s)d_y \end{bmatrix} \quad (3.11)$$

## 3.2 Linearized airship model

In order to linearize the general model and to further simplify the equations, the following assumptions have been introduced:

- the small perturbation theory is applied, that allows decoupling the longitudinal and the lateral-directional problem;

- the velocity components are defined as:

$$\begin{aligned} U &= u + U_e & \phi &= \Phi + \phi_e \\ V &= v + V_e & \theta &= \Theta + \theta_e \\ W &= w + W_e & \psi &= \Psi + \psi_e \end{aligned} \quad (3.12)$$

where  $U_e, V_e, W_e, \phi_e, \theta_e, \psi_e$  are the trim value and the terms  $u, v, w, \Phi, \Theta, \Psi$  represent the perturbations from the initial equilibrium condition. Regarding to the assumption of rectilinear flight, the term  $V_e$  will be zero. The total air speed is then defined as  $V_a = \sqrt{(U^2 + V^2 + W^2)}$ ;

- the director cosine vector can be expressed as:

$$\begin{bmatrix} \lambda_{13} \\ \lambda_{23} \\ \lambda_{33} \end{bmatrix} = \begin{bmatrix} -\Theta \cos \theta_e - \sin \theta_e \\ \Phi \cos \theta_e \\ -\Theta \sin \theta_e + \cos \theta_e \end{bmatrix} \quad (3.13)$$

- the two propellers have been assumed to be “dependent” that means having  $T_s = T_p = T$  and  $\mu_s = \mu_p = \mu$ ;
- the control surface deflections are null at the initial equilibrium condition.

### 3.2.1 Longitudinal equations

The linearized longitudinal equations of motions for an airship are reported in the following:

$$\begin{aligned} m_x \dot{u} + (ma_z - \dot{X}_q) \dot{q} &= X_e - m_z W_e q + \dot{X}_u u + \dot{X}_w w + \dot{X}_q q + \dot{X}_\delta (\delta_e + \delta_r) + \\ &\quad + T_s \cos \mu_s + T_p \cos \mu_p - (mg - B) (\sin \theta_e + \Theta \cos \theta_e) \\ m_z \dot{w} - (ma_x - \dot{Z}_q) \dot{q} &= Z_e + m_x U_e q + \dot{Z}_u u + \dot{Z}_w w + \dot{Z}_q q + \dot{Z}_\delta \delta_e + \\ &\quad - T_s \sin \mu_s - T_p \sin \mu_p + (mg - B) (\cos \theta_e - \Theta \sin \theta_e) \\ J_y \dot{q} - (ma_x - \dot{M}_w) \dot{w} + (ma_z - \dot{M}_u) \dot{u} &= \mathcal{M}_e - (ma_x U_e + ma_z W_e) q + \dot{M}_u u + \\ &\quad \dot{M}_w w + \dot{M}_q q + \dot{M}_\delta \delta_e + T_s (d_z \cos \mu_s - d_x \sin \mu_s) + T_p (d_z \cos \mu_p - d_x \sin \mu_p) + \\ &\quad + (mga_x + Bb_x) (\theta_e \sin \theta_e - \cos \theta_e) - (mga_z + Bb_z) (\sin \theta_e + \Theta \cos \theta_e) \end{aligned} \quad (3.14)$$

To further simplify the longitudinal equations, trim conditions can be applied. Trim conditions assume that the airship is in equilibrium, causing all perturbation variables to reduce to zero. This assumption results in the following equations:

$$\begin{cases} X_e + T_s \cos \mu_s + T_p \cos \mu_p - (mg - B) \sin \theta_e & = 0 \\ Z_e - T_s \sin \mu_s - T_p \sin \mu_p + (mg - B) \cos \theta_e & = 0 \\ \mathcal{M}_e + T_p (d_z \cos \mu_p - d_x \sin \mu_p) + T_s (d_z \cos \mu_s - d_x \sin \mu_s) + \\ \quad - (mga_z + Bb_z) \sin \theta_e - (mga_x + Bb_x) \cos \theta_e & = 0 \end{cases} \quad (3.15)$$

The linearized longitudinal problem is written below in state space form:

$$\underset{(4 \times 4)(4 \times 1)}{\mathbf{M}} \dot{\mathbf{x}} = \underset{(4 \times 4)(4 \times 1)}{\mathbf{A}} \mathbf{x} + \underset{(4 \times 1)}{\mathbf{B}} u \quad (3.16)$$

that divided for the mass matrix becomes:

$$\dot{\mathbf{x}} = \underset{(4 \times 4)(4 \times 1)}{\mathbf{a}} \mathbf{x} + \underset{(4 \times 1)}{\mathbf{b}} u \quad (3.17)$$

where  $\mathbf{x}^T = [x, z, q, \Theta]$  is the state vector, and  $u = \delta_e$

$$M = \begin{bmatrix} m_x & 0 & (ma_z - \dot{X}_{\dot{q}}) & 0 \\ 0 & m_z & -(ma_x + \dot{Z}_{\dot{q}}) & 0 \\ (ma_z - \dot{\mathcal{M}}_{\dot{u}}) & -(ma_x + \dot{\mathcal{M}}_{\dot{w}}) & J_y & 0 \\ 0 & 0 & 0 & 1 \end{bmatrix} B = \begin{bmatrix} \dot{X}_{\delta} \\ \dot{Z}_{\delta} \\ \dot{\mathcal{M}}_{\delta} \\ 0 \end{bmatrix}$$

$$A = \begin{bmatrix} \dot{X}_{\dot{u}} & \dot{X}_{\dot{w}} & (\dot{X}_{\dot{q}} - m_z W_e) & -(mg - B) \cos \theta_e \\ \dot{Z}_{\dot{u}} & \dot{Z}_{\dot{w}} & (\dot{Z}_{\dot{q}} + m_x U_e) & -(mg - B) \sin \theta_e \\ \dot{\mathcal{M}}_{\dot{u}} & \dot{\mathcal{M}}_{\dot{w}} & (\dot{\mathcal{M}}_{\dot{q}} - m_x U_e + m_z W_e) & \left\{ \begin{array}{l} (mga_x + Bb_x) \sin \theta_e + \\ -(mga_z - Bb_z) \cos \theta_e \end{array} \right\} \\ 0 & 0 & 1 & 0 \end{bmatrix}$$

### 3.2.2 Lateral-directional equations

The linearized lateral-directional equations of motion for an airship have been developed, resulting in the following equations:

$$\begin{aligned} m_y \dot{v} - (ma_z + \dot{Y}_{\dot{p}}) \dot{p} + (ma_x - \dot{Y}_{\dot{r}}) \dot{r} &= Y_e + \dot{Y}_v v + (\dot{Y}_p + m_z W_e) + \\ &+ (\dot{Y}_r - m_x W_e) + \dot{Y}_{\delta} \delta_r + (mg - B) \phi \cos \theta_e \\ J_x \dot{p} - J_{xz} \dot{r} - (ma_z + \dot{L}_{\dot{v}}) \dot{v} &= \mathcal{L}_e + \dot{L}_v v + (\dot{L}_p - m_z W_e) p + (\dot{L}_r + m_x U_e) r + \\ &+ \dot{\mathcal{L}}_{\delta} \delta_r - (mga_z + Bb_z) \phi \cos \theta_e \\ J_z \dot{r} - J_{xz} \dot{p} + (ma_x - \dot{N}_{\dot{v}}) \dot{v} &= \mathcal{N}_e + \dot{N}_v v + (\dot{N}_p + m_x W_e) p + (\dot{N}_r - m_x U_e) r \\ &+ \dot{Z}_{\delta} \delta_r + (mga_x + Bb_x) \phi \cos \theta_e \end{aligned} \quad (3.18)$$

Applying the lateral-directional trim conditions, that for the rectilinear flight result all zero ( $Y_e = L_e = N_e = 0$ ), the linearized lateral-directional problem for the airship can be written in state space form as follows:

$$\underset{(4 \times 4)(4 \times 1)}{\mathbf{M}} \dot{\mathbf{x}} = \underset{(4 \times 4)(4 \times 1)}{\mathbf{A}} \mathbf{x} + \underset{(4 \times 1)}{\mathbf{B}} u \quad (3.19)$$

where  $x^T = [v, p, r, \phi]$  is the lateral state vector,  $B^T = [\dot{Y}_{\delta_r}, \dot{\mathcal{L}}_{\delta_r}, \dot{N}_{\delta_r}, 0]$  is the lateral control vector and  $u = \delta_r$  is the rudder input. The control aerodynamic rolling term  $\dot{\mathcal{L}}_{\delta_r}$ , that appears in the lateral control vector, in the reference [12] is omitted, as for the cross empennages configuration the rolling contribution of the two rudders, with respect to the center of volume, is zero; for the three empennages configuration, instead, the only one rudder generate a non zero rolling moment. The lateral stability matrix is obtained dividing the matrix  $\mathbf{A}$  for the mass matrix  $\mathbf{M}$ , as done for the longitudinal case in the Eq. 3.17:

$$\mathbf{A} = \begin{pmatrix} \dot{Y}_v & (\dot{Y}_p + m_z W_e) & (\dot{Y}_r - m_x U_e) & (mg - B) \cos \theta_e \\ \dot{\mathcal{L}}_v & (\dot{\mathcal{L}}_p - m_a z W_e) & (\dot{\mathcal{L}}_r + m_a z U_e) & -(mga_z - Bb_z) \cos \theta_e \\ \dot{N}_v & (\dot{N}_p + m_a x W_e) & (\dot{N}_r - m_a x U_e) & (mga_x + Bb_x) \cos \theta_e \\ 0 & 1 & \tan \theta_e & 0 \end{pmatrix}$$

$$\mathbf{M} = \begin{pmatrix} m_y & -(ma_z + \dot{Y}_p) & (ma_x - \dot{Y}_r) & 0 \\ -(ma_z + \dot{\mathcal{L}}_v) & J_x & -J_{xz} & 0 \\ (ma_x - \dot{N}_v) & -J_{xz} & J_z & 0 \\ 0 & 0 & 0 & 1 \end{pmatrix}$$

The state space problem has been also modified from the reference [12] about the linearized expression of  $\phi$ ; the time derivative of the Euler angle of roll is showed below:

$$\dot{\phi} = p + q \sin \phi \tan \theta + r \cos \phi \tan \theta \quad (3.20)$$

Assuming the small disturbance theory, according to which the longitudinal and lateral motions can be treated as independent for small perturbations about the equilibrium condition, is possible to linearize the Eq. 3.20 as follows, taking in account the contribution of the equilibrium body attitude  $\theta_e$ :

$$\dot{\phi} = p + r \tan \theta_e \quad (3.21)$$

### 3.3 The airship static stability

The static stability of the airships cannot be evaluated by applying the common aircraft methods. In fact due to their features they are affected by a positive  $C_{m\alpha}$ , but also by significant aerodynamic damping effects and by the buoyant lift actions. In order to estimate the stability of the airship it is useful to investigate on the behavior of the dynamic system when is constrained to small perturbation about the equilibrium flight condition. In this way the stability of an airship equilibrium condition is assessed by analyzing the eigenvalues of the plant matrix.

A method [17] based from the geometrical features and the aerodynamic coefficients of the airship has been studied and developed to define the state space problem. The main goal of this approach is the achievement of the state space problem definition without using any numerical methods to linearize a mathematical non-linear model, nor extensive flight data to enable the use of system identification methods. This approach developed by [17] for the longitudinal

problem, with neutral buoyancy, has been fitted to the “heaviness condition” and to the lateral problem. In this way it was possible to compare the two airship tail configurations introduced in the previous chapter. According to the reference method [17], the aerodynamics dimensional longitudinal stability derivatives have been calculated modifying the same expressions used for the aircrafts [19] as follows:

$$\begin{aligned}\dot{X}_u &= \frac{-2C_{D1}q_1S}{U_1} & \dot{X}_w &= \frac{(-C_{D\alpha} + C_{L1})q_1S}{U_1} & \dot{X}_q &= \frac{-C_{Dq}q_1Sc}{2U_1} \\ \dot{Z}_u &= \frac{-C_{L1}q_1S}{U_1} & \dot{Z}_w &= \frac{(-C_{L\alpha} + C_{D1})q_1S}{U_1} & \dot{Z}_q &= \frac{-C_{Lq}q_1Sc}{2U_1} \\ \dot{\mathcal{M}}_u &= \frac{C_{M1}q_1Sc}{U_1} & \dot{\mathcal{M}}_w &= \frac{C_{M\alpha}q_1Sc}{U_1} & \dot{\mathcal{M}}_q &= \frac{C_{Mq} + C_{L1}q_1Sc^2}{2U_1}\end{aligned}\quad (3.22)$$

In order to develop the aerodynamic dimensional lateral stability derivatives from the expressions used for the aircrafts [19], the same criteria of the reference [17] have been applied. According to these, the Mach aerodynamic contribution has been ignored and the geometrical features have been referred to the volume of the airship as in the Eq. 3.23.

$$\begin{aligned}S &= \nabla^{2/3} \\ c &= \nabla^{1/3}\end{aligned}\quad (3.23)$$

The mean aerodynamic chord of an airship coincides with the wingspan, being both functions of the envelope volume.

The following expressions represent the aerodynamics dimensional lateral stability derivatives for the airship, obtained as explained before:

$$\begin{aligned}\dot{Y}_v &= \frac{C_{Y\beta}q_1S}{U_1} & \dot{Y}_p &= \frac{C_{Yp}q_1Sc}{2U_1} & \dot{Y}_r &= \frac{C_{Yr}q_1Sc}{2U_1} \\ \dot{\mathcal{L}}_v &= \frac{C_{\mathcal{L}\beta}q_1Sc}{U_1} & \dot{\mathcal{L}}_p &= \frac{C_{\mathcal{L}p}q_1Sc^2}{2U_1} & \dot{\mathcal{L}}_r &= \frac{C_{\mathcal{L}r}q_1Sc^2}{2U_1} \\ \dot{\mathcal{N}}_v &= \frac{C_{\mathcal{N}\beta}q_1Sc}{U_1} & \dot{\mathcal{N}}_p &= \frac{C_{\mathcal{N}p}q_1Sc^2}{2U_1} & \dot{\mathcal{N}}_r &= \frac{C_{\mathcal{N}r}q_1Sc^2}{2U_1}\end{aligned}\quad (3.24)$$

Finally in Eq. 3.25 are given the control forces and moments, that can be used to determine the longitudinal and the lateral control vectors:

$$\begin{aligned}\dot{X}_{\delta_e} &= C_{D\delta_e}q_1S & \dot{Z}_{\delta_e} &= C_{L\delta_e}q_1S & \dot{\mathcal{M}}_{\delta_e} &= C_{M\delta_e}q_1Sc \\ \dot{Y}_{\delta_r} &= C_{Y\delta_r}q_1S & \dot{\mathcal{L}}_{\delta_r} &= C_{\mathcal{L}\delta_r}q_1Sc & \dot{\mathcal{N}}_{\delta_r} &= C_{\mathcal{N}\delta_r}q_1Sc\end{aligned}\quad (3.25)$$

The expressions of the aerodynamics dimensional stability derivatives [19] [11] are referred to the stability axes ( $X_s, Y_s, Z_s$ ) where the speed  $U_1$  coincides with the total trim speed. The physical quantity with subscript “1”, like the dynamic pressure  $q_1$ , are referred to the equilibrium condition.

The non-dimensional aerodynamic coefficients that figure in the previous expressions could be obtained by semi-empirical approach [19] or by CFD calculation or by wind tunnel testing. The aerodynamic database for the applications has been built on the basis of full three-dimensional CFD RANS (Reynolds Averaged Navier-Stokes) computations, performed by CIRA [2], with the stability reference frame having its origin attached to the center of volume.

### 3.4 Longitudinal trim

For an airship the aerodynamic coefficients have a non-linear behavior at different incidences, so the knowledge of the equilibrium condition is necessary to linearize the dynamic system around it and for evaluating the stability derivatives. For the neutral buoyancy condition, according to the zero incidence, the stability axes coincided with the body axes and the trim equations, balancing the forces acting on the airship, could reach the following simplified expression:

$$\begin{cases} D = T \\ L = 0 \\ \mathcal{M} = m g a_z \sin \theta_e - T d_z \end{cases} \quad (3.26)$$

The Eq. 3.26, where the two only variables are the equilibrium thrust  $T$  and the pitch attitude  $\theta_e$  at the reference speed, have been simplified assuming also the airship statically balanced, that is with the center of gravity beneath the center of volume. Instead, the main problem with a non neutral buoyancy case is the fact that the initial equilibrium condition is characterized by a non zero incidence, that must be calculated from the equilibrium equations. The trim equations represent an indeterminate problem as it has infinite solutions, having more variables than equations.

Assuming the trimmed control forces and moments are zero, assuming the thrust is parallel to the airship reference line and assuming the buoyancy applied at the  $C_V$ , the equilibrium equations may be written as follows:

$$\begin{cases} \frac{1}{2} \rho_A V^2 S (C_L \sin \alpha - C_D \cos \alpha) + T - (m g - B) \sin \theta_e = 0 \\ -\frac{1}{2} \rho_A V^2 S (C_D \sin \alpha + C_L \cos \alpha) + (m g - B) \cos \theta_e = 0 \\ \frac{1}{2} \rho_A V^2 S c C_{\mathcal{M}} + T d_z - m g a_z \sin \theta_e = 0 \end{cases} \quad (3.27)$$

These equations, related to body axes, have been developed from the longitudinal trim equations showed in [12], by expressing the forces and moment according to the aerodynamic lift, resistance and moment coefficients, defined in stability axes. The term  $m g a_z \sin \theta_e$  represents the righting moment due to the buoyant lift.

Under these assumptions, the problem, setting the speed, is reduced to have only three variables:  $T$ ,  $\alpha$ ,  $\theta_e$ , that are uniquely determined. Knowing the equilibrium condition is possible to evaluate the stability coefficients and the dimensional longitudinal stability derivatives. Furthermore the expressions of the dimensional stability derivatives, calculated in the stability axes, as defined before, have to be transformed to the body axes, by a rotation matrix.

### 3.5 Application of the method

In this section is reported the application of proposed method to the unmanned non-rigid airship "AIUX15". The comparison between the two possible airship

Table 3.1: AIUX15 trim conditions

Item	Name	$\alpha(^{\circ})$	$\theta(^{\circ})$	$T(N)$
1	Cross +	1.962	10.601	84.774
2	Inverted Y	2.286	17.647	94.097

empennages configurations on the same envelope, has been carried out, with regard to the stability and the response to control, at the nominal speed. The number and the size of the empennages have a significative influence on weight and trim, affecting the payload especially for a small airship.

The comparison between the “cross” and the “inverted Y” configuration is carried out assuming the same weight condition that could be reached improving the payload. The airship is in a heaviness condition, with an exceeded weight of about 8kg that, however, can be sustained in hovering by the vectorable thrust. For this airship, as mentioned before, the aerodynamic models and data for the four and three empennages configurations are available, whose main coefficients are given in table 2.2. All the aerodynamic reference data used for the applications have been performed by CIRA. [2]

### 3.5.1 “Cross” configuration results

The method explained before has been applied by setting a “Mathcad” worksheet. The longitudinal and the lateral results regarding the stability analysis of the airship configurations, have been carried out for the nominal speed of 40kmh at sea level. The calculated trim condition are showed in the table 3.1.

The added mass terms have been evaluating applying the theoretical formula for the prolate ellipsoid [4] (see Appendix A); these formula take in account the added mass effects of the only envelope, without empennages; however the fins contribution is such smaller that could be safely ignored. According to this assumption about the added mass terms, the longitudinal and lateral mass matrices, respectively named  $\mathbf{M}_l$  and  $\mathbf{M}_{l_a}$  do not change with the tail configurations and are showed below:

$$M_l = \begin{pmatrix} 146.84 & 0 & 156.78 & 0 \\ 0 & 262.74 & 0 & 0 \\ 156.78 & 0 & 4856 & 0 \\ 0 & 0 & 0 & 1 \end{pmatrix}$$

$$M_{l_a} = \begin{pmatrix} 262.74 & -156.78 & 0 & 0 \\ -156.78 & 580.74 & -265.45 & 0 \\ 0 & -265.45 & 4419 & 0 \\ 0 & 0 & 0 & 1 \end{pmatrix}$$

For the four empennages configuration in heaviness condition, the matrices  $\mathbf{a}_l$  and  $\mathbf{a}_{l_a}$  have been obtained from the application of the developed method. The stability characteristics of the system, that are related to the eigenvalues of the plant matrices  $\mathbf{a}_l$  and  $\mathbf{a}_{l_a}$ , have been reported in the table 3.2. It's to

Table 3.2: AIUX15 cross configuration-stability results

Long. eigenvalues	Characteristics	Lat. eigenvalues	Characteristics
-1.834	t=0 545s	-1.616	t=0 619s
-0.667	t=1 501s	-0.698	t=1 443s
-0.095	t=10 514s	-0.402 + 1.783i	$\omega = 1 828\text{rads}$
-0.191	t=5 235s	-0.402 + 1.783i	$\zeta = 0.220$

notice that the longitudinal stability modes of motion of the cross configuration are all exponential subsidence modes, characterized by real roots, while the lateral stability denotes oscillatory rolling motions. In order to view the stability modes the longitudinal and the lateral small perturbations equations, from the reference equilibrium condition, are applied for the input command of a  $5^\circ$  elevator step, and subsequently for a  $5^\circ$  rudders step. The longitudinal responses for the cross empennages configuration are plotted in the figure 3.2. The lateral results, for the same configuration, are plotted in the figure 3.4.

$$a_l = \begin{pmatrix} -12.68 & 9.71 & -59.02 & -76.83 \\ -13.90 & -202.86 & 435.59 & -14.3843 \\ 7.48 & 218.55 & -9082 & -1511 \\ 0 & 0 & 1 & 0 \end{pmatrix} \quad b_l = \begin{pmatrix} -1.68 \\ -71.16 \\ -446.47 \\ 0 \end{pmatrix}$$

$$a_{la} = \begin{pmatrix} -196.50 & 99.97 & -435.96 & 76.83 \\ 7.85 & -396.81 & 1993 & -1511 \\ -218.42 & -11.55 & -7345 & 0 \\ 0 & 1 & 0.187 & 0 \end{pmatrix} \quad b_{la} = \begin{pmatrix} 72.51 \\ 2.48 \\ -433.45 \\ 0 \end{pmatrix}$$

### 3.5.2 “Inverted Y” configuration results

The stability analysis has been carried for the three empennages configuration, for the reference trim condition reported in the table 3.1.

Regarding to the longitudinal response to control in Figure 3.3, the increase in drag is to ascribe to the equilibrium attitude that arise from balancing the longitudinal moment of the aerodynamic actions with the stability buoyant moment. Through the elevator control at equilibrium, it could be possible to reduce the attitude angle and therefore the drag. From the eigenvalues of the plat matrices, as can be seen in table 3.3, the longitudinal stability modes denote oscillatory motions as well the lateral stability modes of motions. The “inverted Y” tail airship, even if it is provided with only one rudder, demonstrate a good lateral-directional control as shows in the figure 3.5.

$$a_l = \begin{pmatrix} -12.66 & 9.37 & -80.40 & -74.48 \\ -13.46 & -168.60 & 727.77 & -23.69 \\ 22.014 & 551.88 & -7489 & -1465 \\ 0 & 0 & 1 & 0 \end{pmatrix} \quad b_l = \begin{pmatrix} 2.06 \\ -62.43 \\ -374.85 \\ 0 \end{pmatrix}$$

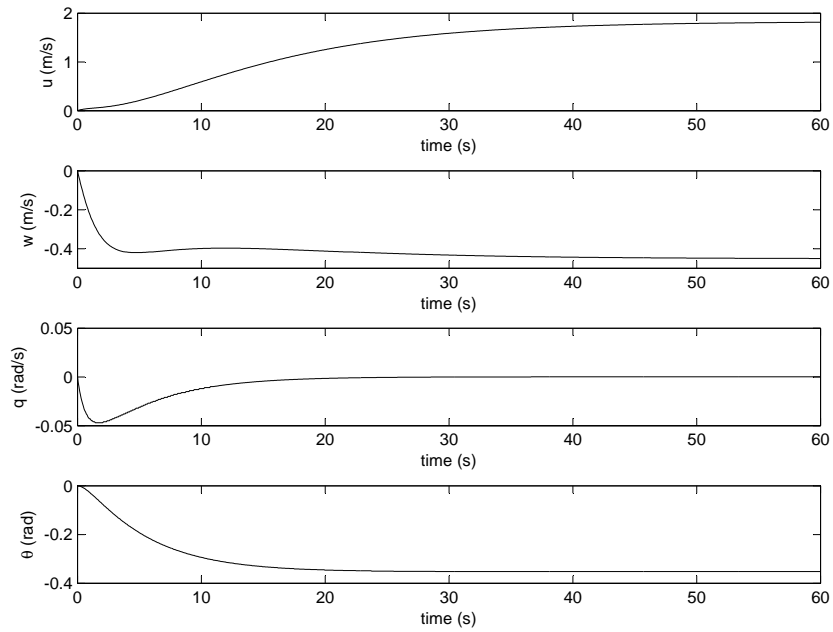


Figure 3.2: AIUX15 cross configuration-longitudinal response to a  $5^\circ$  elevators step

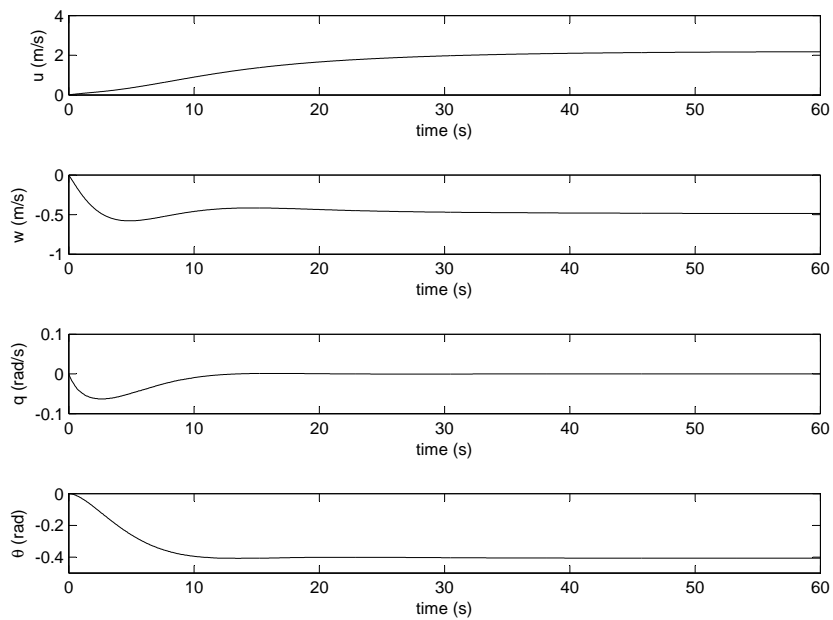


Figure 3.3: AIUX15 inverted Y configuration-longitudinal response to a  $5^\circ$  elevators step

Table 3.3: AIUX15 inverted Y configuration-stability results

Long. eigenvalues	Characteristics	Lat. eigenvalues	Characteristics
-1.721	t=0.581s	-1.525	t=0.656s
-0.086	t=11.691s	-0.297	t=3.368s
$-0.254 + 0.236i$	$\omega = 0.347\text{rads}$	$-0.336 + 1.793i$	$\omega = 1.824\text{rads}$
$-0.254 - 0.236i$	$\zeta = 0.733$	$-0.336 + 1.793i$	$\zeta = 0.184$

$$a_{la} = \begin{pmatrix} -162.48 & 116.42 & -727.05 & 74.48 \\ 22.01 & -347.44 & 1970 & -1465 \\ -551.44 & -11.09 & -5741 & 0 \\ 0 & 1 & 0.318 & 0 \end{pmatrix} \quad b_{la} = \begin{pmatrix} 36.03 \\ 7.05 \\ -216.73 \\ 0 \end{pmatrix}$$

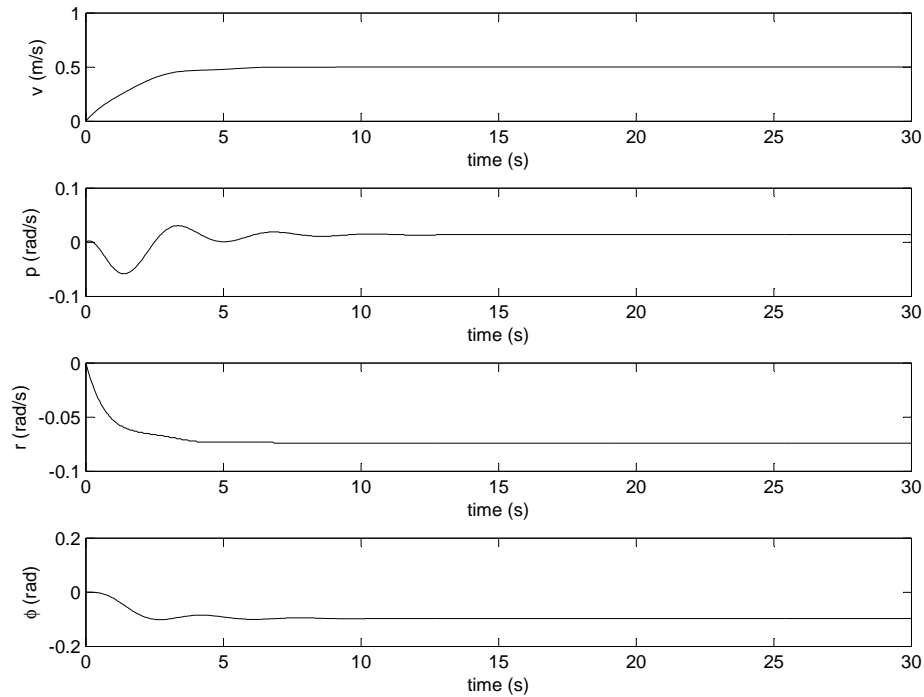


Figure 3.4: AIUX15 cross configuration-lateral response to a 5° rudders step

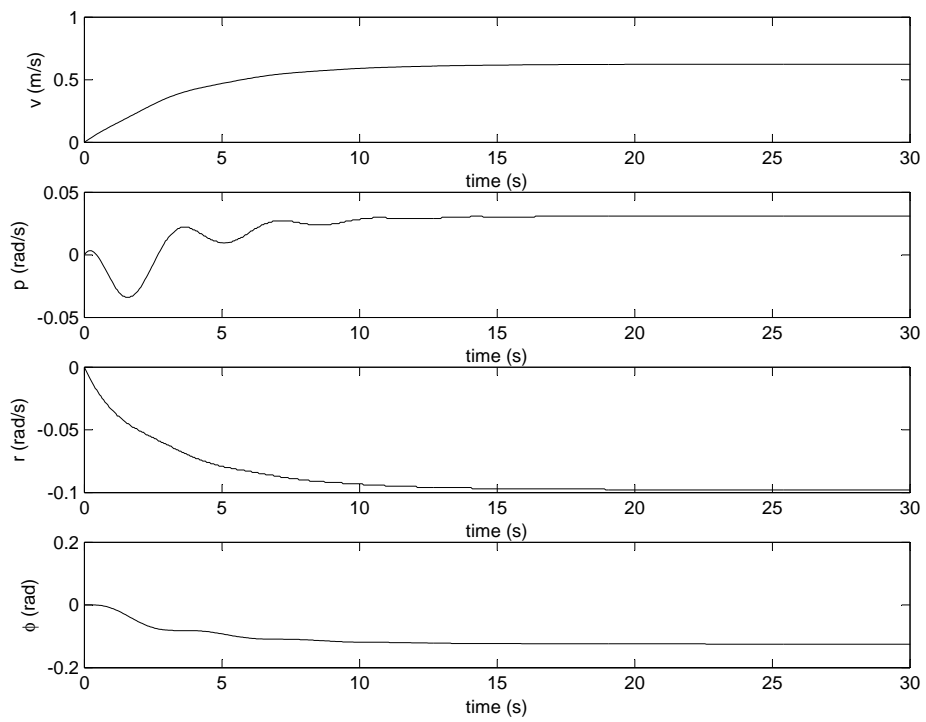


Figure 3.5: AIUX15 inverted Y configuration-lateral response to a  $5^\circ$  rudder step

## Chapter 4

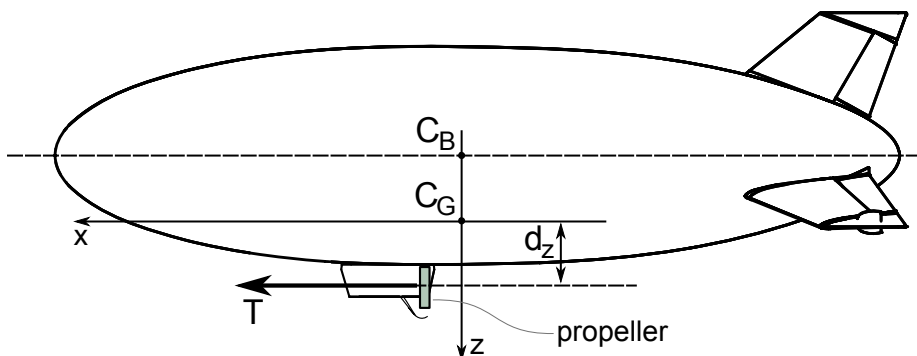
# Longitudinal Simulation Model

### 4.1 Longitudinal equation of motion

THE longitudinal equations of motion for an airship represent a second order differential problem of three equations in the body fixed reference frame. Differently from the standard practise, the airship presents the body-fixed reference frame having its origin attached to the  $C_G$  and not to the CV ( the center of volume coincides with the center of buoyancy  $C_B$  see Figure 4.1). The airship model incorporates the standard aerostatics and aerodynamics terms, and a special treatment of added-mass terms as external forces. The model have been implemented using the Simulink toolbox of Matlab. In particular all the assumptions made enabled the use of the Simulink *3DoF Body Axes/Euler Angle* block in order to describe the dynamics of the system. This block solves the differential equations by using numerical integration according to the algorithm ode45 by Runge-Kutta. The resulting 3DoF dynamic model for the airship is given by the following equation:

$$\mathbf{M} \begin{bmatrix} \dot{U} \\ \dot{W} \\ \dot{q} \end{bmatrix} = \mathbf{F}_d(U, W, q) + \mathbf{A}(U, W, q) + \mathbf{G}(\Theta) + \mathbf{C} + \mathbf{P} + \mathbf{F}_{\text{add}} \quad (4.1)$$

On the left-hand side of system (4.1) the term  $\mathbf{M}$  is  $3 \times 3$  generalized mass matrix, and  $[U, W, q]^T$  is the vector of state variables, i.e. the airship velocity component along the x and the z axis and the pitch angular velocity component in the body axes. On the right-hand side, the term  $\mathbf{A}$  is an aerodynamic generalized force vector depending on the above mentioned velocity and on angular velocity components. The quantity  $\mathbf{C}$  is a control generalized force vector depending also on the aero-surface deflections at the tail. The term  $\mathbf{G}$  is a generalized gravity force vector depending on the Eulerian angle  $\Theta$ . The term  $\mathbf{F}_d$  is a dynamic-effect generalized force vector depending on  $(U, W, q)$ . The added mass effects are not built into the mass matrix of the airship [12, 13] but are modelled as external inertial actions in the vector  $\mathbf{F}_{\text{add}}$  depending on the ve-

Figure 4.1: Reference frame with origin in the  $CG$ 

locity and angular velocity rates  $(\dot{U}, \dot{W}, \dot{q})$ . This model, whose terms are going to be detailed in the following, represents the first step in the achievement of a simulation model that takes in account all the 6DoF of motions of the airship.

The aerodynamic generalized force are calculated as:

$$\begin{cases} D = 1/2 \rho V^2 S C_D \\ L = 1/2 \rho V^2 S C_L \\ \mathcal{M} = 1/2 \rho V^2 S c C_M \end{cases} \quad (4.2)$$

They are referred to the wind axis system centered at the CV. In order to evaluate the aerodynamic actions in the body fixed reference frame centered at the  $CG$  a transport of the forces and a rotation matrix (4.3) depending on the angle of attack, were introduced in the model:

$$R_\alpha = \begin{bmatrix} \cos \alpha & 0 & -\sin \alpha \\ 0 & 1 & 0 \\ \sin \alpha & 0 & \cos \alpha \end{bmatrix} \quad (4.3)$$

The longitudinal aerodynamic coefficients that figure in the (4.2) have been organized into Simulink “look-up tables” as function of the angle of attack and of the normalized pitch speed.

Following the same criteria, the longitudinal aerodynamic control forces and moments have been calculated as follows:

$$\begin{cases} D = 1/2 \rho V^2 S \Delta(C_D) \\ L = 1/2 \rho V^2 S \Delta(C_L) \\ \mathcal{M} = 1/2 \rho V^2 S c \Delta(C_M) \end{cases} \quad (4.4)$$

The longitudinal control coefficients have been implemented into “look-up tables” assuming as parameters the angle of attack and the elevators deflections. The vector  $\mathbf{P}$  in equation (4.1) depends on the propulsive model. In the general case the thrust vector has a varying direction, always belonging to the body-fixed longitudinal plane  $XZ$ . The propulsive actions are then given by the following:

$$\begin{cases} X_p = 2T \cos \mu \\ Z_p = -2T \sin \mu \\ \mathcal{M}_p = 2T(d_z \cos \mu - d_x \sin \mu) \end{cases} \quad (4.5)$$

In our simulation model the propeller thrust has been assumed as a constant and held aligned with the airship longitudinal X axis , assuming a null value of the  $\mu$  angle. The gravitational actions represented by the column matrix  $\mathbf{G}$  in equation (4.1) depend on the buoyant lift magnitude  $B$ . The latter is a function of the helium purity  $\eta_h$  and density  $\rho_h$ , and of the air density  $\rho$ . The air density is assumed constant according to the low operational altitude of the airship. The expressions that give the three elements of  $\mathbf{G}$  are reported in the following:

$$\begin{cases} X_g = -\sin \theta (mg - B) \\ Z_g = \cos \theta \cos \phi (mg - B) \\ \mathcal{M}_g = -\sin \theta \quad b_z B \end{cases} \quad \text{where } B = (\rho - \rho_h)\eta_h g \nabla \quad (4.6)$$

Finally the longitudinal added mass forces and moment of the airship have been evaluated as follows:

$$\begin{cases} X_{\text{add}} = \dot{X}_{\dot{U}}\dot{U} - \dot{Z}_{\dot{W}}\dot{W}q - \dot{X}_{\dot{q}}\dot{q} \\ Z_{\text{add}} = \dot{Z}_{\dot{W}}\dot{W} - \dot{X}_{\dot{U}}\dot{U}q - \dot{Z}_{\dot{q}}\dot{q} \\ \mathcal{M}_{\text{add}} = \dot{\mathcal{M}}_{\dot{q}}\dot{q} - \dot{\mathcal{M}}_{\dot{W}}\dot{W} - \dot{\mathcal{M}}_{\dot{U}}\dot{U} \end{cases} \quad (4.7)$$

where  $\dot{X}_{\dot{q}} = \dot{Z}_{\dot{q}} = \dot{\mathcal{M}}_{\dot{W}} = \dot{\mathcal{M}}_{\dot{U}} = 0$ .

For an airship the added mass effects can be reasonably approximated by considering only the envelope volume, enabling the application of the theoretical formulas for the prolate ellipsoid [4].

## 4.2 The Simulink 3DoF model

The longitudinal equations of motion have been implemented in Matlab/Simulink. Each type of external forces and pitching moment acting on the airship, have been introduced and evaluated into subsystems.

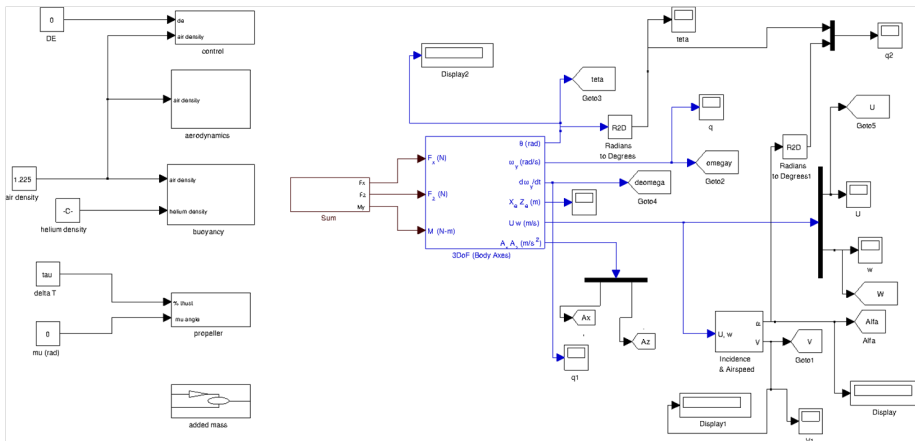


Figure 4.2: Airship 3DoF implemented Matlab/Simulink model

In Figure 4.2 is presented the general view of longitudinal airship model. The whole longitudinal aerodynamic database, the mass and all the airship reference

dimensions, required by the model, have been collected in a Matlab M-file. Even the initial velocity and attitude value to give to the model have been defined in the main M-file.

In this way, standing the Matlab/Simulink model, it's easy to develop different airships simulation model, or different configurations of the same airship by only changing the reference data in the M-file.

For the purpose of the applications the *AIUX15* airship in cross empennage configuration has been implemented and analyzed for the neutral buoyancy condition. The trim conditions descend from the 4.8 for the nominal speed of 40 km/h at sea level.

$$\begin{cases} D = T \\ L = 0 \\ Td_z = -mga_z \sin \theta_e \end{cases} \quad (4.8)$$

The response to the following input have been reported and analyzed; for each input command the velocity and the external force and moment components have been observed in order to check qualitatively the behavior of the dynamic system:

1. 10° elevator step (see Figure 4.2);
2. 5° elevators up, 5° elevators down (see Figure 4.2);
3. 10% thrust increase (see Figure 4.2);
4. 10% thrust increase with  $\mu = 45^\circ$  (see Figure 4.2).

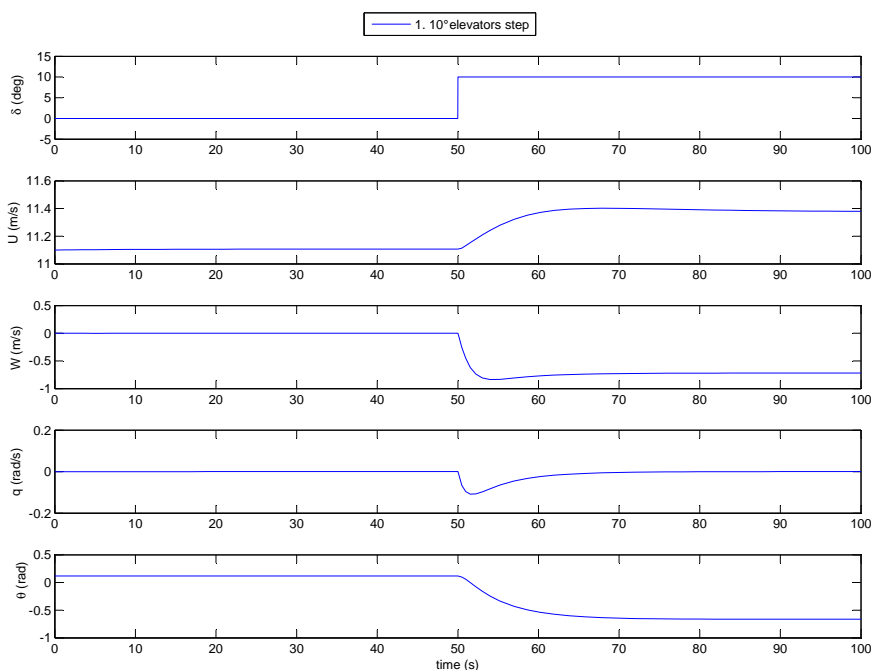


Figure 4.3: Airship longitudinal response to 10° elevator step

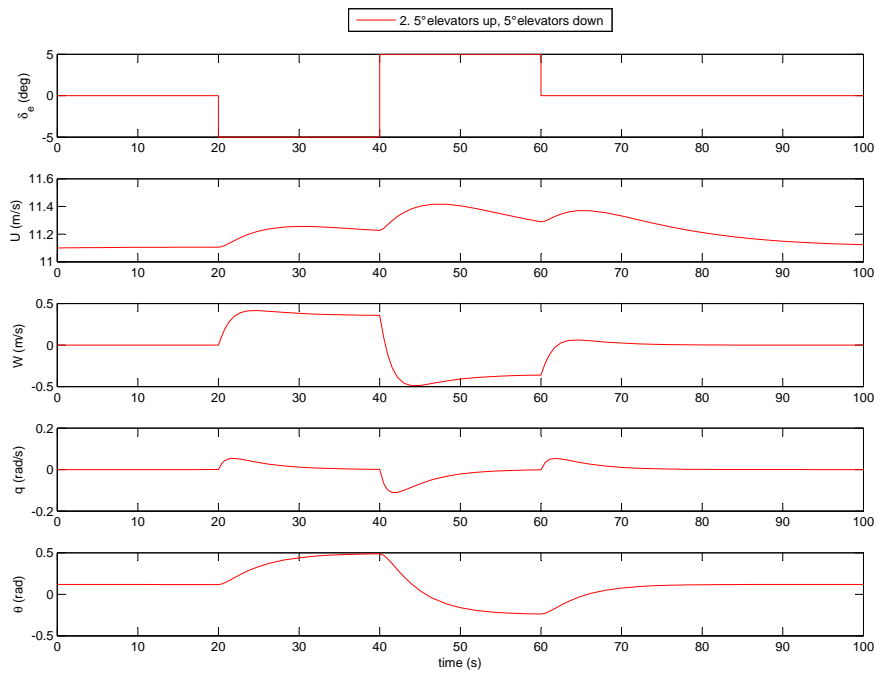
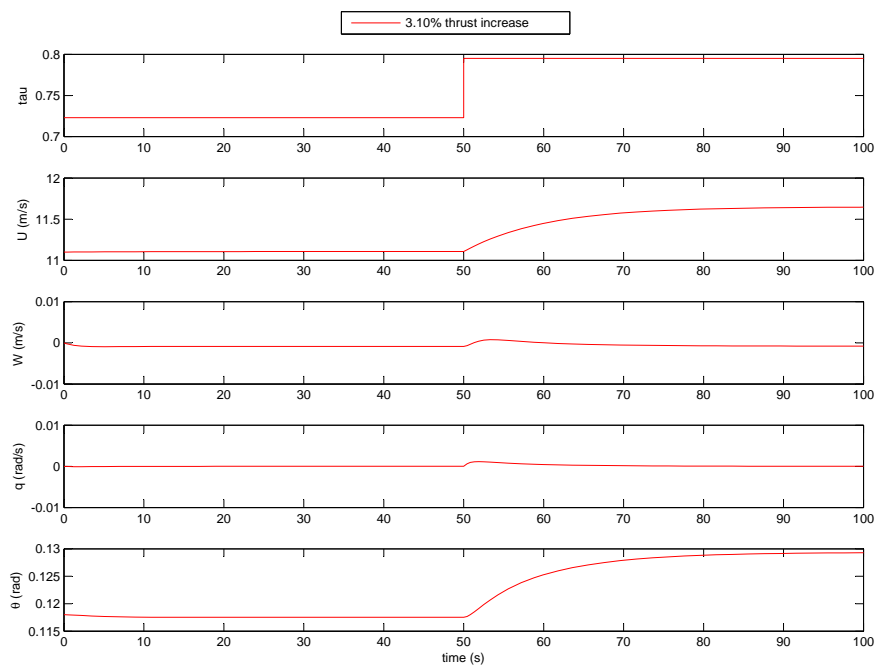
Figure 4.4: Airship longitudinal response to  $+5^\circ -5^\circ$  elevator input

Figure 4.5: Airship longitudinal response to 10% thrust increase

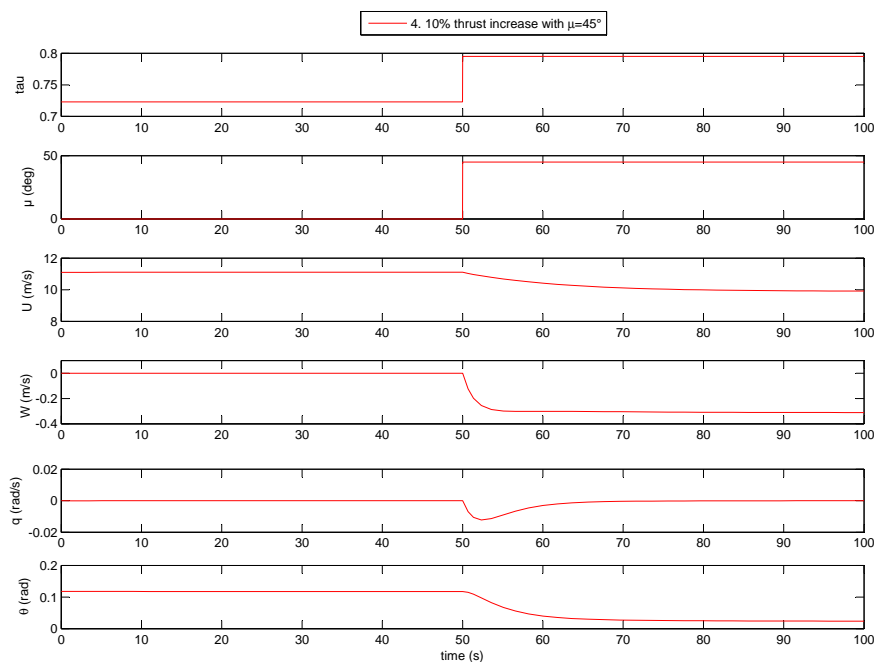


Figure 4.6: Airship longitudinal response to 10 % thrust increase with  $\mu = 45^\circ$

1.  $10^\circ$  elevator step

The positive deflection of the elevator, as expected caused a “nose down” response of the airship. The control forces are mainly balanced by the aerodynamic actions. The aerodynamic force component along the  $X$  axis,  $F_{AX}$  is not the aerodynamic drag as could be notice in the 4.9:

$$\begin{cases} -(D \cos \alpha - L \sin \alpha) = F_{AX} \\ -(D \sin \alpha + L \cos \alpha) = F_{AZ} \end{cases} \quad (4.9)$$

Instead the longitudinal moment induced by the elevators is balanced by the buoyant lift moment 4.10 that justifies the high attitude angle.

$$Ba_z \sin \Theta = \mathcal{M}_{BY} \quad (4.10)$$

2.  $5^\circ$  elevators up,  $5^\circ$  elevators down

This type of input is made by a negative elevator deflection hold for 20s and by a positive elevator deflection, finally set to zero. The airship longitudinal response to this input denote the tendency of the system to return to its initial state after removing the control action:

3. 10 % thrust increase

The third examined input was an increment of 10% in the propulsive thrust, without deflecting the control surfaces. As expected the thrust increase determines an increase in speed and drag, while the moment due to the propellers action modify the attitude angle:

4. 10 % thrust increase with  $\mu = 45^\circ$

Finally the last input presents an increment of 10% in thrust with propellers tilted at  $45^\circ$  with respect to the airship reference line. At the

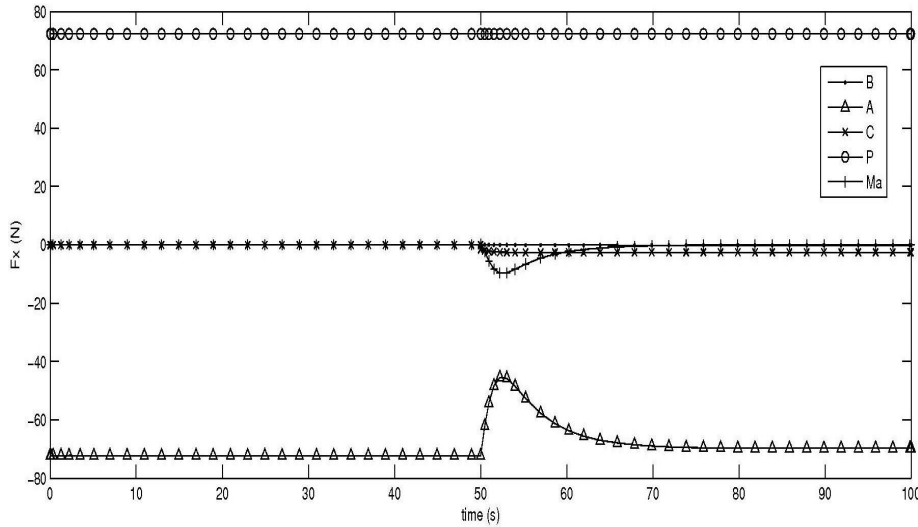


Figure 4.7: Case 1: Axial Forces

nominal speed of 40 km/h the propeller control plays a minor role with respect to the aerodynamic control. Instead at low speed it would be the opposite. It' to be noticed that to simulate the vertical take off and the landing of the airship is necessary to model the aerodynamic behavior of the system even at very high incidences.

### 4.3 Method comparison

The longitudinal linear model of the airship, introduced and developed in the previous chapter, has been compared to the longitudinal simulation model. This comparison has been carried out by superimposing the responses to a same input of  $5^\circ$  of elevator deflection for two different airship weight conditions. In Figure 4.19 are reported the longitudinal responses, to the above mentioned input, for the airship in neutral buoyancy condition; this weight condition presents  $(mg - B) = \alpha = W_e = 0$ . In order to compare the results, only the perturbations from the initial equilibrium condition have been plotted. In Figure 4.20, instead, are compared the longitudinal responses for the airship having 8 kg of exceeding weight with respect to the buoyancy, for which there is a non-zero incidence at equilibrium. As could be noticed, the linear model matches with low gaps the simulation model, for both the weight configurations. The differences on the attitude angle is due to the small angle hypothesis on the linear model. The main difference for the neutral buoyant condition is in the axial velocity  $u$ ; according to the liner model the component  $W_e$  is zero and the added mass contribution  $m_z W_e q$  during the transient phase, remains null. In fact this problem does not significantly affect the  $u$  response of the non-neutral buoyant condition transient phase.

However the final equilibrium values of  $u$  is different from the linear model,

as the value of  $C_{D\alpha}$  has been evaluated approximately without taking in account the parabolic behavior of  $C_D$ .

All the small differences between the responses are to be referred to hypothesis of the linear model regarding the small perturbation behavior from the equilibrium condition; in this way, assuming the velocity  $V$  as constant, all the aerodynamic forces are evaluated with a constant dynamic pressure differently from the reality. Clearly, the smaller the perturbation is, the better the responses match.

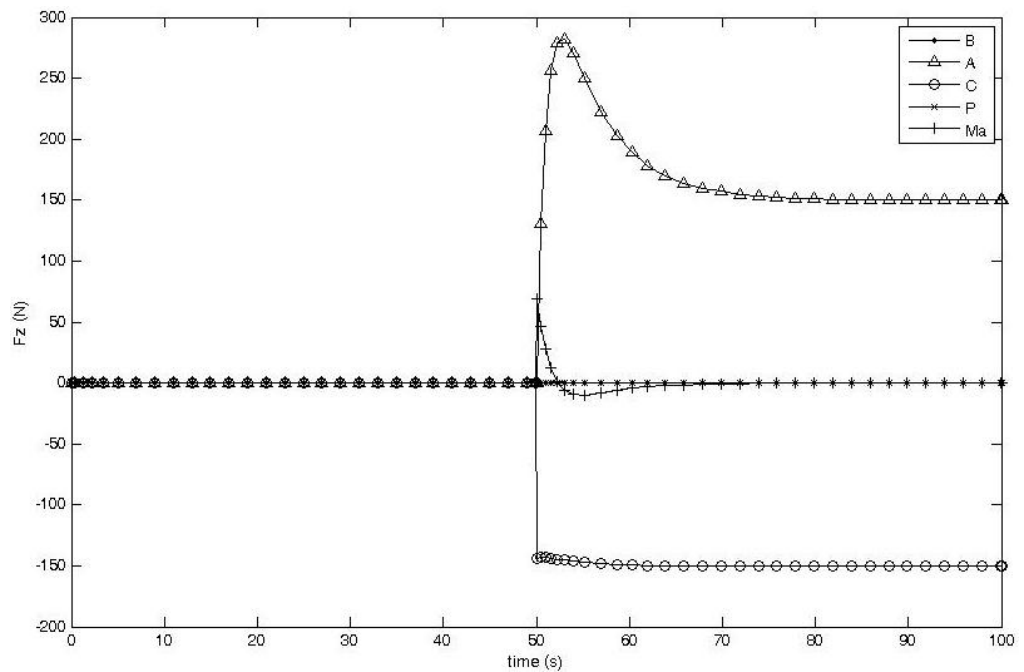


Figure 4.8: Case 1: Normal Forces

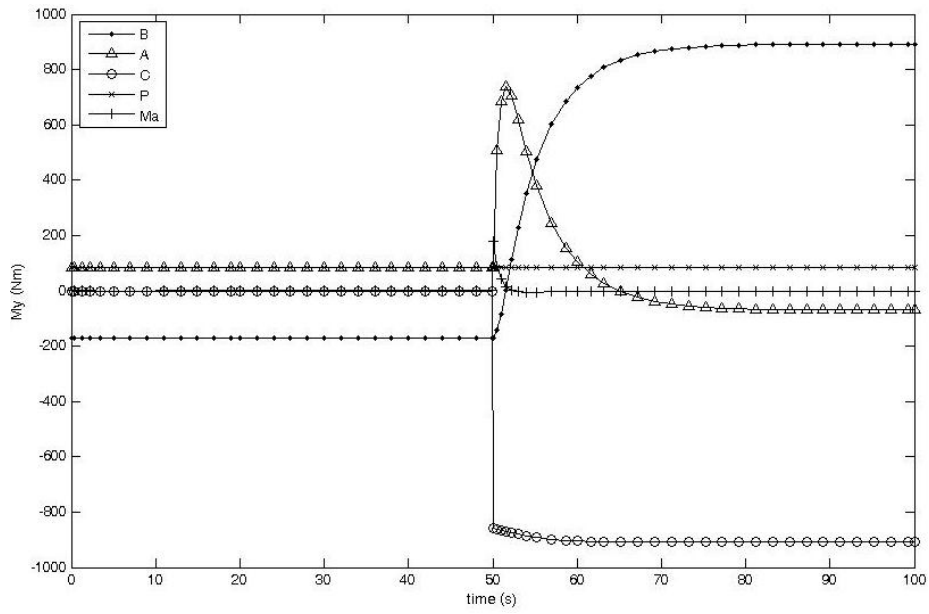


Figure 4.9: Case 1: Pitching Moments

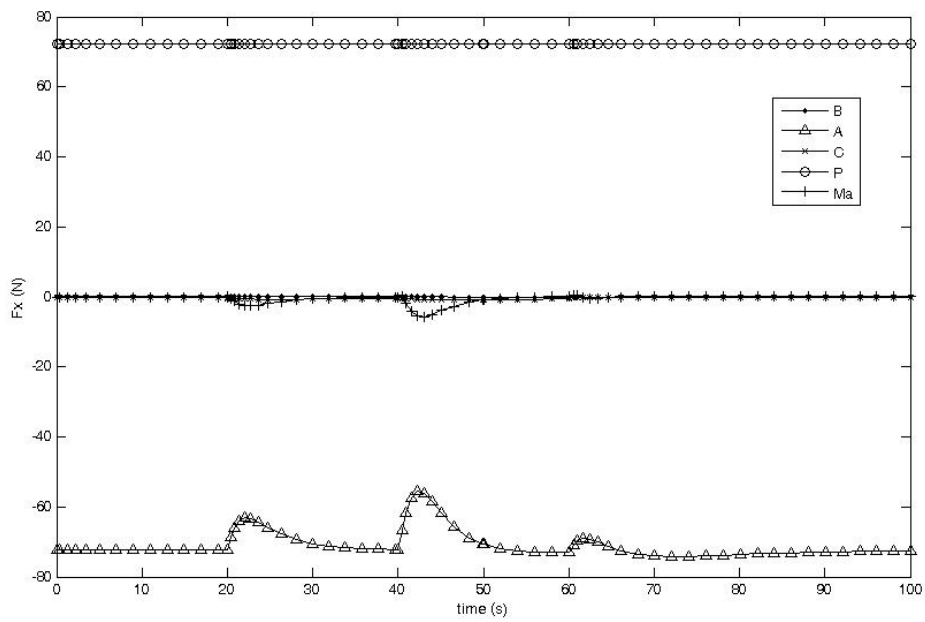


Figure 4.10: Case 2: Axial Forces

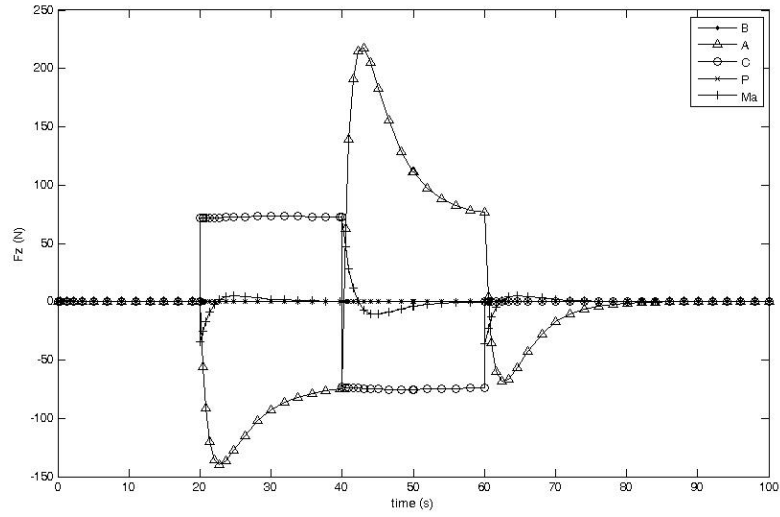


Figure 4.11: Case 2: Normal Force

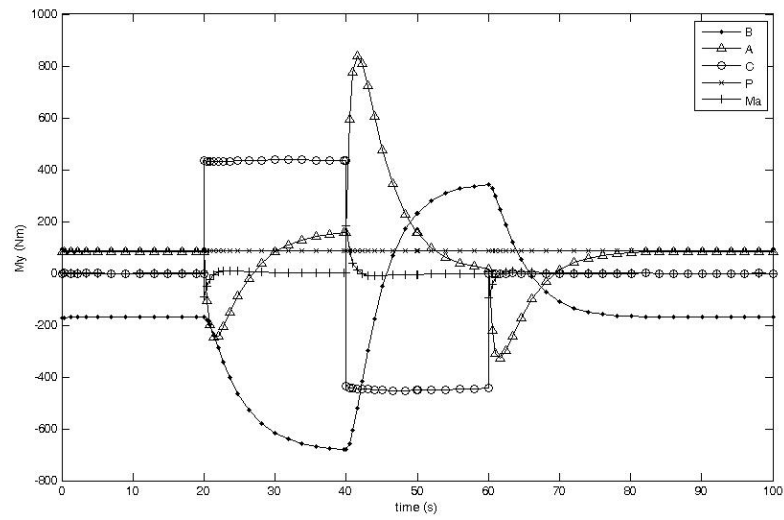


Figure 4.12: Case 2: Pitching Moments

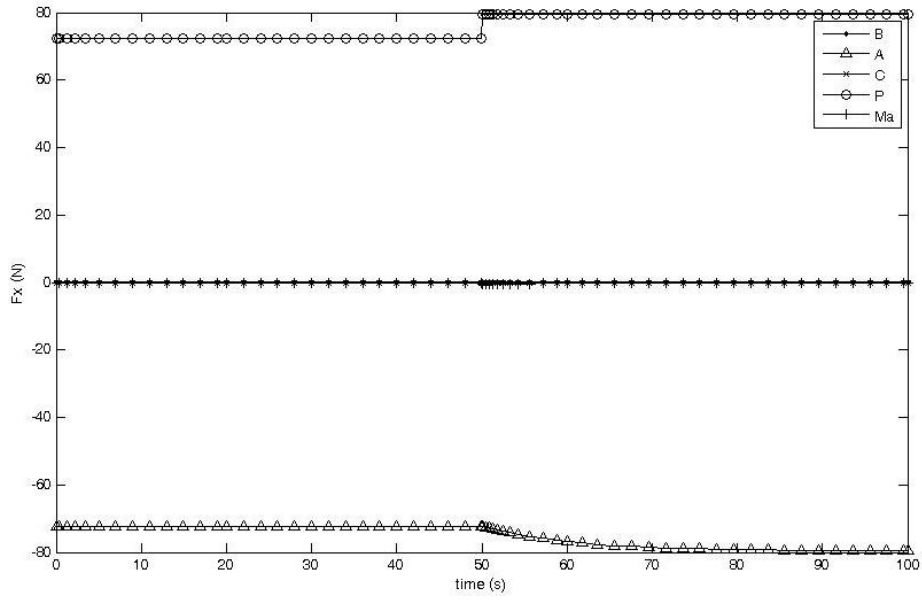


Figure 4.13: Case 3: Axial Forces

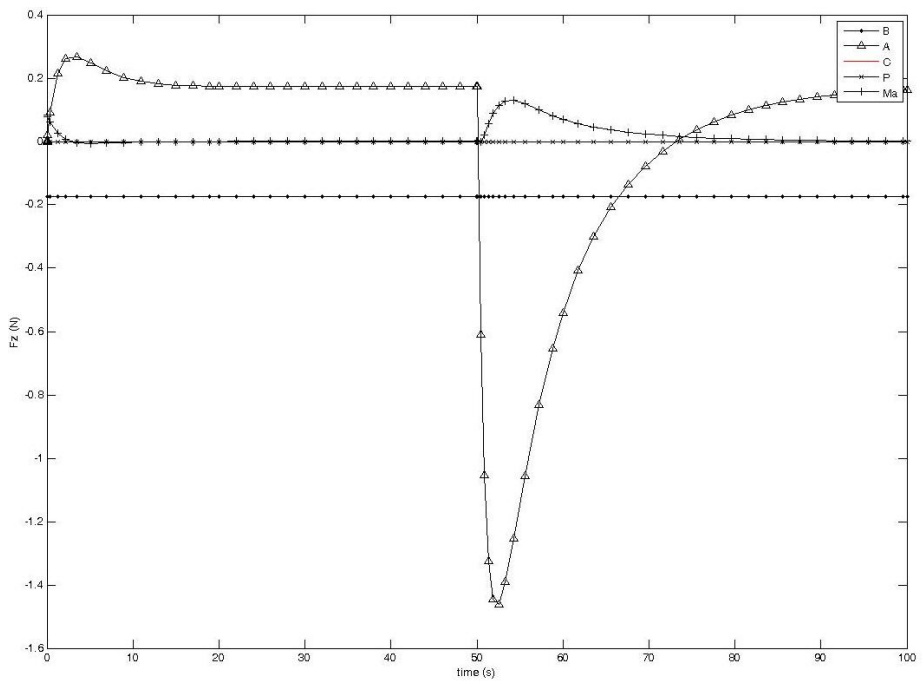


Figure 4.14: Case 3: Normal Force

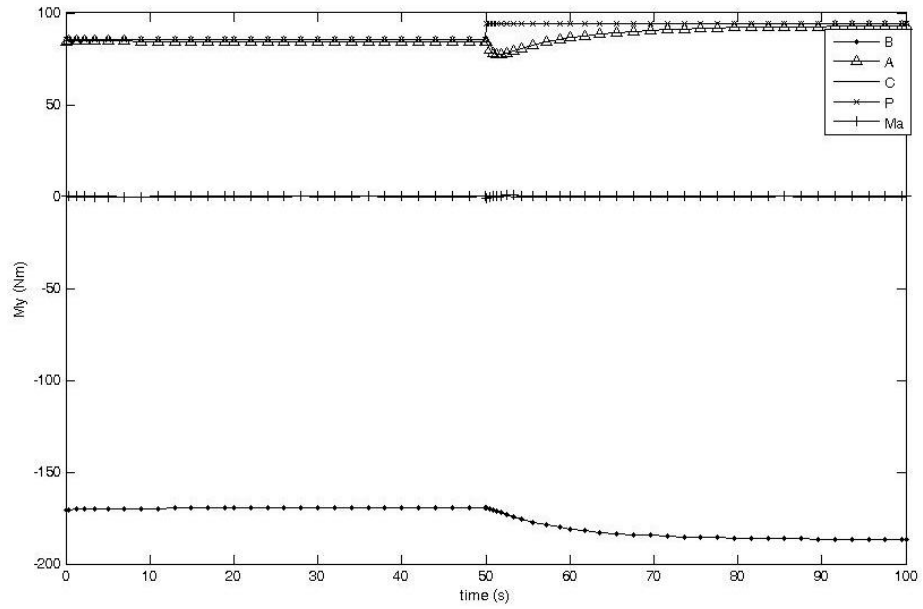


Figure 4.15: Case 3: Pitching Moments

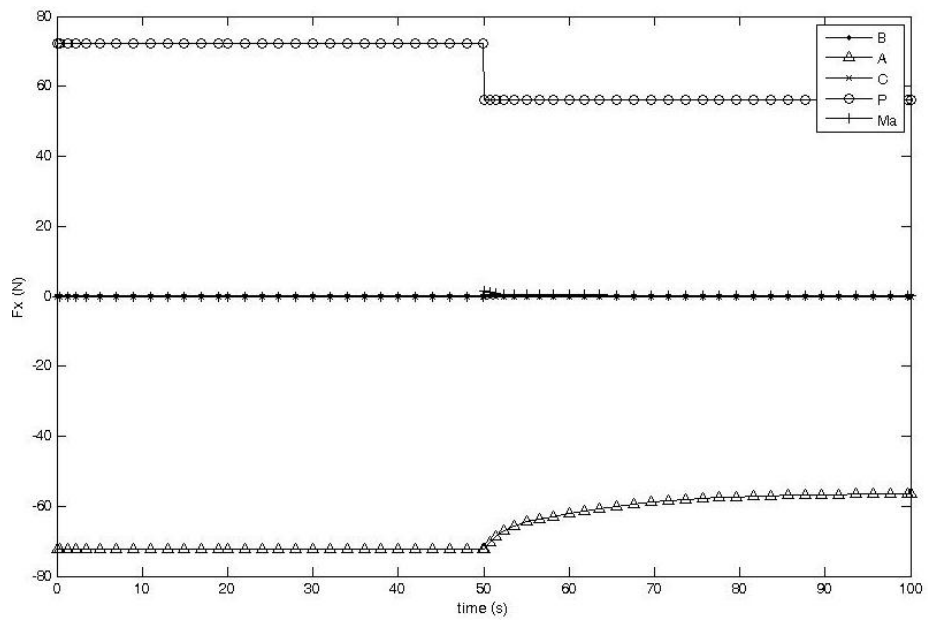


Figure 4.16: Case 4: Axial Forces

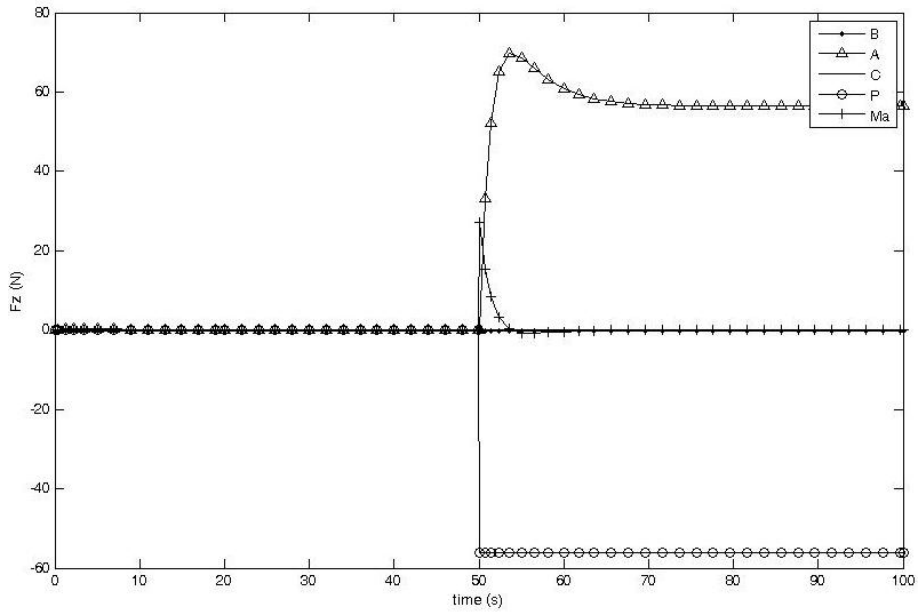


Figure 4.17: Case 4: Normal Force

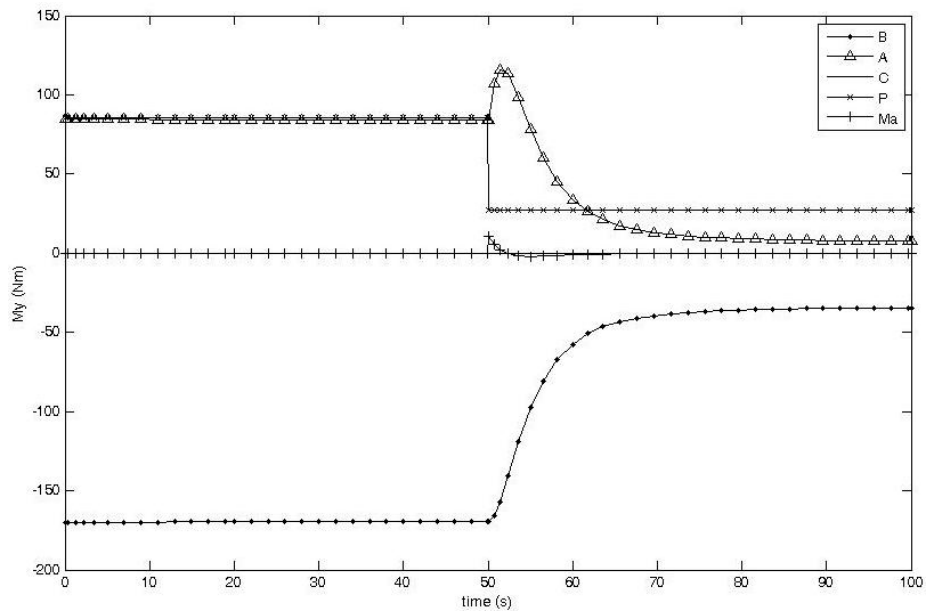


Figure 4.18: Case 4: Pitching Moments

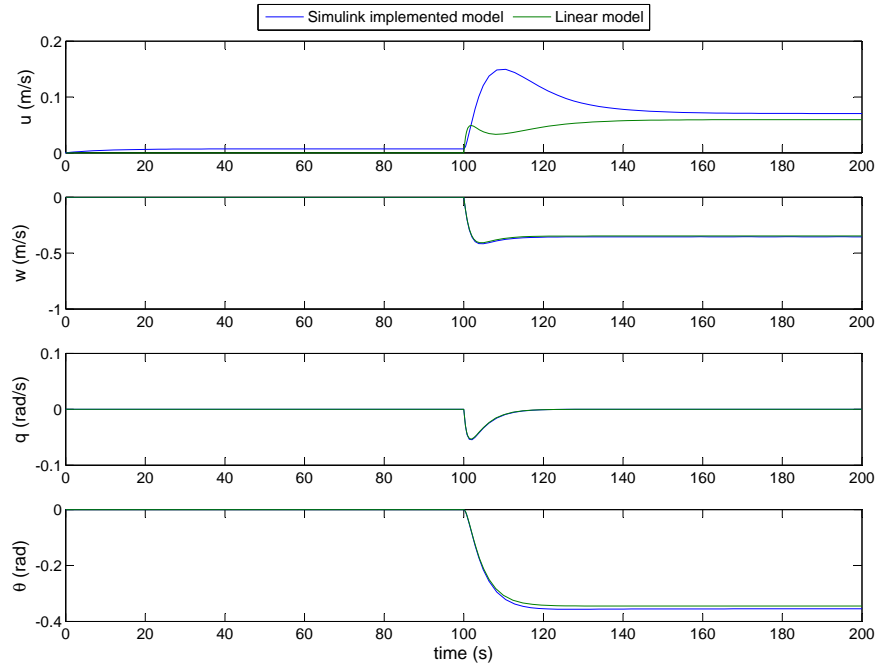


Figure 4.19: Neutral buoyancy condition: model responses comparison

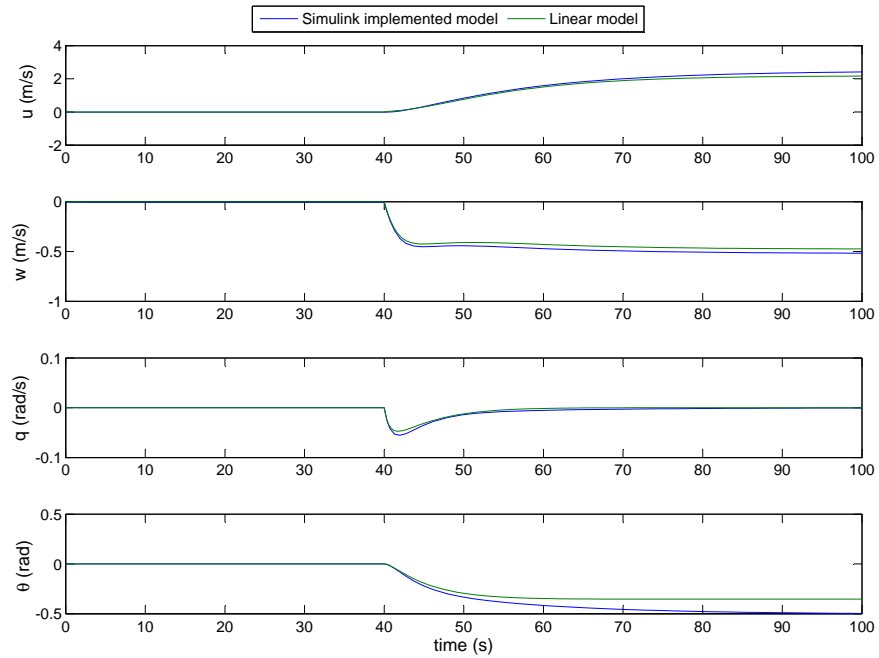


Figure 4.20: Non-neutral buoyancy condition: model responses comparison

## Chapter 5

# Six-degree-of-freedom Simulation Model

### 5.1 Implemented equation of motion

THE 6DoF simulation model for the *AIUX15* unmanned airship has been developed and implemented in Matlab/Simulink. This airframe is treated as a rigid body, symmetric respect to the center-line vertical plane, with a fixed center of gravity, as previously assumed for the 3DoF model. This assumption descend from some important features of this type of unmanned airship: the *AIUX15* is designed for constant low altitude operations and it is provided with electric engine coupled with vectored propellers, and does not require a ballonets system.

The revisited FDM for this type of airship, differently from the standard practise [9, 12, 13], presents the body-fixed reference frame having its origin attached to the  $C_G$  and not to the CV. The CV is also assumed to coincide with the gross center of buoyancy (CB), i.e. point  $C_B$  in Figures 2.2 and 2.3.

As for the 3DoF simulation model, the airship 6DoF model, given in the Eq. 5.1, includes the standard aerostatics and aerodynamics terms, and does not model the added-mass terms within the mass matrix.

$$\underset{(6 \times 6)}{\mathbf{M}} \begin{bmatrix} \dot{U} \\ \dot{V} \\ \dot{W} \\ \dot{p} \\ \dot{q} \\ \dot{r} \end{bmatrix} = \underset{(6 \times 1)}{\mathbf{F}_d} + \underset{(6 \times 1)}{\mathbf{A}} + \underset{(6 \times 1)}{\mathbf{G}} + \underset{(6 \times 1)}{\mathbf{C}} + \underset{(6 \times 1)}{\mathbf{P}} + \underset{(6 \times 1)}{\mathbf{F}_{add}} \quad (5.1)$$

in the above equation, the matrix dimensions are indicated for clarity.

On the left-hand side of system (5.1) the term  $\mathbf{M}$  is a generalized mass matrix, and  $[U, V, W, p, q, r]^T$  is the vector of state variables, i.e. the airship velocity and angular velocity components on the body axes. On the right-hand side, the term  $\mathbf{A}$  is an aerodynamic generalized force vector depending on the velocity and on angular velocity. The quantity  $\mathbf{C}$  is a control generalized force vector depending also on the aero-surface deflections at the tail. The term  $\mathbf{G}$  is a generalized gravity force vector depending on the direction cosines ( $\lambda_{13}, \lambda_{23}, \lambda_{33}$ )

of the body frame with respect to the inertial frame. The term  $\mathbf{F}_d$  is a dynamic-effect generalized force vector depending on  $(U, V, W, p, q, r)$ . The added mass effects are not built into the mass matrix of the airship [12, 13] but are modeled as external inertial forces and moments in the vector  $\mathbf{F}_{\text{add}}$ . The generalized added mass force, occurring in accelerated flight, depend on the velocity and angular velocity rates  $(\dot{U}, \dot{V}, \dot{W}, \dot{p}, \dot{q}, \dot{r})$ .

The available forces and the moments are calculated as:

$$\begin{cases} D = 1/2 \rho V_a^2 S C_D \\ Y = 1/2 \rho V_a^2 S C_Y \\ L = 1/2 \rho V_a^2 S C_L \end{cases} \quad \begin{cases} \mathcal{L} = 1/2 \rho V_a^2 S c C_{\mathcal{L}} \\ \mathcal{M} = 1/2 \rho V_a^2 S c C_{\mathcal{M}} \\ \mathcal{N} = 1/2 \rho V_a^2 S c C_{\mathcal{N}} \end{cases} \quad \text{with } V_a^2 = U^2 + V^2 + W^2 \quad (5.2)$$

They are referred to the wind axis system centered at the CV (point  $C_B$ ). In order to evaluate the aerodynamic actions in the body fixed reference frame centered in  $C_G$  (see Figure 2.2), a transport of the forces was introduced into the model (recalling that  $\psi = -\beta$ ), by means also of a rotation matrix:

$$R_\alpha R_{-\beta} = \begin{bmatrix} \cos \alpha \cos \beta & -\cos \alpha \sin \beta & -\sin \alpha \\ \sin \beta & \cos \beta & 0 \\ \sin \alpha \cos \beta & -\sin \alpha \sin \beta & \cos \alpha \end{bmatrix} \quad (5.3)$$

In the Eq. 5.4 and Eq. 5.5 are shown the aerodynamic coefficients, in the body axes, by means of the rotation matrix:

$$\begin{bmatrix} C_X \\ C_Y \\ C_Z \end{bmatrix}_{\text{body axes}} = R_\alpha R_{-\beta} \begin{bmatrix} -C_D \\ C_Y \\ -C_L \end{bmatrix}_{\text{wind axes}} \quad (5.4)$$

$$\begin{bmatrix} C_{\mathcal{L}} \\ C_{\mathcal{M}} \\ C_{\mathcal{N}} \end{bmatrix}_{\text{body axes}} = R_\alpha R_{-\beta} \begin{bmatrix} C_{\mathcal{L}} \\ C_{\mathcal{M}} \\ C_{\mathcal{N}} \end{bmatrix}_{\text{wind axes}} + \begin{bmatrix} C_Y a_z \\ C_D a_z \\ 0 \end{bmatrix} \quad (5.5)$$

The aerodynamic database for the purpose of the airship FDM, has been collected on the basis of full three-dimensional RANS computations. The control coefficients have been calculated assuming as parameters the aero-surface deflections  $\delta_a$  and  $\delta_r$ . In Section 2.3 are reported the the airship aerodynamic coefficient variations at different control surface deflections for both the empennage configurations, obtained by the CFD computations. They enable the calculation of the aerodynamic forces and moments variations as follows:

$$\begin{cases} \Delta D = 1/2 \rho V_a^2 S \Delta(C_D) \\ \Delta Y = 1/2 \rho V_a^2 S \Delta(C_Y) \\ \Delta L = 1/2 \rho V_a^2 S \Delta(C_L) \end{cases} \quad \begin{cases} \Delta \mathcal{L} = 1/2 \rho V_a^2 S c \Delta(C_{\mathcal{L}}) \\ \Delta \mathcal{M} = 1/2 \rho V_a^2 S c \Delta(C_{\mathcal{M}}) \\ \Delta \mathcal{N} = 1/2 \rho V_a^2 S c \Delta(C_{\mathcal{N}}) \end{cases} \quad (5.6)$$

These are the control generalized forces that populate the column matrix  $\mathbf{C}$  in equation (5.1).

The vector  $\mathbf{P}$  in equation (5.1) depends on the propulsive model. The airship propulsive system is characterized by two tilting propellers powered by

an electrical engine. In the general case the thrust vector has a varying direction, always belonging to the body-fixed longitudinal plane  $XZ$ . The propulsive actions are then given by the following:

$$\begin{cases} X_p = 2T \cos \mu \\ Z_p = -2T \sin \mu \\ \mathcal{M}_p = 2T(d_z \cos \mu - d_x \sin \mu) \end{cases} \quad \text{with } Y_p = \mathcal{L}_p = \mathcal{N}_p = 0 \quad (5.7)$$

In our simulation model the propeller thrust has been assumed as a constant and held aligned with the airship longitudinal axis  $X$ , assuming a null value of the angle  $\mu$  (see Figure 2.2).

The airship thrusters are two ducted fans mounted on the gondola. This type of propulsion system affects the aerodynamic flow in the vicinity of the airship tails. The global effect is modelled by taking into account the increase of tail efficiency. The following multiplicative factor[8]:

$$f_{\text{tail}} = \left( 1 + \sqrt{1 + \frac{T}{4\rho S_{\text{prop}} V_a^2}} \right)^2 \quad (5.8)$$

has been introduced in the simulation model as an enhanced tail authority factor. This means that the input variables  $\delta_a$  and  $\delta_r$  are replaced by  $f_{\text{tail}}\delta_a$  and  $f_{\text{tail}}\delta_r$  respectively.

The airship is assumed to be neutral buoyant and statically balanced (buoyancy equals weight). Regarding to the usual weight arrangement, the airship with the gondola under the envelope, has its center of gravity beneath the center of volume. This condition is required for the buoyant vehicles in order to ensure the static stability. The gravitational actions, represented by the column matrix  $\mathbf{G}$  in equation (5.1), depend on the buoyant lift magnitude  $B$ . The latter is a function of the helium purity  $\eta_h$  and density  $\rho_h$ , and of the air density  $\rho$ . The air density is assumed constant according to the low operational altitude of the airship. The expressions that give the six elements of  $\mathbf{G}$  are the following:

$$\begin{cases} X_g = -\sin \theta (mg - B) \\ Y_g = \cos \theta \sin \phi (mg - B) \\ Z_g = \cos \theta \cos \phi (mg - B) \end{cases} \quad \begin{cases} \mathcal{L}_g = -\cos \theta \sin \phi b_z B \\ \mathcal{M}_g = -\sin \theta b_z B \\ \mathcal{N}_g = 0 \end{cases} \quad (5.9)$$

where  $B$  has been still defined in Eq. 4.6

Finally, on the right-hand side of equation (5.1) the added mass effects are modelled as external inertial forces and moments. For this type of airship the added mass effects can be reasonably approximated by considering only the envelope volume. Applying the theoretical formulas for the prolate ellipsoid [4], it is possible to evaluate the added mass terms of the airship with respect to

the CV as follows:[12]

$$\begin{cases} X_{\text{add}} = \dot{X}_{\dot{U}}\dot{U} + \dot{Z}_{\dot{W}}Wq - \dot{Y}_{\dot{V}}Vr - \dot{X}_{\dot{q}}\dot{q} \\ Y_{\text{add}} = \dot{Y}_{\dot{V}}\dot{V} + \dot{X}_{\dot{U}}Ur - \dot{Z}_{\dot{W}}Wp - \dot{Y}_{\dot{p}}\dot{p} - \dot{Y}_{\dot{r}}\dot{r} \\ Z_{\text{add}} = \dot{Z}_{\dot{W}}\dot{W} - \dot{X}_{\dot{U}}Uq - \dot{Y}_{\dot{V}}Vp - \dot{Z}_{\dot{q}}\dot{q} \end{cases} \quad (5.10)$$

$$\begin{cases} \mathcal{L}_{\text{add}} = \dot{\mathcal{L}}_{\dot{p}}\dot{p} - \dot{\mathcal{L}}_{\dot{V}}\dot{V} - \dot{\mathcal{L}}_{\dot{r}}\dot{r} \\ \mathcal{M}_{\text{add}} = \dot{\mathcal{M}}_{\dot{q}}\dot{q} - \dot{\mathcal{M}}_{\dot{W}}\dot{W} - \dot{\mathcal{M}}_{\dot{U}}\dot{U} \\ \mathcal{N}_{\text{add}} = \dot{\mathcal{N}}_{\dot{r}}\dot{r} - \dot{\mathcal{N}}_{\dot{V}}\dot{V} - \dot{\mathcal{N}}_{\dot{p}}\dot{p} \end{cases}$$

The added mass actions  $X_{\text{add}}, Y_{\text{add}}, \dots, \mathcal{N}_{\text{add}}$  given by (5.10) occur in accelerated flight and are given by a sum of terms proportional to the airship linear and angular accelerations and angular velocities (state variables and their derivatives). The coefficients  $\dot{X}_{\dot{U}}, \dot{Z}_{\dot{W}}, \dots, \dot{\mathcal{N}}_{\dot{p}}$  in equations (5.10) are calculated on the basis of the envelope geometry and most of them are zero for axial-symmetrical bodies (see Appendix A). The above added mass actions are referred to the CV. For the purpose of our flight dynamics model they have been transported to the  $C_G$ .

## 5.2 The implemented Simulink model

The 6DoF implemented model has been developed and checked by means of the 3DoF model introduced in the Section 4.2.

In order to model the two different airship configurations, it is possible to use the same interface by only changing the Matlab initialization file, in which are defined all the variables declared in the Simulink model.

In the following figures are reported some pictures of the implemented 6DoF Simulink model for the airship. The Figure 5.1 shows the main part of the model, with the *6DoF Euler Angle* Simulink built-in block and the subsystems that evaluate all the external forces and moments acting on the airship.

The connections between subsystem are handled by means of *Go-to/From-to* Simulink tags. Both the aerodynamic and the control actions are built from an aerodynamic coefficient database organized in look-up tables (see Figure 5.2).

In Figure 5.4 and Figure 5.5 are respectively shown the propulsive and the added mass subsystems, implementing the corresponding Eq. 5.7 and Eq. 5.10.

It's to be noticed that in the gravitational subsystem (see Figure 5.3), differently from the Eq. 5.9, are modeled only the buoyancy actions as the weight effects are evaluated within the *6DoF Euler Angle* block.

Finally the open loop responses to several input commands, from the trim condition regarding the operational speed of 40 km/h at sea level, have been obtained and analyzed. Some results for the cross configuration airship are reported in the Figures 5.6, 5.7, 5.8, 5.9 and 5.10; the term  $\Delta T$  represents the percentage increase in thrust. As could be noticed, the airship responses are all exponential type, with the exception of the rolling motions.

In order to check the 6DoF model was also verified the correct matching of the longitudinal behavior with the previously defined 3DoF simulation model.

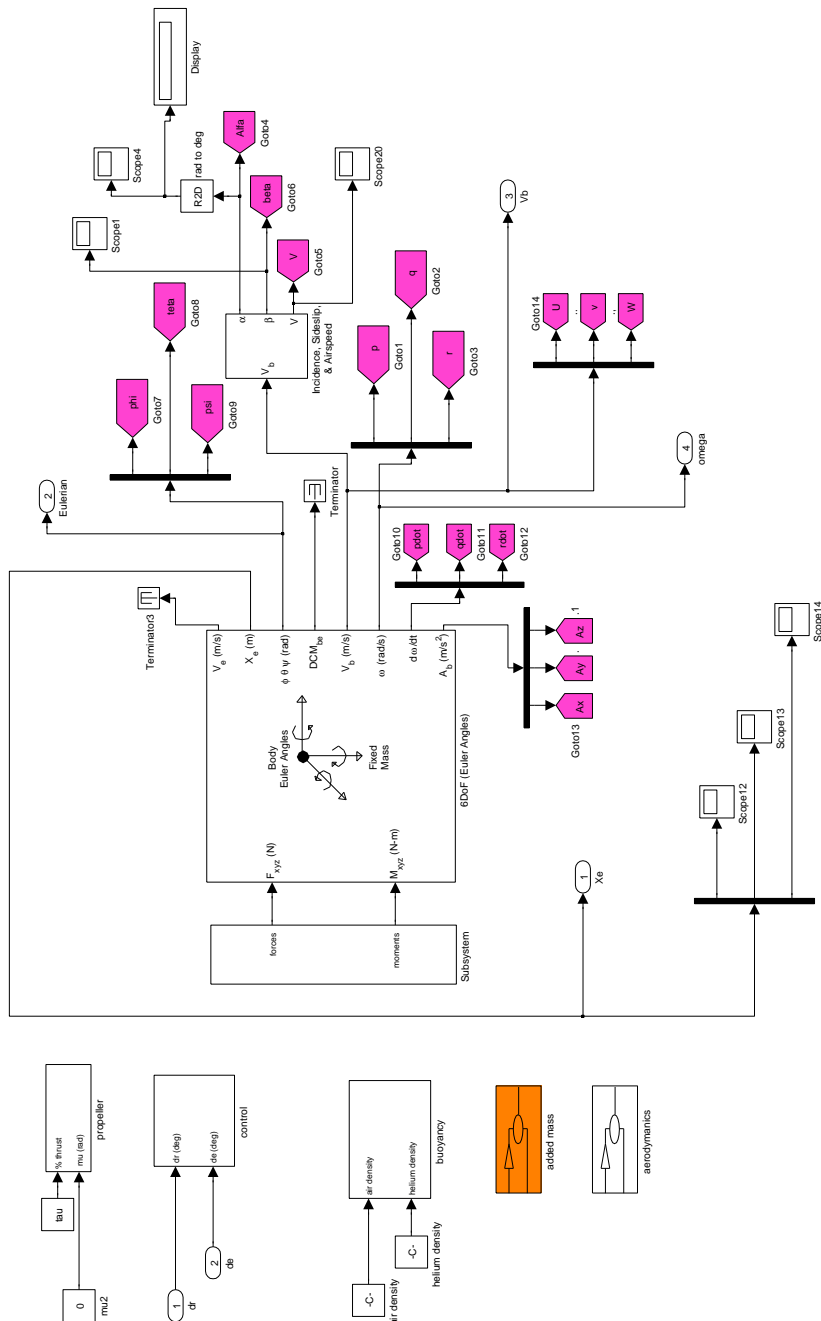


Figure 5.1: 6DoF implemented Simulink model

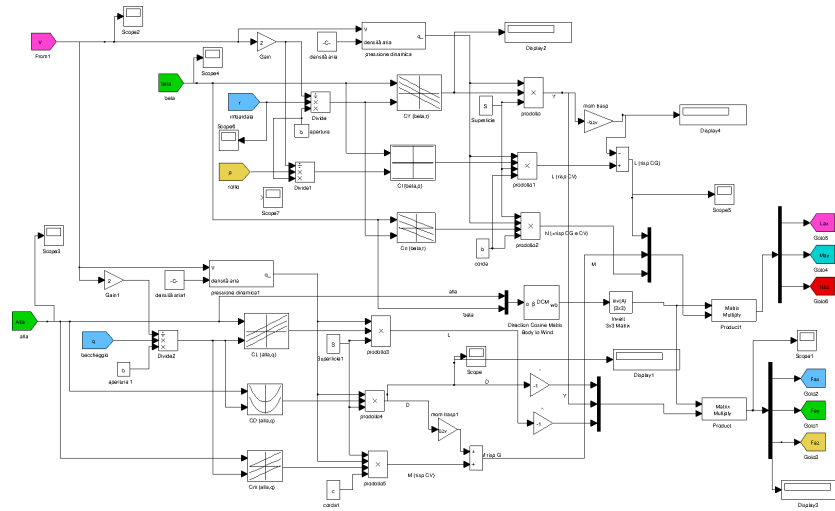


Figure 5.2: 6DoF aerodynamic subsystem

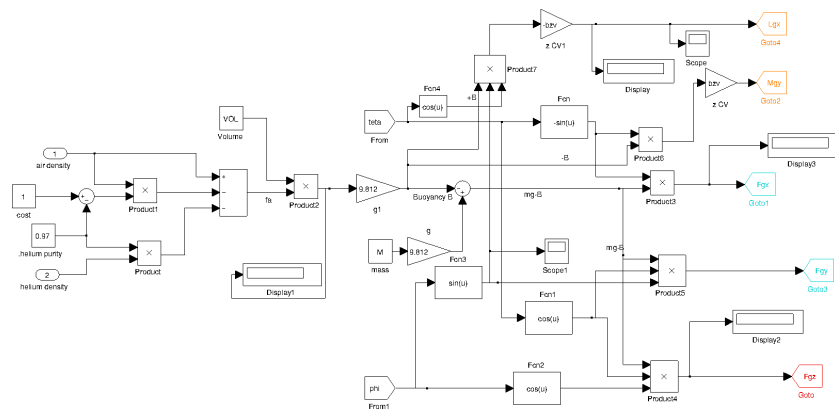


Figure 5.3: 6DoF gravitational subsystem

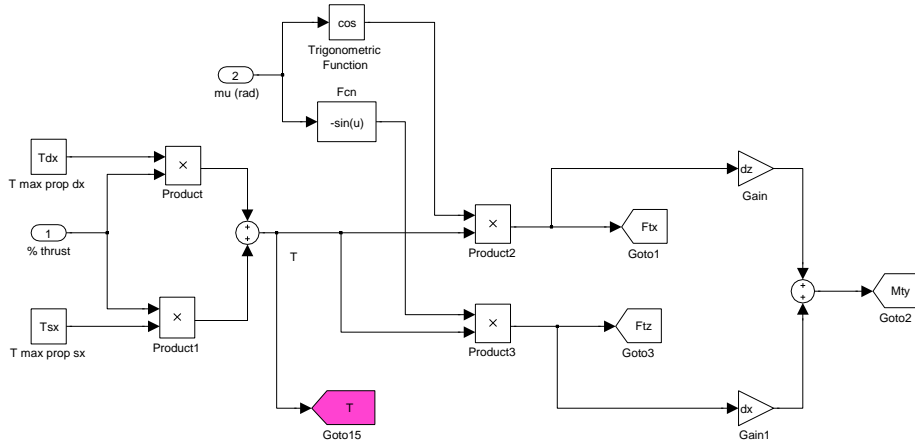


Figure 5.4: 6DoF propulsive subsystem

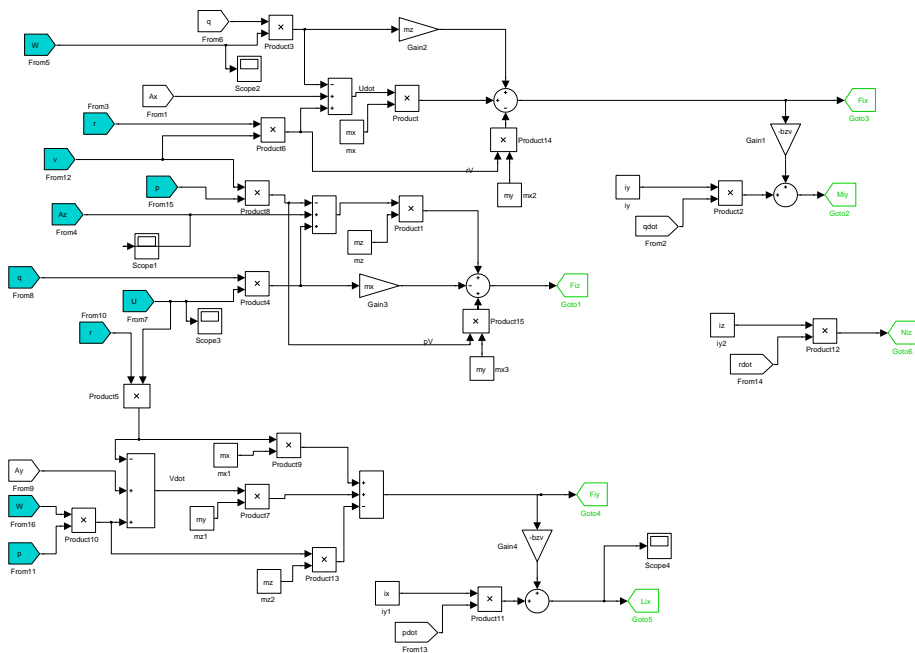


Figure 5.5: 6DoF added mass subsystem

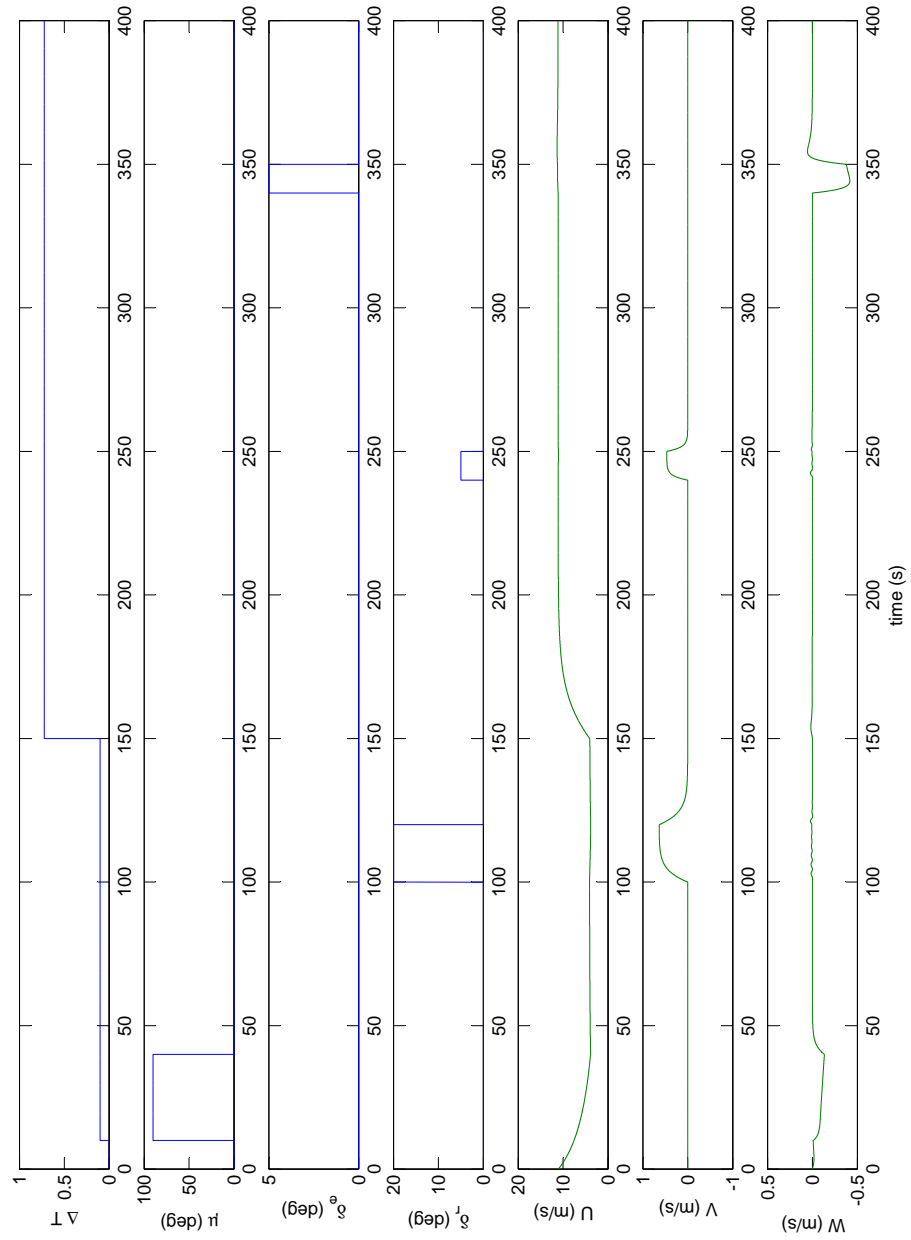


Figure 5.6: 6DoF implemented model responses – velocity in the body-fixed frame

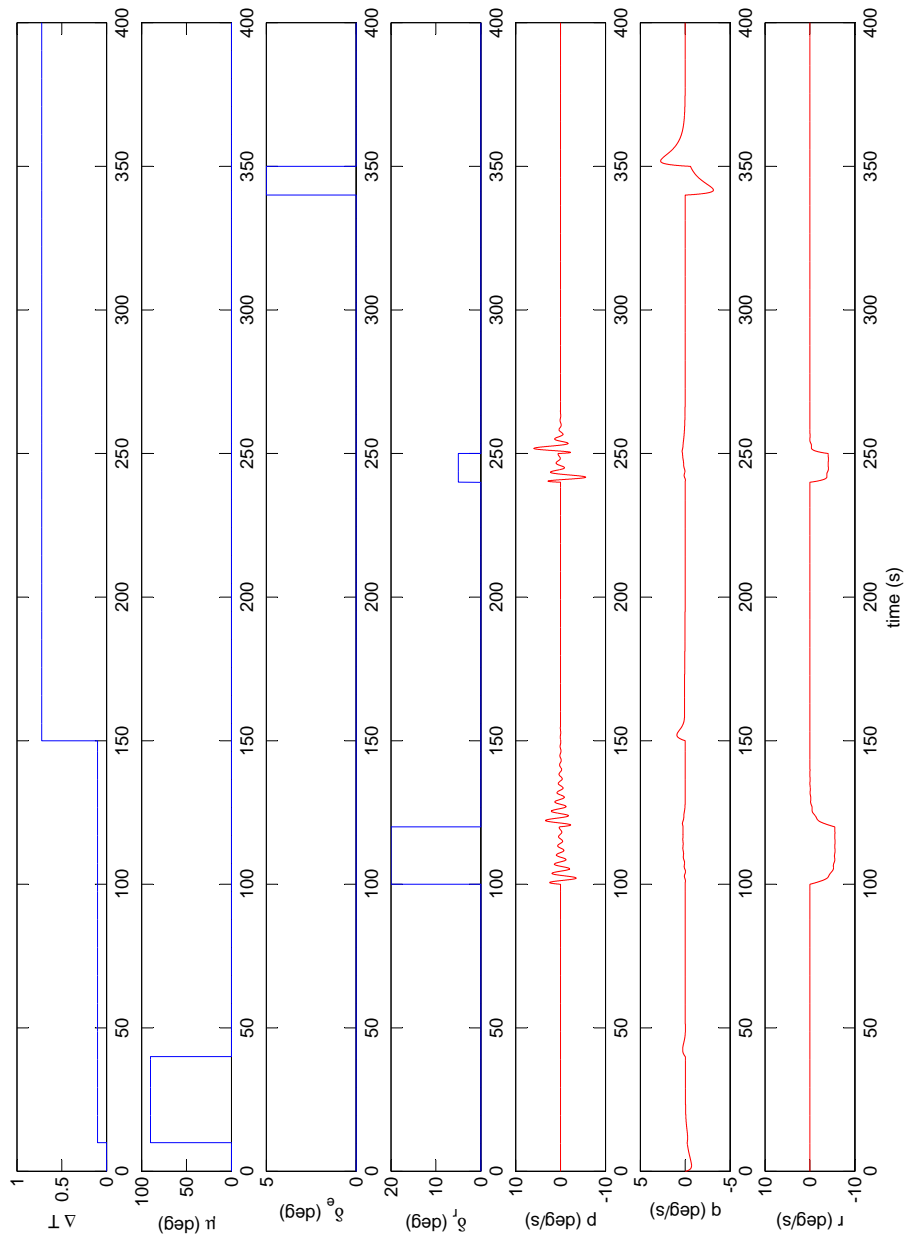


Figure 5.7: 6DoF implemented model responses – angular rates in body-fixed axes

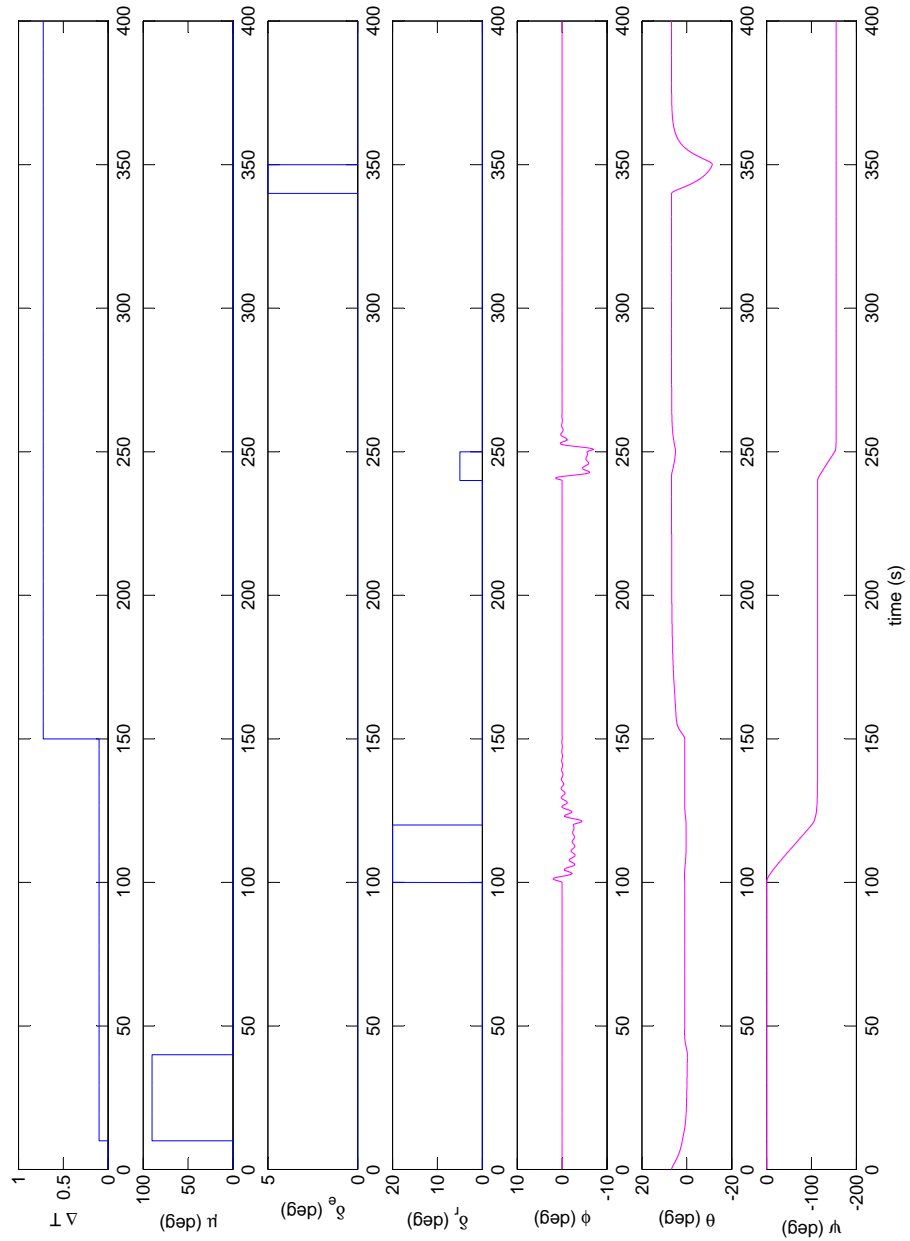


Figure 5.8: 6DoF implemented model responses – Euler rotation angles

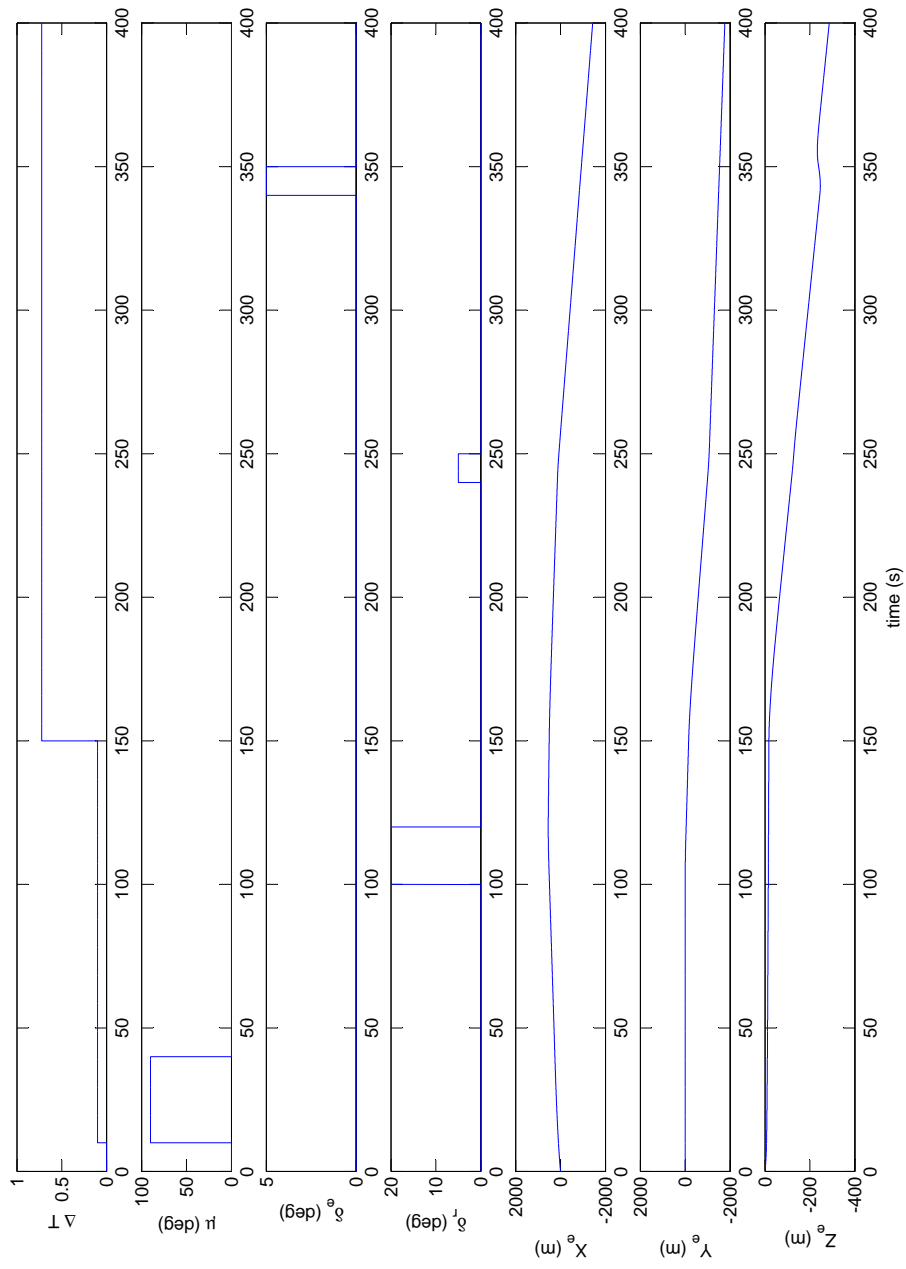


Figure 5.9: 6DoF implemented model responses – position in inertial axes

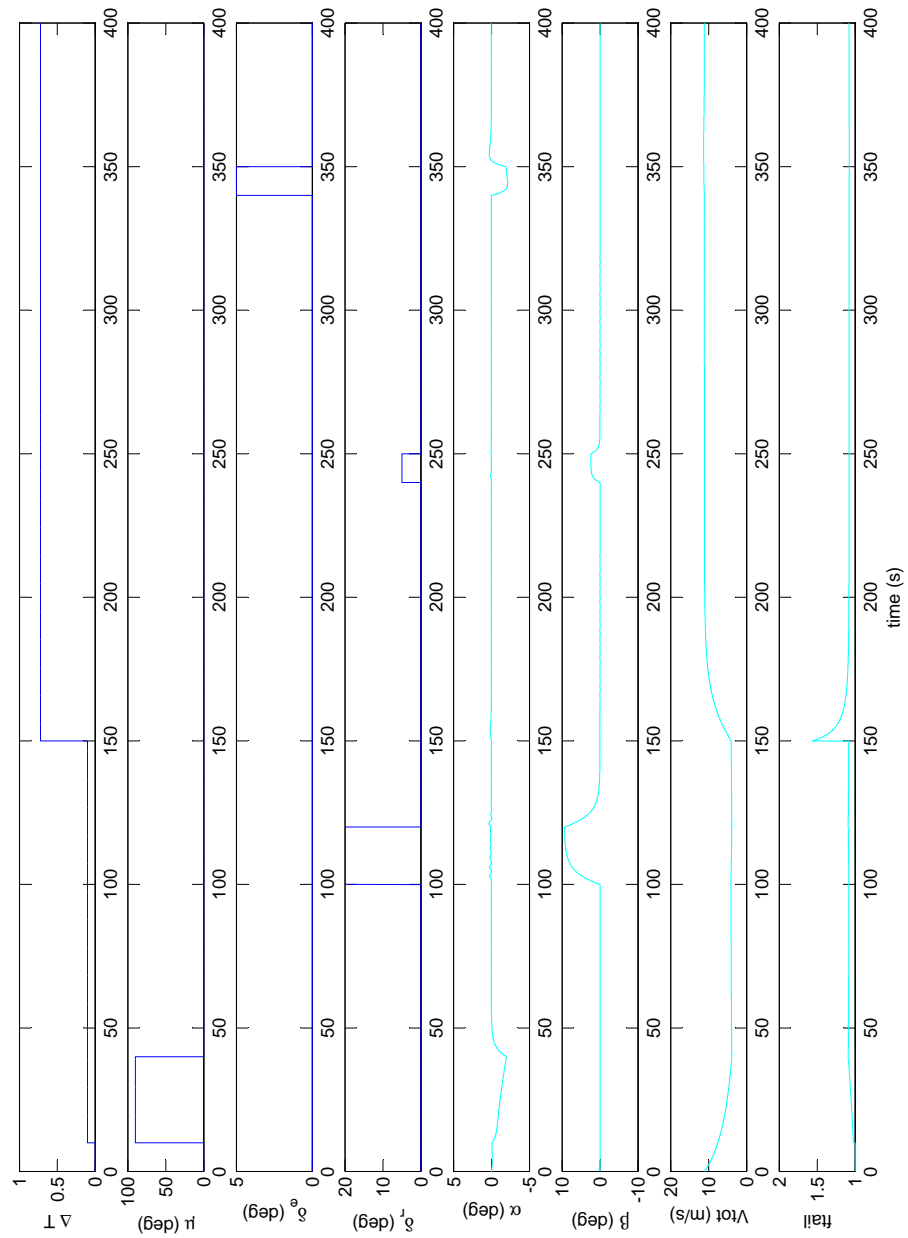


Figure 5.10: 6DoF implemented model responses – incidence, airspeed and *ftail*

## Chapter 6

# Airship Control in Steady Air

### 6.1 Implemented equation of motion

ONE of the main goals of the research concerned the achievement of a satisfying roll control system that reduces the airship high-frequency oscillatory motions, in a stationary atmosphere. These are an annoying source of trouble for the video and picture acquisition systems, which represent the typical payload of this kind of vehicles. For a typical configuration airship, the oscillatory rolling motions arise as undesired effect from the rudder deflections (due to the  $C_G$  offset with respect to the envelope longitudinal centerline). In our analysis (see for example Figure 5.7 and Figure 5.8) undesired oscillatory rolling motions have been found for both the configurations.

Two feedback control algorithms, regarding two different approaches have been developed. The airship lateral-directional closed-loop control, for both the tails configurations, has been carried out by acting on the rudders control only.

Then a feedback control law on both the rudders and the ailerons have been implemented after introducing an aileron control into the simulation model. For ailerons it means the elevators in the case of the cross configuration, when they are deflected anti-symmetrically. In the case of the inverted Y configuration the ailerons are the movable aerosurfaces placed on the two lower empennages.

The closed-loop flight control has been achieved by means of the state-space approach. The state space representation of the dynamic system is carried out by linearizing the 6DoF model around the reference equilibrium condition. Applying the small disturbance theory for airships [12] the longitudinal and lateral equations are decoupled and written in the state space form. The state space lateral control problem is formulated for both the above discussed approaches as follows:

$$\begin{aligned} \dot{\mathbf{x}} &= \underset{(4 \times 1)}{\mathbf{A}} \mathbf{x} + \underset{(4 \times 1)}{\mathbf{B}} \delta_r \\ \text{(I approach, only } \delta_r) \end{aligned} \quad (6.1)$$
$$\dot{\mathbf{x}} = \left( \underset{(4 \times 4)}{\mathbf{A}} - \underset{(4 \times 1)(1 \times 4)}{\mathbf{B}} \mathbf{k}^T \right) \mathbf{x} + \underset{(4 \times 1)}{\mathbf{B}} \delta_r$$

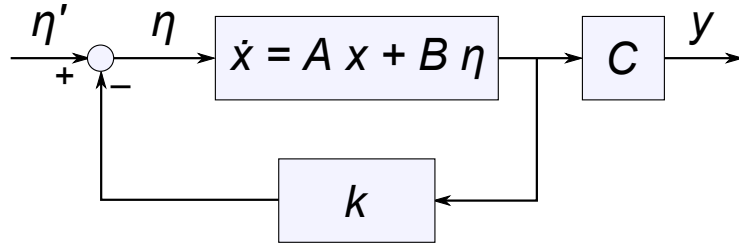


Figure 6.1: Block diagram of the linear system with state feedback.

Table 6.1: Control characteristics and controller gains

Airship Configuration	$M_o$	$T_s$	Controller gains $\mathbf{k}^T$	Controller gains $\mathbf{k}_p^T$
cross	5%	3 s	[23.94 17.37 -45.06 102.05]	$\begin{bmatrix} 32.84 & -254.68 & -131.88 & 43.00 \\ 10.54 & -33.36 & -20.55 & -20.38 \end{bmatrix}$
inverted Y	5%	3 s	[26.86 12.39 44.53 74.17]	$\begin{bmatrix} -67.55 & 32.78 & -133.14 & 96.02 \\ -21.70 & -2.61 & 21.24 & 56.22 \end{bmatrix}$

$$\dot{\mathbf{x}} = \mathbf{A} \mathbf{x} + \mathbf{B} \boldsymbol{\eta}$$

$(4 \times 1) \quad (4 \times 4)(4 \times 1) \quad (4 \times 2)(2 \times 1)$

(II approach,  $\boldsymbol{\eta} = [\delta_a \ \delta_r]^T$ )

$$\dot{\mathbf{x}} = \left( \mathbf{A} - c \mathbf{B} \mathbf{k}_p^T \right) \mathbf{x} + \mathbf{B} \boldsymbol{\eta}$$

$(4 \times 1) \quad (4 \times 4) \quad (4 \times 2)(2 \times 4) \quad (4 \times 1) \quad (4 \times 2)(2 \times 1)$

(6.2)

In the above equations the state vector has been defined as  $\mathbf{x} = [v \ p \ r \ \phi]^T$ . In the first approach—system (6.1)—there is only the rudder deflection  $\delta_r$ , i.e. the input vector is  $\boldsymbol{\eta} = [\delta_r]$ , a  $1 \times 1$  matrix. In the second approach—system (6.1)—the inputs are  $\boldsymbol{\eta} = [\delta_a \ \delta_r]^T$ . In the latter case the constant  $c = 1$  was set. These models are schematically represented in Figure 6.1.

## 6.2 The pole placement method

The controller gains have been determined according to the pole-placement method. The knowledge of the poles that guarantee the desired behavior of the system is linked to the design criteria of the controller, such as the overshoot and the settling time, from which the damping and the real part of the poles descend. The design criteria of the closed loop controllers have been set as: Overshoot ( $M_o$ ) less than 5% and Settling Time ( $T_s$ ) less than 3 s, that lead respectively to a damping coefficient of 0.7 and a pole real part of  $-1.94$ .

The feedback control laws with the controller gains obtained from the state space linear analysis (see Table 6.1) have been subsequently introduced in the simulation models to compare the closed-loop results to the open-loop responses. In order to avoid deflections at which the control surfaces do not work properly (beyond ranges), saturation blocks have been introduced in the simulation model, imposing upper and lower limits on the input signal from the feedback control law. These limits are assumed to be  $-25^\circ$  and  $25^\circ$ , that are the surface deflections at which the maximum absolute values of the aerodynamic coefficients are achieved.

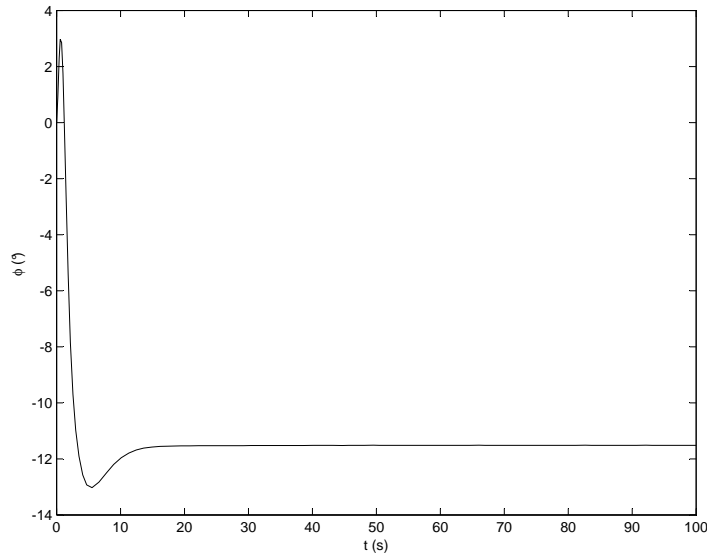


Figure 6.2: simulink roll response with feedback control to an initial rudder step of  $25^\circ$

### 6.3 Applications and results

The two control strategies have been applied to both the airship tail configurations for different initial rudder deflections. The first roll control strategy, involving only the rudders, achieves for both the configurations a reduction of the oscillatory motions. This control strategy continues to reduce the oscillatory rolling motion up to  $25^\circ$  of initial rudder deflection.

In Figures 6.2 and 6.3 are shown some examples for the cross configuration; the same is true for the three empennage airship. The second control strategy involving both rudder and ailerons, is considered to be not satisfactory especially for the four empennage airship; moreover in some conditions, even it could worsen the stability characteristics of the airship that could lead to instability of the feedback control system. Regarding to the cross configuration for initial rudder step greater than about  $10^\circ$ , the control response denotes an undamped harmonic behavior: this is linked to the saturation features on the ailerons that cuts the deflections beyond range (see Figure 6.4 and Figure 6.5). The same instability occurs for the inverted Y configuration, but for greater initial rudder step, as the aileron control power for this configuration is comparable to the rudder one. In Figure 6.6 and Figure 6.7 are shown, respectively for the four and three empennages airship, the lateral-directional closed loop responses to a unit rudder step input, for both the control approaches, compared to the open

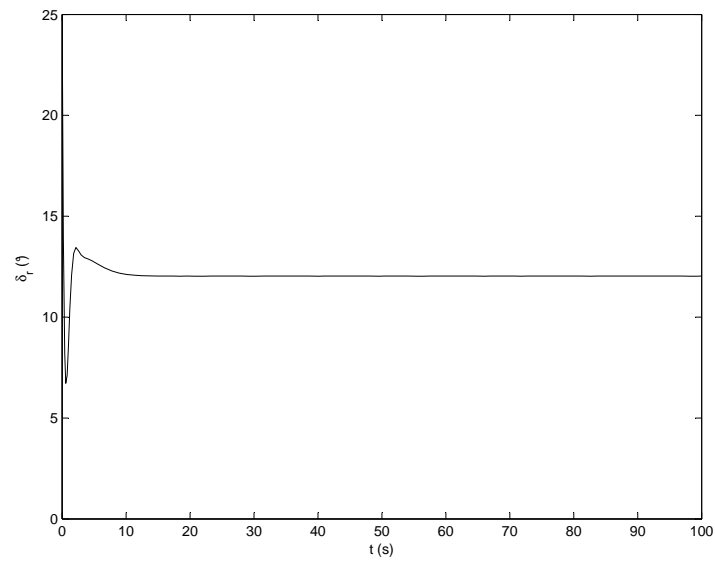


Figure 6.3: rudder input with feedback control, from the initial step of  $25^\circ$

loop behavior.

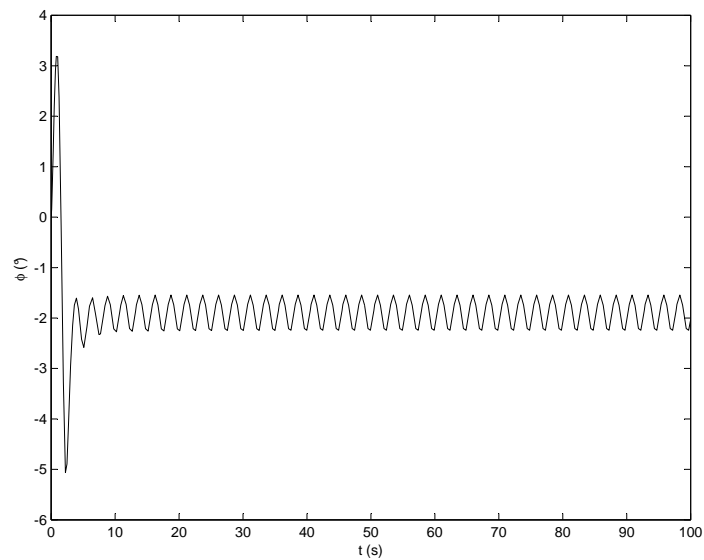


Figure 6.4: simulink roll response with feedback control to an initial rudder step of  $15^\circ$ , aileron case

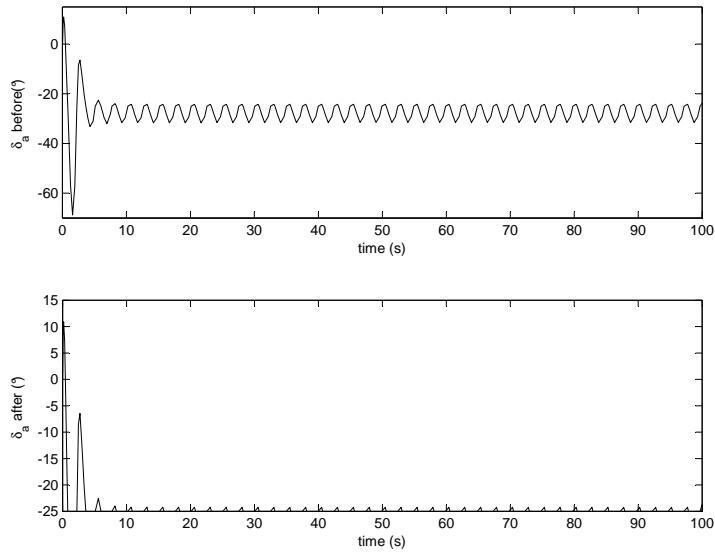


Figure 6.5: aileron deflection after and before the saturation block

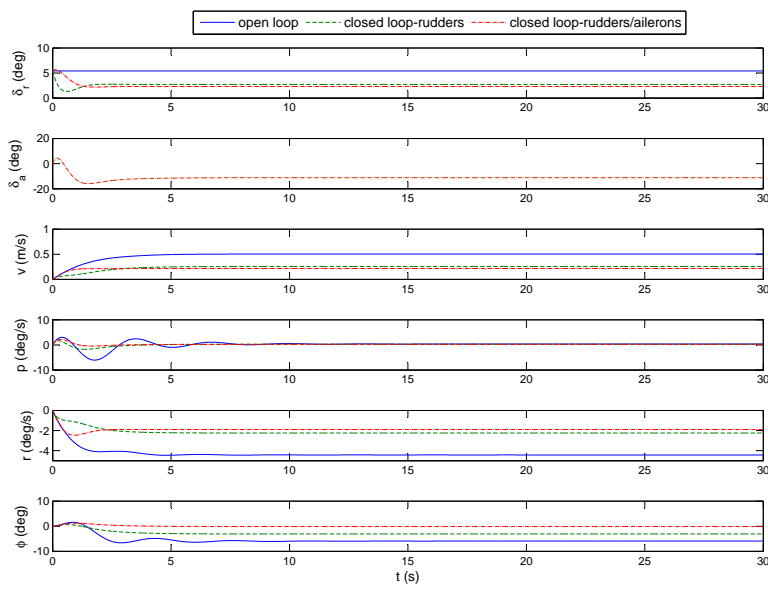


Figure 6.6: Cross configuration lateral responses without and with control

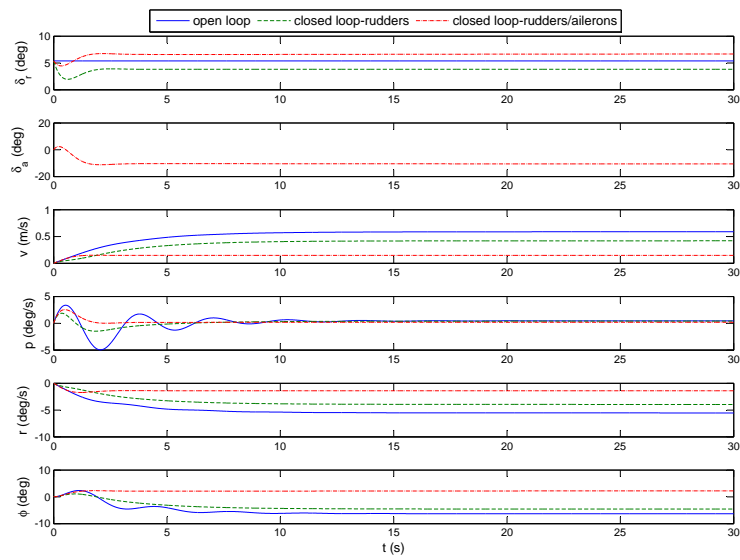


Figure 6.7: Inverted Y configuration lateral responses without and with control

## Chapter 7

# Airship Control in Turbulent Air

### 7.1 The turbulence model

IN the second part of the research work regarding the airship lateral-directional control, the atmospheric turbulence model has been introduced.

The turbulence is a random process which describes the chaotic motion of the air, in terms of velocity component fluctuations superposed on a mean wind. For the purpose of the control application the mean wind velocity has been set to zero.

The model chosen to represent the atmospheric turbulence is based on the Power Spectral Density (PSD) function (7.1) of Dryden.[7, 8] The Dryden Continuous Wind Turbulence Model Simulink built-in block has been used to implement the turbulent air into the simulation; this block is based on the Dryden spectral representation( see Eq. 7.1) to add turbulence to the aerospace model by passing band-limited white noise through appropriate forming filters.

$$\begin{aligned}\Phi_u(\omega) &= \frac{2\sigma_u^2 L_u}{\pi V} \frac{1}{1 + (L_u \omega / V)^2} & \Phi_p(\omega) &= \frac{\sigma_w^2}{L_w V} \frac{0.8(\pi L_w / 4b)^{1/3}}{1 + (4b\omega / \pi V)^2} \\ \Phi_v(\omega) &= \frac{\sigma_v^2 L_v}{\pi V} \frac{1 + 3(L_v \omega / V)^2}{[1 + (L_v \omega / V)^2]^2} & \Phi_r(\omega) &= \frac{(\omega / V)^2}{1 + (3b\omega / \pi V)^2} \Phi_v(\omega) \\ \Phi_w(\omega) &= \frac{\sigma_w^2 L_w}{\pi V} \frac{1 + 3(L_w \omega / V)^2}{[1 + (L_w \omega / V)^2]^2} & \Phi_q(\omega) &= \frac{(\omega / V)^2}{1 + (4b\omega / \pi V)^2} \Phi_w(\omega)\end{aligned}\tag{7.1}$$

The intensity of turbulence is assumed as isotropic, having a maximum value of  $\sigma_u = \sigma_v = \sigma_w = 7$  m/s. [8] An unitary noise seeds has been also assumed and the aircraft wingspan that figures in the above equation, has been referred to the airship envelope volume:  $b = \nabla^{1/3}$ . The scale for the wave length of the atmospheric turbulence has been chosen according to the low altitude model. [7]

The vector of the wind velocity plus gust is used to calculate the airship air velocity affecting the aerodynamic and control actions.

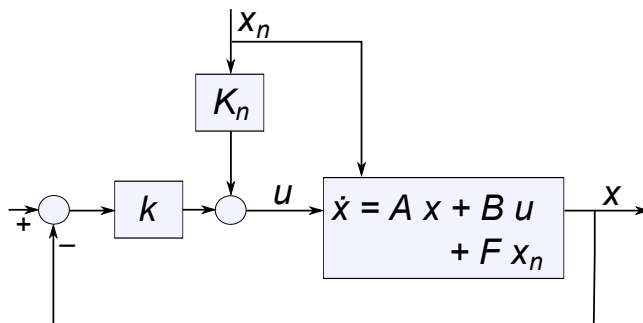


Figure 7.1: Block diagram of the linear system with turbulence and state feedback.

## 7.2 The pole placement with noise

In order to reduce the lateral-directional motions of the airship in turbulence, the two control strategies have been fit to this more realistic scenario. The pole placement method with noise [6] has been applied at first to the control strategy that uses only the rudders; the state space representation with turbulence has been written as follows:

$$\dot{\mathbf{x}} = \mathbf{A} \mathbf{x} + \mathbf{B} u + \mathbf{F} \mathbf{x}_n \quad (7.2)$$

$(4 \times 1) \quad (4 \times 4)(4 \times 1) \quad (4 \times 1) \quad (4 \times 4)(4 \times 1)$

The noise coefficient matrix  $\mathbf{F}$  has been assumed as an identity matrix, while the noise vector  $\mathbf{x}_n$  represents the turbulence effect, acting as an input for the closed-loop system. A schematic diagram of the full-state feedback regulator with noise is shown in Figure 7.1.

To place the closed-loop poles at desired locations while counteracting the effect of the noise, a full-state feedback regulator has been designed, based on the following control-law:

$$u = -\mathbf{K} \mathbf{x} - \mathbf{K}_n \mathbf{x}_n \quad (7.3)$$

$(1 \times 4)(4 \times 1) \quad (1 \times 4)(4 \times 1)$

The state space representation in turbulence has been carried out also for the control approach involving both rudder and ailerons:

$$\dot{\mathbf{x}} = \mathbf{A} \mathbf{x} + \mathbf{B} \mathbf{u}_p + \mathbf{F} \mathbf{x}_n \quad (7.4)$$

$(4 \times 1) \quad (4 \times 4)(4 \times 2) \quad (4 \times 2)(2 \times 1) \quad (4 \times 4)(4 \times 1)$

Table 7.1: Controller gains with turbulence

Airship Configuration	$\mathbf{K}_n^T$	Controller gains $\mathbf{K}_{np}^T$
cross	$[-2.42 \ 8.48 \ 7.34 \ 0]$	$\begin{bmatrix} -20.20 & 48.05 & -62.17 & 0 \\ -4.71 & 13.92 & 0.29 & 0 \end{bmatrix}$
inverted Y	$[-2.73 \ 10.70 \ 14.50 \ 0]$	$\begin{bmatrix} -18.62 & 47.41 & -38.50 & 0 \\ -0.19 & 4.23 & 19.75 & 0 \end{bmatrix}$



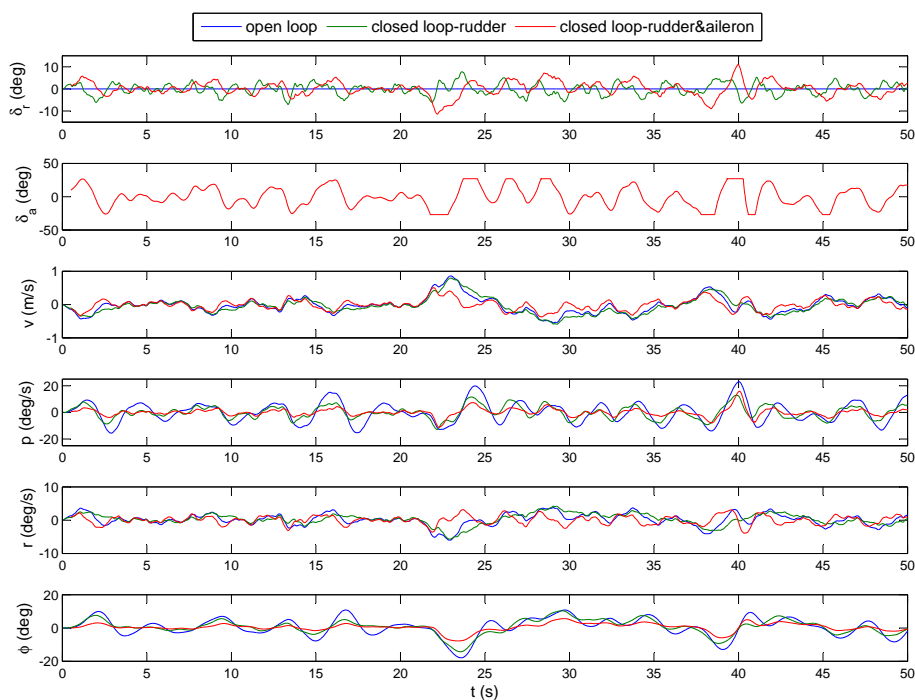


Figure 7.3: Cross configuration lateral responses in turbulence.

### 7.3 Linear quadratic optimal control

Optimal control provides an alternative design strategy producing the best possible control system for a given set of performance objectives. This is done by formulating an objective function which is to be minimized in the design process. In this case, the expenditure of the control signal energy is the main concern. For vehicles with electric control system the term  $[u(t)]^2$  represents the expenditure of battery energy and must be restricted to save the energy for long missions.

The linear quadratic regulator (LQR) is an optimal control technique that realizes the feedback control loop through the optimization of the following scalar function:

$$J = \int_0^{\infty} (\mathbf{x}^T \mathbf{Q} \mathbf{x} + \mathbf{u}^T \mathbf{R} \mathbf{u}) dt \quad (7.6)$$

The symmetrical matrices  $\mathbf{Q}$  and  $\mathbf{R}$ , respectively semi-positive and positive defined, are called “weight or cost matrices”. Assuming the dynamic system controllable, the gain vector is given by:

$$\mathbf{K} = \mathbf{R}^{-1} \mathbf{B}^T \mathbf{P} \quad (7.7)$$

where  $\mathbf{P}$  is the positive defined solution of the algebraical “Riccati equation”:

$$\mathbf{A}^T \mathbf{P} + \mathbf{P} \mathbf{A} - \mathbf{P} \mathbf{B} \mathbf{R}^{-1} \mathbf{B}^T \mathbf{P} + \mathbf{Q} = 0 \quad (7.8)$$

In this particular control problem it is convenient to introduce into the cost function definition (7.6) an exponential decay of rate. [14] Two new vectors  $\bar{\mathbf{x}} =$

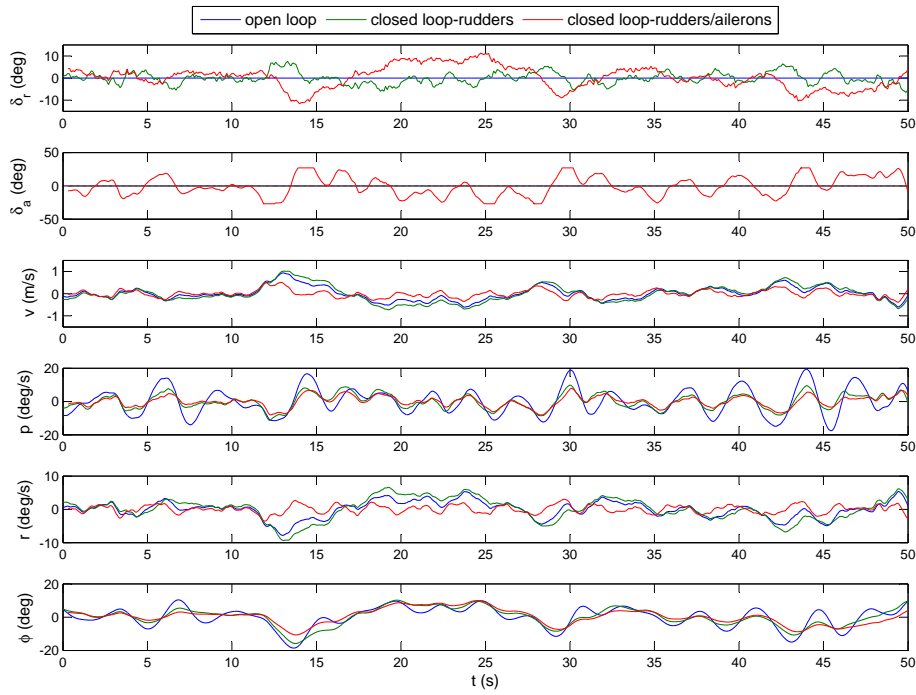


Figure 7.4: Inverted Y configuration lateral responses in turbulence.

$\mathbf{x}e^{\alpha t}$  and  $\bar{\mathbf{u}} = \mathbf{u}e^{\alpha t}$  have been introduced—which differ from the actual  $\mathbf{x}$  and  $\mathbf{u}$  by the exponential term  $e^{\alpha t}$ —that enable to redefine the scalar function  $J$  as follows:

$$J = \int_0^{\infty} e^{2\alpha t} (\mathbf{x}^T \mathbf{Q} \mathbf{x} + \mathbf{u}^T \mathbf{R} \mathbf{u}) dt \quad (7.9)$$

In this case, the plant matrix that goes into the Riccati equation (7.8), taking in account the exponential decay of rate  $\alpha$ , becomes  $(\mathbf{A} + \alpha \mathbf{I})$ . Similarly,  $\mathbf{K}$  becomes  $\mathbf{K}_{p\alpha}$ . In order to observe the influence of the exponential decay of rate on the poles of the lateral-directional dynamics, in Figures 7.5 and 7.6 have been respectively reported the roots of the augmented stability matrix  $\mathbf{A} - \mathbf{B} \mathbf{K}_{p\alpha}^T$  for different values of  $\alpha$ , compared to the poles chosen according to the pole placement specifications.

In Figure 7.7 are shown the Matlab/Simulink 6Dof airship model with the optimal controller in turbulence. It has been decided to apply the optimal control technique in turbulence only to the control strategy involving both the rudders and the ailerons that seemed to be the more suitable approach. For the purpose of the optimal control the following cost matrices have been assumed, as the best trade-off of a trial and error approach:

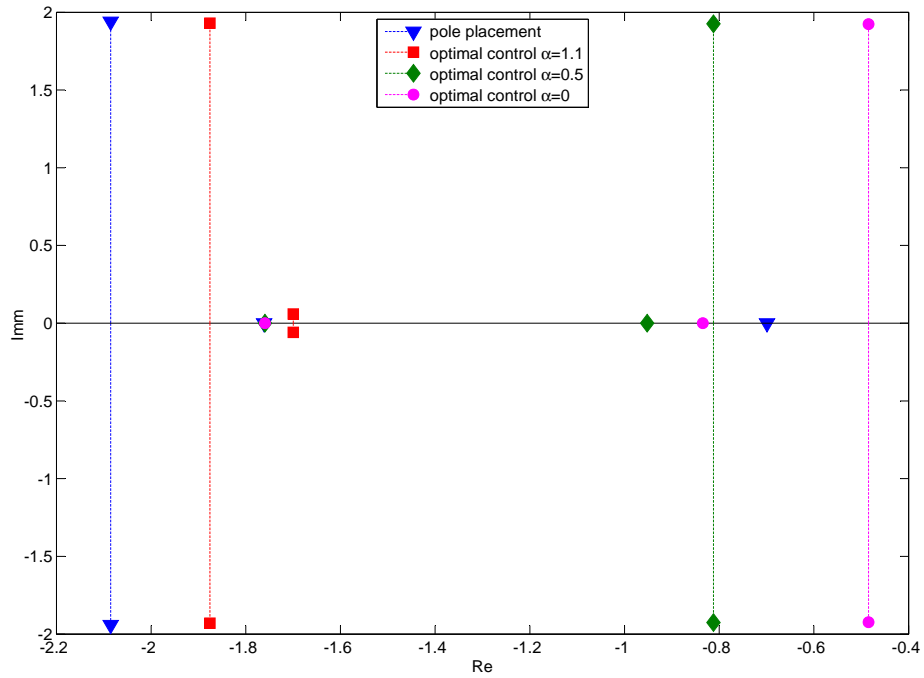


Figure 7.5: root locus analysis, cross configuration

$$Q = \begin{pmatrix} 1 & 0 & 0 & 0 \\ 0 & 20 & 0 & 0 \\ 0 & 0 & 10 & 0 \\ 0 & 0 & 0 & 200 \end{pmatrix} \quad R = \begin{pmatrix} 0.1 & 0 \\ 0 & 1 \end{pmatrix} \quad (7.10)$$

The resulting optimal control gain matrices are showed in Table 7.2.

Table 7.2: LQR controller gains with  $\alpha = 1.1$ 

Airship Configuration	$K_{\rho\alpha}^T$
cross	$\begin{bmatrix} 35.14 & -154.30 & -89.30 & -147.14 \\ 12.05 & 4.11 & -18.20 & 14.20 \end{bmatrix}$
inverted Y	$\begin{bmatrix} -256.13 & 128.54 & -291.49 & -42.14 \\ 0.66 & -0.10 & 17.02 & 19.58 \end{bmatrix}$

From the applications it could be noticed that the use of both rudder and aileron is more suitable for the purpose of the lateral-directional regulation in turbulence. In Figures 7.8 and 7.9 are plotted the optimal control results for this strategy, assuming the exponential decay of rate  $\alpha = 1.1$ . This particular value comes from the analysis carried out in the previous section—see Figure 7.5 and 7.6.

Finally, for both the airship configurations, in Figures 7.10(a) and 7.10(b) is shown a comparison between the terms  $\mathbf{u}^T \mathbf{u}$  descending from the applications of the pole placement with noise method and from the LQR with exponential decay of rate technique. As is observed, the optimal control presents a lower

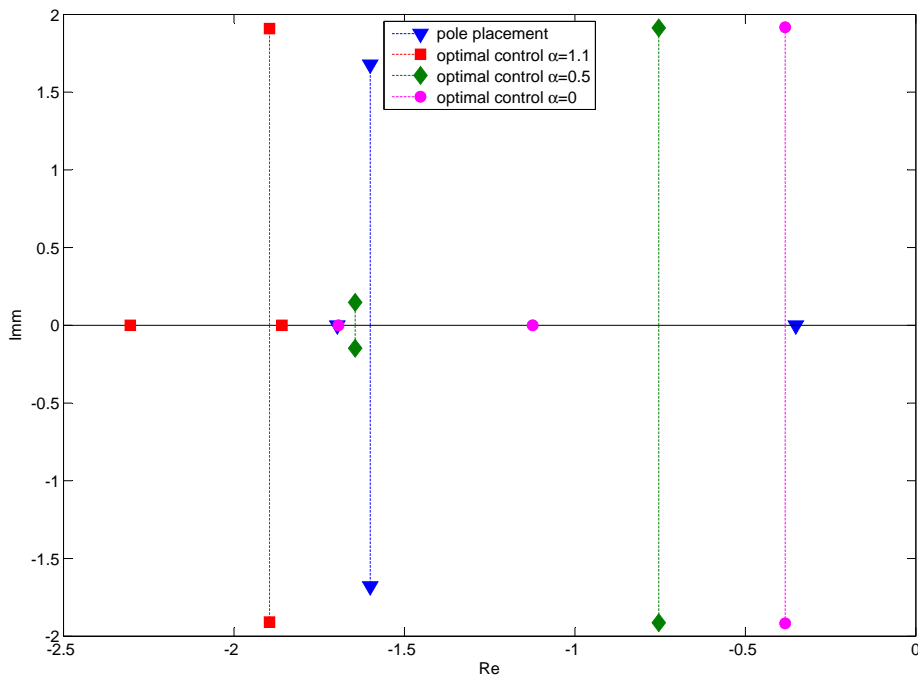


Figure 7.6: root locus analysis, inverted Y configuration

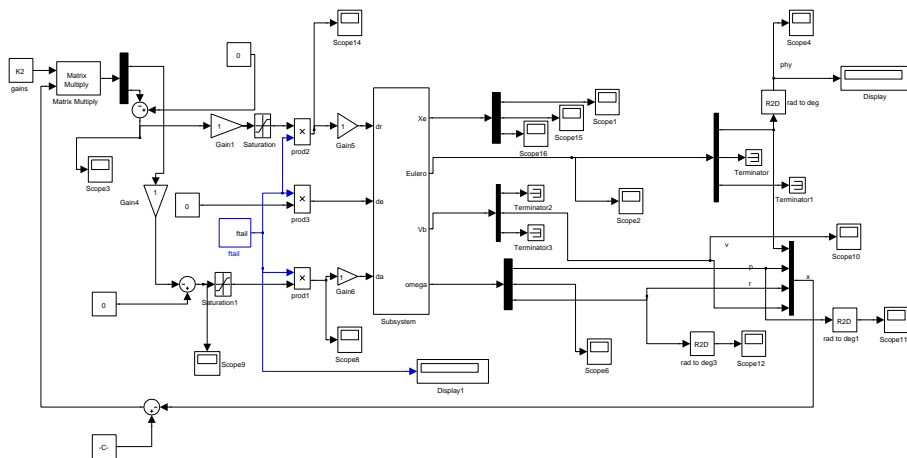


Figure 7.7: Matlab/Simulink 6DOF airship model with turbulence optimal control method.

value of the term  $\mathbf{u}^T \mathbf{u}$ , whose integral with respect to the time means a lower work on the control surfaces.

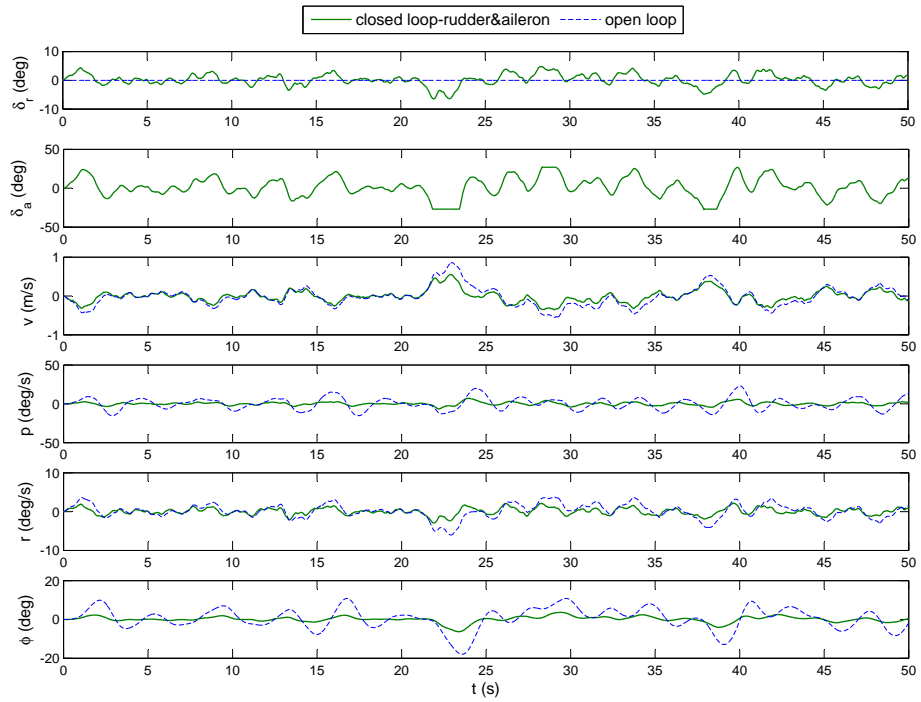


Figure 7.8: Optimal control responses in turbulence, cross configuration

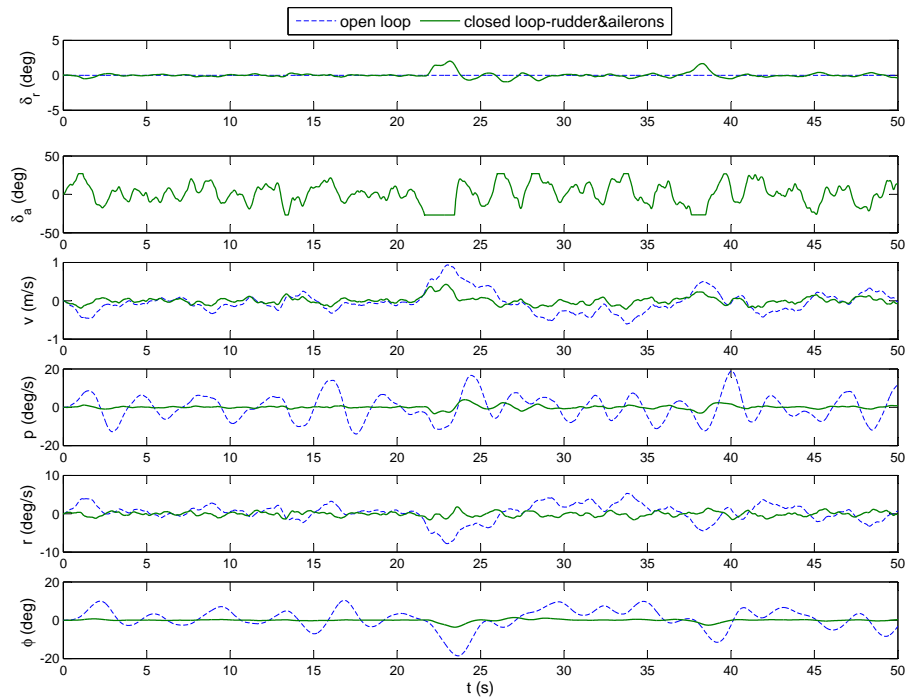


Figure 7.9: Optimal control responses in turbulence, inverted Y configuration

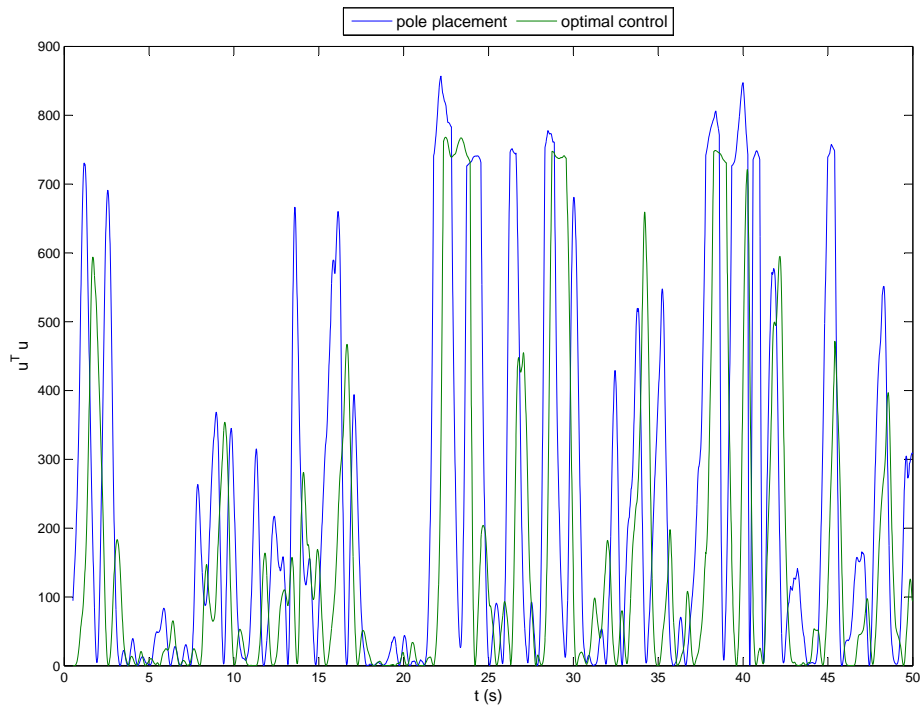
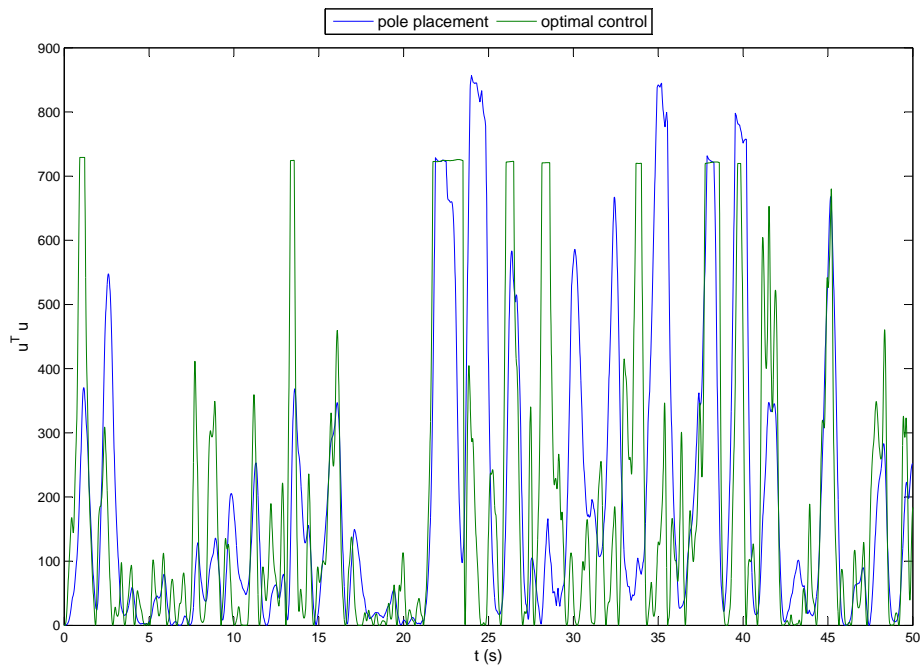
(a)  $u^T u$ , cross configuration(b)  $u^T u$ , inverted Y configuration

Figure 7.10: Surface deflections efforts in turbulence atmosphere.

## Chapter 8

# General Layout of the Experimental Tests

### 8.1 Introduction

IN the last part of the research work, a preliminary study regarding experimental tests on the airship *AIUX15* has been carried out: the aim of this project is to validate the airship aerodynamic database obtained by CFD RANS computations with experimental data. A new method for the calculation of the longitudinal airship stability derivatives by using a towing tank, has been developed; for the symmetry of the problem, once evaluated the longitudinal aerodynamic coefficients, even the lateral-directional coefficients could be estimated.

The towing tank, differently from the wind tunnel, allows to reach higher Reynolds numbers with smaller model dimensions and flow velocity; the main characteristics of the towing tank of the Department of Marine Engineering (DIN) at the University of Naples "Federico II" (see Figure 8.1 ) are shown in Table 8.1:

### 8.2 The mathematical model

The experimental tests are based on a 1-degree of freedom mathematical mass-spring-damper model, defined as follows 8.1:

$$I_y \ddot{\theta} + b_\theta \dot{\theta} + (k_0 + \Delta k_0) - M(t) = F(t)a \quad (8.1)$$

where:

Table 8.1: Towing tank characteristics

Length	Beam	Depth	Max Velocity	Max Deceleration
140.2 m	9.0 m	4.25 m	10.0 m/s	3.0 m/s <sup>2</sup>



Figure 8.1: The towing tank of the DIN

- $I_y$  is the airship moment of inertia, without taking in account the effects of the added mass;
- $M(t) = M_\theta\theta + M_{\dot{\theta}}\dot{\theta} + M_{\ddot{\theta}}\ddot{\theta}$  represents the hydrodynamic action arising from the airship oscillations. In particular the term  $M_{\ddot{\theta}}$  represent the moment of inertia due to the added mass, the term  $M_{\dot{\theta}}$  is the hydrodynamic damping;
- $b_\theta = \frac{2a_\theta k_0}{\omega}$  is the structural damping coefficient, depending on the restrain characteristics;
- $k_0 + \Delta k_0$  is the elastic constant of the restrain. For the particular geometry of the restrain, the elastic constant could change according to the different loads applied on it; the term  $\Delta k_0$  represents the variation of the elastic constant due to drag and the lift acting on the model that, as will be explained in the following, could be safely ignored;
- $F(t)a$  is the external moment applied to excite the system. The harmonic force could be expressed as  $F(t) = Fe^{i\omega t} = (F' + iF'')e^{i\omega t}$ .

The experimental method is based on the comparison of the exciting forces applied on the airship model at zero speed and in motion, as reported in the following equations:

$$M_{\dot{\theta}} = \frac{2a_\theta I_y \omega_0^2}{\omega_v} \left( 1 - \frac{F''_v}{F''_0} \right) \quad M_\theta = A\omega_0^2 I_y - \omega_v^2 (I_y - M_{\ddot{\theta}}) \quad (8.2)$$

Table 8.2: Airship model characteristics

$V_m$	$c = \nabla^{1/3}$	$l_m$	$d_m$	$\nabla$	$R_N$
4.5 m/s	0.355 m	1.050 m	0.272 m	0.045 0 m <sup>3</sup>	1.0 · 10 <sup>6</sup>

where:

- $F''_0$  is the imaginary force component at zero speed with frequency  $\omega_0$ ;
- $F''_v$  is the imaginary force component for the airship moving in the water, with frequency  $\omega_v$ ;
- $A = \frac{k_0 + \Delta k_0}{k_0}$  takes in account the increment in elastic constant due to the drag and the lift acting on the airship.

After evaluating respectively the damping and the elastic term of the hydrodynamic moment, the sought aerodynamic coefficients can be evaluated as follows:

$$C_{m\alpha} = \frac{M_\theta}{q_\infty S c} \quad C_{mq} = \frac{2M_{\dot{\theta}} V_\infty}{q_\infty S c^2} \quad (8.3)$$

The method introduced in this paragraph has been applied in a previous research work to evaluate the stability derivatives for an aircraft by wind tunnel tests [20].

### 8.3 Preliminary analysis

The dimensions of the airship model, the maximum forces and moments on the restrain, and the speed of the model during the tests have been determined on the basis of preliminary analysis carried out from the CFD aerodynamic database, having  $R_N = 4.7 \cdot 10^6$ . The Reynolds number for the airship *AIUX15* has been calculated, assuming the reference cord ( $c = \nabla^{1/3}$ ), the airship maximum velocity of 50 km/h and the air temperature at sea level as 15°.

Some consideration on the maximum weight and size of the model, related to the towing tank characteristics, led to the choice of the following model dimensions (Table 8.2). The scale factor have been assumed to be  $\lambda = 14$ : this is the best compromise to obtain a model that realized a significative  $R_N$  and remaining manageable.

Another advantage in using a towing tank instead of a wind tunnel is the reduction in the frequency of the oscillation for the test. In Table 8.3 are compared the preliminary values of the natural frequencies of the airship motion in air and in water. These values, that during the test will be measured to evaluate the experimental stability derivatives 8.2, in this analysis have been obtained from the numerical CFD stability derivatives. The comparison has

Table 8.3: Frequency comparison

Fluid	$\lambda$	$\omega_0(1/s)$	$\omega_v(1/s)$	$\frac{\omega_v}{\omega_0}$	$\frac{F''_v}{F''_0}$	$V_m$ m/s
AIR	6.5	22.2	19.97	0.90	395.8	20.0
WATER	14	4.78	2.19	0.46	84.1	4.5

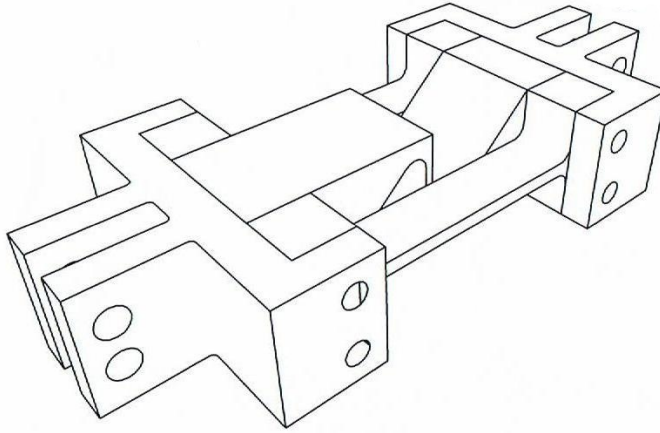


Figure 8.2: Cross flexure pivot

been carried out for the same Reynolds number of  $1.0 \cdot 10^6$  and assuming an initial  $k = 150 \text{ N m/rad}$ . The significant advantages in using water as test fluid are the reduction in speed, in model dimensions and in frequencies; there is also a lower value of the ratio  $\frac{\omega_v}{\omega_0}$  that means lower error on the measurements.

The restraint chosen and designed for the test is a cross flexure pivot shown in Figure 8.2. Cross flexure pivots do not require lubrication and are of very simple and robust construction, but they are not suitable for very large angle of rotation. For the design of this restraint the method developed by Wittrick [22] has been followed, obtained for the dimensions shown in Table 8.4 a value of  $k_0 = 295 \text{ N m/rad}$  and  $A = 1$  as, from the calculations, the term  $\Delta k_0$  could be safely ignored.

## 8.4 Model test arrangement

In the last part of this work, the model arrangement inside the towing tank has been expected. The main problem with an underwater test is the need to match the deep water condition. In this way a good correlation between the

Table 8.4: Cross flexure pivot main dimensions

Length	Beam of each strip	Thickness
80 mm	25 mm	3 mm

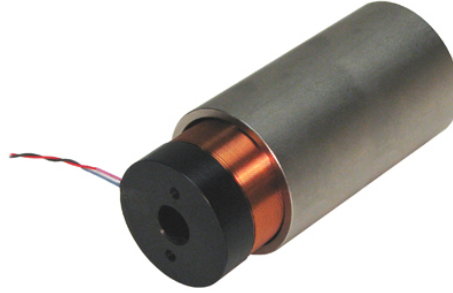


Figure 8.3: Voice coil actuator

model test data and the real data is ensured. The model should not generate free surface effects, so the airship has to be placed enough underwater. According to the standard practice for the submarine [21], the deep water depth  $h$  has to be three-four times the maximum diameter of the body: in this case  $h = 1.20$  m. During the test will be also used a carter with an aerodynamic section to cover the connection beam at the free surface in order to limit the undesirable wave generation.

It was also estimated that the maximum force  $F = 43$  N, that the actuator must exert on the model of the airship in order to cause an oscillation of  $\theta = 2.5^\circ$ , applied at a distance of about 30 cm from the constraint. The exciting force will be applied by using a voice coil 8.3: this is a small linear actuator that uses a permanent magnet field and a coil winding to produce a force proportional to the current applied to the coil. The main advantage in using a voice coil actuator is the possibility to easily introduce a servo control on the intensity and on the frequency of the exciting force.

# Chapter 9

## Conclusion

### 9.1 Linear analysis

The main objective of this research work has regarded the development of new methods in analyzing and evaluating the stability and the control of the airship. The theoretical approach to airship dynamic model and then the numerical approach in developing the 3DoF and 6DoF simulation models represented basis of the work.

At first the mathematical linearized longitudinal model has been applied to a small airship at the nominal speed and solved with an approximate approach. Airships static stability, due to their fuselage shape without wing and due to their nature of buoyant lift cannot refer to the aircraft standard methods in appraising static stability. In the performed analysis the effects of the weight have been taken in account, and the trim equations in heaviness condition have been developed and solved.

With the introduction of an innovative method, based on the knowledge of the main geometrical and aerodynamical characteristics of the airship, it was possible to demonstrate that an airship could carry more weight without relevant consequences on stability and drag.

Observing the numerical test cases on the AIUX15, the airship in heaviness condition could have the same stability characteristic of the neutral buoyancy one's, keeping down the excess of weight. Furthermore, thanks to the thrust vectoring the airship at hover could sustain the exceeded weight aiming vertical take-off and landing too. As expected, the stability modes were quite distinct exponential subsidence modes for these cases.

For significant excess of weight, instead, the airship would required high incidence to flight. Regarding to the AIUX15, the stability at equilibrium in the range of negativity of  $C_{m\alpha}$ , over  $15^\circ$  of incidence has been investigated. In this conditions the airship seemed to be stable too, but with a significant total drag, that would require a thrust increase, and with oscillatory modes of motion.

All that confirmed that for an airship the value of  $C_{m\alpha}$  has not the same relevance on the stability as for a conventional aircraft. The significant difference between a neutral buoyancy condition and the heaviness conditions, as could guessed, was due to the effect of the excess weight on  $X$  and  $Y$  axes, ( $mg -$

$B) \cos \Theta_e$  and  $(mg - B) \sin \Theta_e$  respectively, which tended to reduce or increase the total speed according to its direction were nose up or nose down.

Then the proposed method had been extended also to the lateral motions, to compare the stability and control characteristics of two different typical tail arrangement configuration. The cross empennages airship in a heaviness condition denoted a drag lower than the inverted Y airship drag, due to the equilibrium attitude without control. The main advantage in having a three empennages configuration is the improvement of the airship payload (approximately 10% increase), reducing the fins number.

## 9.2 Simulation model

In the second part of the research, it was reported about the development of the FDM model for an unmanned airship in stationary and turbulence atmosphere, intending this vehicle for use at low altitude operations. The details of the implementation of a specific Matlab/Simulink dynamic model were also reported. This model has been applied to analyze the lateral-directional behavior at the nominal speed for two different empennages configurations. A satisfying closed-loop control system that reduces the airship oscillatory rolling motions was achieved. The simulation of flight responses to assigned conditions and inputs enabled to compare two different control strategies regarding the use of rudders (two vertical aero-surfaces in the “cross” tail configuration and one in the “inverted-Y” tail configuration) and of the ailerons (i.e. elevators with imposed anti-symmetrical rotations, both in the “cross” and in the “inverted-Y” tail configuration). The analysis of the feedback control laws for the 6DoF model has been carried out by linearization around the operational trim conditions. The closed-loop flight control by means of the state-space approach were achieved, in order to limit the oscillatory rolling motions induced by the rudder deflections. A low ailerons roll control power, as compared to the rudders control power, resulted from our analysis, leading initially to an unsatisfactory closed-loop control, especially for the four empennages configuration.

A Dryden power spectral density function was implemented to model the atmospheric turbulence in the simulation. The closed-loop control in turbulence was achieved firstly by applying the pole placement with noise method. Both the control strategies for the two airship configurations reduced the oscillatory motions in turbulence. The control approach using both the rudders and the ailerons resulted quite satisfactory.

Finally the LQR optimal control technique was introduced with an exponential decay rate applied to the strategy involving both rudder and aileron. Using this method it was possible to reduce the amount of control surface work to control the lateral-directional oscillations in turbulent air.

# Appendix A

## The Added Mass

The added mass contribution, in the equations of motion, is taken into account; in fact the airship motions accelerate the surrounding air, yielding to it energy. For the airship, the added mass effects could be approximately referred only to the envelope, for which the added mass term could be calculated using the theoretical formulas for the prolate ellipsoid [4], for which, due to the symmetry of the body, the added mass matrix is diagonal:

$$\begin{aligned} X_{\dot{u}} &= -\frac{4}{3}\pi\rho_A ab^2 k_1 \\ Y_{\dot{v}} &= Z_{\dot{w}} = -\frac{4}{3}\pi\rho_A ab^2 k_2 \end{aligned} \quad (\text{A.1})$$

where:

$$k_1 = \frac{\alpha_0}{2 - \alpha_0} \quad k_2 = \frac{\beta_0}{2 - \beta_0}$$

and  $\rho_A$  is the density of the fluid. For a prolate spheroid with  $a > b$ , where  $b$  represents the maximum radius of the airship, the two coefficients assume the following expression [4]:

$$\alpha_0 = \frac{2(1 - e^2)}{e^3} \left( \frac{1}{2} \ln \frac{1 + e}{1 - e} - e \right) \quad \beta_0 = \frac{1}{e^2} - \frac{1 - e^2}{2e^3} \ln \frac{1 + e}{1 - e} \quad (\text{A.2})$$

where  $e$  is the eccentricity of the longitudinal section:

$$e = \sqrt{\left(1 - \frac{a^2}{b^2}\right)}$$

The additional moments of inertia are given by [4]:

$$\begin{aligned} K_{\dot{p}} &= 0 \\ N_{\dot{r}} &= M_{\dot{q}} = -\frac{4}{3}\pi\rho_A ab^2 \frac{b^2 + a^2}{5} k' \end{aligned} \quad (\text{A.3})$$

where:

$$k' = \frac{e^4 (\beta_0 - \alpha_0)}{(2 - e^2) [2e^2 - (2 - e^2) (\beta_0 - \alpha_0)]}$$

The added mass matrix of an airship, due to the presence of the fins, is not strictly diagonal; however, the non-diagonal terms are such smaller than the others, that could be safely ignored [18].

# Bibliography

- [1] A. Colozza, J. L. Dolce, *High-Altitude, Long-Endurance Airships*, NASA Technical Memorandum, National Aeronautics and Space Administration, John H. Glenn Research Center at Lewis Field Cleveland, Ohio, 2005.
- [2] G. Andreutti, P. Iannelli, A. Carozza, *Sintesi delle attività di aerodinamica svolte dal CIRA sul progetto ZSFERA*. CIRA (Italian Aerospace Research Centre), 2009.
- [3] G. Kantor, D. Wettergreen, J. P. Ostrowski, S. Singh, *Collection of Environmental Data From an Airship Platform*. Proceedings of the SPIE Conference on Sensor Fusion and Decentralized Control IV. 2001. pp. 76-83.
- [4] H. Lamb, *The Inertia Coefficients of an Ellipsoid Moving in Fluid*. Aeronautical Research Council Report 623, Aeronautical Research Council, 1918.
- [5] J. Carvalho, E. de Paiva, J. Azinheira, P. Ferreira, J. Ramos, S. Bueno, M. Bergerman, S. Maeta, L. Mirisola, L. Faria, A. Elfes, *Classic and robust PID heading control for an unmanned robotic airship*. SIRS'2001 Int. Conf., Toulouse, France, Jul 2001, pp. 61-70.
- [6] A. Tewari, *Modern Control Design with Matlab and Simulink*. John Wiley & Sons Ltd, ISBN 0 471 496790, 2002.
- [7] C. G. Justus, C. W. Campbell, M. K. Doubleday, D. L. Johnson, *New Atmospheric Turbulence Model for Shuttle Applications*. NASA Technical Memorandum 4168, NASA, 1990.
- [8] J. R. Azinheira, E. Paiva, J. J. G. Ramos, S. S. Bueno, M. Bergerman, *Extended Dynamic Model for AURORA Robotic Airship*. AIAA Lighter-Than-Air Technology Conference, Akron, 2001.
- [9] J. Rao, Z. Gong, Z. Xie, *A Flight Control and Navigation System of a Small Size Unmanned Airship*. IEEE International Conference on Mechatronics & Automation, Niagara Falls, Canada, 2005, pp. 1491-1496.
- [10] L. G. B. Mirisola, J. Lobo, J. Dias, *Stereo Vision 3D Map Registration for Airships*. IASTED International Conference on Robotics and Applications (RA '06). Honolulu, Hawaii, 2006. pp. 102-107.
- [11] M. Munk, *The aerodynamic forces on airship hulls*. NACA Report 184, NACA, 1924.

- [12] M. V. Cook , *Stability and Control*. Chap. IV in Airship technology, by Khoury G.A. and Gillett J.D., Cambridge University Press, 1999.
- [13] S. B. V. Gomes, J. Jr. G. Ramos, *Airship Dynamic Modeling for Autonomous Operation*. IEEE International Conference on Robotics & Automation, Leuven, Belgium, 1998, pp. 3462-3467.
- [14] Y. J. Liang, G. Y. Tang, H. Ma, *Optimal Control with Exponential Decay Rate for Offshore Platform Subjected to Irregular Wave Force*. IEEE International Conference on Control and Automation, Xiamen, China, June 2010.
- [15] M. V. Cook, *The linearized small perturbation equations of motion for an airship*, College of Aeronautics Reports, WP8, Cranfield Institute of Technology, 1990.
- [16] F. Goineau and M. V. Cook, *The stability and control characteristics of the neutrally buoyant non-rigid airship*, College of Aeronautics Reports, Cranfield Institute of Technology, 1999.
- [17] E. A. Kulczycki, J. R. Johnson, *On The Development of Parameterized Linear Analytical Longitudinal Airship Model*, AIAA Guidance, Navigation And Control Conference And Exhibit, Paper No.7260, Honolulu (Hawaii), 2008.
- [18] N. La Gloria, *Simultaneous localization and mapping applied to an airship with inertial navigation system and camera sensor fusion*, CISAS, Phd Thesis, University of Padua , 2008.
- [19] J. Roskam, *Flight dynamics of rigid and elastic airplanes*, Vol.1, Published by the author, Kansas City, USA, 1972, Chap. 4.
- [20] L. Lecce and V. Gentile, *Wind Tunnel Tests to Determine Longitudinal Dynamic Stability Derivatives on Models in Forced Oscillation* , Proceedings of the V National Conference of the AIDAA, Milano, Italy, 26-29 Ott. 1979. Published on "Aerotecnica , Missili e Spazi", Vol. 59, No. 4, December 1980, pp. 314-321.
- [21] *Principles of Naval Architects* published by the Society of Naval Architects and Marine Engineers - SNAME.
- [22] H. Wittrick, *The Theory of Symmetrical Crossed Flexure Pivots* , Australian Journal of Scientific Research, Series A: Physical Sciences, vol. 1, pp.121, 1948.
- [23] V. R. Cortes, J. R. Azinheira, E. C. Paiva, B. Faria, J. Ramos, S. Bueno, *Experimental Identification of Aurora Airship*, IAV2004 – 5th IFAC/EURON Symposium on Intelligent Autonomous Vehicles, Instituto Superior Técnico, Lisboa, Portugal July 2004.
- [24] A. Kornienko, *System Identification Approach for Determining Flight Dynamical Characteristics of an Airship from Flight Data*, IFF, PhD Thesis, University of Stuttgart, August 2006.

- [25] J. Kim, J. Keller, R. V. Kumer, *Design and Verification of Controllers for Airships*, Departmental Papers (MEAM), University of Pennsylvania, 2003.
- [26] E. N. Goncalves, R. M. Palhares, R. H. C. Takahashi,  $\mathcal{H}_2/\mathcal{H}_\infty$  *Robust PID Synthesis for Uncertain Systems*, Proceedings of the 45th IEEE Conference on Decision & Control, San Diego, CA, USA, December 2006, pp. 4375-4380.
- [27] P. G. Thomasson, *Equations of Motion of a Vehicle in a Moving Fluid*, Journal of Aircraft Vol. 37, No. 4, AIAA-2645-634, August 2000, pp.630-639.
- [28] Y. Li, M. Nahon, *Modeling and Simulation of Airship Dynamics*, Journal of Guidance Control and Dynamics, Vol. 30, No. 6, AIAA-29061-200, December 2007, pp. 1691-1700.
- [29] B. L. Nagabhushan, *Control Configuration of a Relaxed Stability Airship*, Journal of Aircraft Vol. 28, No. 9, AIAA-46064-520, September 1991, pp. 558-563.
- [30] B. L. Nagabhushan, S. B. Tan, *Directional Control of an Advanced Airship*, Journal of Aircraft Vol. 33, No. 5, AIAA-47032-268, October 1996, pp. 895-900.
- [31] A. Moutinho, J. R. Azinheira, *Stability and Robustness Analysis of the AURORA Airship Control System using Dynamic Inversion*, Proceedings of the 2005 IEEE International Conference on Robotics and Automation Barcelona, Spain, April 2005, pp. 2265-2270.
- [32] B. L. Nagabhushan, *Dynamic Stability of a Buoyant Quad-Rotor Aircraft*, Journal of Aircraft, Vol. 20, No. 3, AIAA-44859-486, March 1983, pp. 243-249.
- [33] A. Moutinho, *Modeling and Nonlinear Control for Airship Autonomous Flight*, PhD Thesis, University of Lisboa, December 2007.
- [34] N. E. Leonard, J. G. Graver, *Model-Based Feedback Control of Autonomous Underwater Gliders*, IEEE Journal of Oceanic Engineering, Vol. 26, No. 4, October 2001, pp. 633-645.
- [35] B. H. Beheshti, F. Wittmer, R. S. Abhari, *Flow visualization study of an airship model using a water towing tank*, Aerospace Science and Technology, August 2009, pp. 450-458.
- [36] L. Valera, B. L. Nagabhushan, *Design Trends and Global Developments in Modern Lta Vehicles*, ICAS Congress, 2002.
- [37] T. Lutz, P. Funk, A. Jakobi, S. Wagner, *Summary of Aerodynamic Studies on the Lotte Airship*, 4th International Airship Convention and Exhibition, Cambridge, England, July 2002.
- [38] T. Lutz, P. Funk, A. Jakobi, S. Wagner, *Aerodynamic Investigations on Inclined Airship Bodies*, 2th International Airship Convention and Exhibition, Bedford, Great Britain, June 1998.

## Publications

- [39] Acanfora, M., De Marco, A., Lecce, L., *Development of a Flight Dynamics Model of a Small Unmanned Airship*. Proceedings of the The 58th CASI Aeronautics Conference - AERO 2011 , Montreal , Quebec, Canada, April 2011.
- [40] M. Acanfora, A. De Marco, L. Lecce, *Development, Modeling and Simulation of Multiple Design Concepts for a Small Unmanned Airship*, Proceedings of the AIAA Modeling and Simulation Technology Conference, Portland, Oregon, USA, AIAA-MST 2011-6521-967, August 2011.
- [41] M. Acanfora, A. De Marco, L. Lecce, *Stability and Control Analysis for a Non-Rigid Unmanned Airship with Different Tail Configurations*, Proceedings of the Specialists Meeting NATO AVT-189/RSM-028, Portsmouth West, UK, October 2011.
- [42] AM. Acanfora, L. Lecce, *On the Development of the Linear Longitudinal Model for Airship's Stability in Heaviness Condition*, Accepted on "Aerotecnica Missili e Spazio" 07/09/2011.